ACOUSTICAL PROPERTIES OF CLAY-BEARING ROCKS

A DISSERTATION
SUBMITTED TO THE DEPARTMENT OF GEOPHYSICS
AND THE COMMITTEE ON GRADUATE STUDIES
OF STANFORD UNIVERSITY
IN PARTIAL FULFILLMENT OF THE REQUIREMENTS
FOR THE DEGREE OF
DOCTOR OF PHILOSOPHY

By
Carol Ann Tosaya

June 1982

TABLE OF CONTENTS

TABLE OF CONTENTS (Continued)

LIST OF FIGURES

LIST OF FIGURES (Continued)

LIST OF TABLES

ACOUSTICAL PROPERTIES OF CLAY-BEARING ROCKS

ABSTRACT

Occurrences of clay-rich shaly formations in association with petroleum reservoirs have posed numerous problems over the years for geophysicists and reservoir engineers. The dominant method of identifying subsurface lithologies and detailing subsurface structural geometries has been through the correlation of seismic reflection data with data obtained from strictly controlled laboratory measurements of rock properties. Most rock types, including sandstones, limestones, and igneous and metamorphic rocks, have been comprehensively studied in the laboratory, and, hence, there exists a large body of information concerning the physical and acoustical properties of a wide range of materials. Shales, however, constitute a large class of rocks to which little study has been devoted. This dissertation seeks to substantially broaden existing knowledge of the acoustical and the physiochemical behavior of shales under test conditions that were designed to address important problems of current research and applications interest.

The work is divided into three experiments, all involving ultrasonic-frequency, transient-pulse measurements through cylindrical cores of rocks that are isolated at elevated confining and pore pressures.

The first experiment focuses primarily on the delineation of abnormal pore pressures in subsurface shaly lithologies. Variation with depth of the transmitted first-arrival, zero-to-peak P-wave amplitude, inversely related to attenuation through the sample, is found to be the most sensitive acoustic parameter for delimiting pore pessures in clay-rich rocks.

The second experiment deals with the acoustical identification of lithologies based on systematic dependencies of compressional- and shear-wave velocities on pore fraction and volumetric clay content within a few percent error in the detrital silicate rocks selected for the study over ranges of porosity and clay content that span 4 - 20 percent and 0 - 72 percent, respectively.

The final experiment treats intrinsic acoustical anisotropy, a property that is strongly characteristic of shales due to high degrees of preferred orientation of morphologically platy clay minerals. The five independent elastic constants determined for a hexagonally symmetrical shale are seen to diverge with increasing differential pressure. This increase in anisotropy with depth should continue, tending toward the intrinsic crystallographic anisotropy of the statistically weighted volume fractions of the constituent minerals.

I. INTRODUCTION

INTRODUCTION

In recent years seismologists have become increasingly interested in the acoustical properties of clay-bearing rocks. The continued development of high-resolution seismic techniques for locating and evaluating petroleum reservoirs and subsurface stratigraphy has necessitated detailed, accurate knowledge about the response of rock to acoustic-wave disturbances. Particular interest has focused on: (1) shortcomings of the time-average equation (Rinehart, et al., 1961; Geertsma, 1961; Geertsma and Smit, 1961) when applied to clay-bearing rocks, (2) development of acoustical tools for delineating abnormal pore pressures that are frequently associated with the presence of low-permeability shales that are underconsolidated or normally consolidated, and (3) evaluation of the elastic constants of anisotropic rocks in order to correct for tilted formations or horizontally bounded, intrinsically anisotropic units. Strict control of significant parameters in laboratory studies provides a highly useful means of assessing the influence of subsurface environmental conditions on the physical properties of rocks.

The time-average equation, an empirically derived expression (Wyllie, et al., 1956, 1958) relating bulk-rock velocity to porosity and to fluid and matrix velocities, does not adequately describe the effect of detrital matrix clays on measured longitudinal and shear velocities. Even a small amount of matrix clay can significantly influence frame compressibility, as shown in Chapter IV. Although there are numerous theoretical models concerning the effects of porosity, pore and contact shape, and fluid and matrix moduli on the elastic properties of rocks, little experimental and petrographic work has been done in this area (e.g., see Walsh and Grosenbaugh, 1979; Mavko and Nur, 1978; Brown and Korringa, 1975; Gassmann, 1951, Biot, 1956).

Present seismic techniques employed in the detection of abnormally high pore-pressures in shale rely on identifying stratigraphic regions of anomalously low velocity and are based on the assumption of undercompaction or volumetric clay contents larger than 50% in these units (Chapter III). However, undercompaction and high clay content are not requisite criteria identifying overpressured shales (Bradley, 1975; Carstens and Dypvik, 1981; Tosaya, this volume). It is well documented that clays physiochemically interact with pore fluids principally as a result of two conditions: (1) small particle size and platy morphology resulting in high specific surface area (surface area per unit volume or per unit mass of clay) and (2) a net electrical charge resulting from isomorphous ionic substitutions in the crystal lattices and ionic adsorption associated with broken bonds and free surfaces (Lambe and Whitman, 1971; Mitchell, 1969; Van Olphen, 1977). Yet, lack of knowledge about the precise manner in which pore-water/clay interactions affect acoustical measurements has prevented development of suitable exploration tools. Diagnostic characteristics seen in strictly controlled laboratory acoustical studies have direct applicability to the nature of fluid/clay interactions at depth in well consolidated shales and may lead to the development of highly definitive pore-pressure sensitive stratigraphic-evaluation tools.

It is well documented that treatment of the earth's crust as an elastically isotropic medium yields results that are erroneous in the evaluation of media that are not isotropic on the wavelength scales of seismic or sonic exploration techniques. Descriptions of elastic-wave propagation in transversely isotropic media based on periodic layering of isotropic media range from the zero-porosity models of Voigt and Reuss

(Dieter, 1961) to various long-wavelength, grossly homogeneous, anisotropic-equivalent, lamellae-stacking theories including those of Postma (1955), Rytov (19560, Helbig (1981), Backus (1962), Anderson (1961), Uhrig and Van Melle (1955), and Love (1934). Although these models of long-wave equivalents to horizontally layered isotropic media adequately describe observed crystal anisotropics due to layering of isotropic materials, large errors result when they are applied to intrinsically, highly anisotropic materials such as shales.

Careful, direct laboratory measurement of directional elastic-wave propagation in shales is the most accurate method of determining the elastic constants of intrinsically anisotropic media. Anisotropy data from samples of Green River shale (Podio, et al., 1968), Pierre shale (Jones and Wang, 1981), and Cotton Valley silty shale (Tosaya, this volume) provide widely applicable, realistic values of acoustical anisotropy in these media over a range of simulated <u>in situ</u> conditions.

REFERENCES

Anderson, D.L., 1961, Elastic wave propagation in layered anisotropic media: J. Geophys. Res., Vol. 66, p. 2953-2963.

Backus, G.E., 1962, Long-wave elastic anisotropy produced by horizontal layering: J. Geophys. Res., Vol. 67, p. 4427-4440.

Biot, M.A., 1956, Theory of propagation of elastic waves in fluid-saturated porous solid: Parts I and II: J. Acoust. Soc. Am., Vol. 28, p. 168-191.

Bradley, J.S., 1975, Abnormal formation pressure: Amer. Assoc. Petroleum Geol. Bull., Vol. 59, p. 957-973.

Brown, R.J.S., and Korringa, J., 1975, On the dependence of the elastic properties of a porous rock on the compressibility of the pore fluid: Geophysics, Vol. 40, p. 608-616.

Carstens, H., and Dypvik, H., 1981, Abnormal formation pressure and shale porosity: Amer. Assoc. Petroleum Geol. Bull., Vol. 65, p. 344-350.

Dieter, J.E., Jr., 1961, Mechnical Metallurgy, Metallurgy and Metallurgical Engineering Series, McGraw-Hill Book Co., New York, 615 pp.

Gassmann, F., 1951, Elastic waves through a packing of spheres, Geophysics, Vol. 16, p. 673-685.

Geertsma, J., 1961, Velocity-log interpretation: the effects of rock bulk compressibility: Soc. Petroleum Engr. Jour., p. 235-248.

_____ and Smit, D. C., 1961, Some aspects of elastic wave propagation in fluid-saturated porous solids: Geophysics, Vol. 26, p. 169-181.

Helbig, K., 1981, Systematic classification of layer-induced anisotropy: Geophysical Prospecting, Vol. 29, p. 550-577.

Jones, L.E.A., and Wang, H.F., 1981, Ultrasonic velocities in cretaceous shales from the Williston Basin: Geophysics, Vol. 46, p. 288-297.

Love, A.E.H., 1934, A treatise on the mathematical theory of elasticity, Cambridge Univ. Press, Cambridge.

Mavko, G.M., and Nur, A.M., 1978, The effect of nonelliptical cracks on the compressibility of rocks: J. Geophys. Res., Vol. 83, p. 4459-4468.

Podio, A.L., Gregory, A.R., and Gray, K.E., 1968, Dynamic properties of dry and water-saturated Green River shale under stress: Soc. Petroleum Engr. Jour., Vol. 8, p. 389-404.

Postma, G.W., 1955, Wave propagation in a stratified medium: Geophysics, Vol. 20, p. 780-806.

Reinhart, J.S., Fortin, J.-P., and Burgin, L., 1961, Propagation velocity of longitudinal waves in rocks. Effect of state of stress, stress level of the wave, water content, porosity, temperature, stratification and texture, in Colorado School of Mines, Mining Engineering Series Third Technical Session, p. 119-135.

Rytov, S.M., 1956, Acoustical properties of a thinly laminated medium: Soviet Physics — Acoustics, Vol. 2, p. 68-80.

Uhrig, L.F., and Van Melle, F.A., 1955, Velocity anisotropy in stratified media: Geophysics, Vol. 20, p. 774-779.

Walsh, J.B., and Grosenbaugh, M.A., 1979, A new model for analyzing the effect of fractures on compressibility: J. Geophys. Res., Vol. 84, p. 3532-3536.

Wyllie, M.R.J., Gregory, A.R., and Gardner, L.W., 1956, Elastic wave velocities in heterogeneous and porous media: Geophysics, Vol. 21, p. 41-70.

II. EXPERIMENTAL TECHNIQUE

EXPERIMENTAL TECHNIQUE

INTRODUCTION TO ULTRASONIC MEASUREMENTS

All of the experiments presented in this volume were conducted at frequencies close to one megahertz. Transient pulse/sample interaction parameters at ultrasonic frequencies are optimized for small sample dimensions relative to experiments at longer wavelengths. In addition, since time durations of experiments with fluid-saturated shales at elevated differential pressures are lengthy because of the low fluid permeabilities that are characteristic of these rocks, small sample dimensions minimized the times required for equilibration of pore pressure throughout the cores with each incremental increase in confining pressure.

The experiments of Chapters III and IV utilized rock plugs that were 2.5 cm in diameter and 1.4 cm in length. The length was constrained by the high degree of fissility of the Pierre shale. Other cores were matched to this length in order to permit direct comparisons of transmitted-amplitude data. An important consideration in the selection of rocks for these experiments, then, was that the cores must have been homogeneous over the scale of the Pierre shale sample dimensions. Average grain dimensions of the three rocks used in these two experiments were: Pierre shale: 3μ diameter x .3μ thickness, Cotton Valley silty shale: 7μ diameter x .5μ thickness, and Berea sandstone: 140μ diameter, approximately equant grains. Therefore, even the largest-grained Berea sandstone measured approximately 100 grains along the direction of wave propagation.

The most significant parameter considerations in the pulse-transmission experiments dealt with minimization of wave-energy dissipation of the transient pulse due to diffraction, scattering, and reflection phenomena. These effects were greatly reduced by optimizing the transient pulses with respect to the range of variation in physical characteristics of the three samples.

Maximum wavelength, λ, of the transmitted pulse should be constrained by the sample radius, r. If $r < \lambda$, then the pulse does not propagate at the longitudinal wave velocity, but travels at a reduced velocity that tends toward the bar velocity as r becomes small with respect to λ (Schreiber, 1973).

The ratio of the pulse wavelength to the pulse travel length, λ/L, must be less than 1 to assure that the pulse transmits through the core rather than displacing the sample uniformly (Kolsky, 1953). The maximum peak frequency observed at the compressional receiver transducer was 1.2 megahertz. The upper limit for compressional velocities was close to 4.8 kilometers per second, measured in fully saturated Cotton Valley silty shale. These numbers correspond to a maximum compressional wavelength of 4.0 mm. The maximum shear wavelength was 4.6 mm for a frequency of .65 megahertz.

There is also a minimum wavelength (maximum frequency) constraint in order to avoid diffraction effects from grains and pores (Plona and Tsang, 1979). The ratio of wavelength to grain or pore diameter, $\lambda_{s,p}$:d, should be greater than 3. The maximum grain diameter observed by thin-section and scanning-electron microscopy was .7 mm, the upper limit for the grain-size distribution of St. Peter sandstone. The minimum shear velocity measured in the saturated St. Peter sample at low differential pressure was 2.3 km/sec. Thus, the maximum shear-wave frequency limited by diffraction effects was

(2.3 km/sec)(.7 mm)$^{-1}$(3)$^{-1}$, or 1.1 megahertz. Similarly, the maximum limit for compressional-wave frequency was 2.1 megahertz.

An additional constraint on sample length was that the length-to-diameter ratio, L/d, should be less than 5 to avoid reductions in first-arrival amplitudes caused by delays from sidewall reflections.

TRANSDUCER ARRAYS AND BUFFER ROD/ENDPLUG DESIGN

The ceramic piezoelectric transducers (lead zirconium Titanate, PZT-5A) were affixed to titanium endplug/buffer rods with a thin film of stiff-curing, silver-filled, conductive epoxy. Titanium was selected as the endplug/buffer-rod material because of its high corrosion resistance to brine solutions. The length of the titanium pieces was sufficiently large to assure that reflected arrivals from the sample/endplug interfaces would be delayed so as not to interfere with first-arrival amplitudes. Figure 1 contains schematic drawings of the sample/endplug assembly configuration, the transducer array used for the experiments of Chapters III and IV (transducer mosaic 1), and the array used for the acoustical anisotropy experiment of Chapter V (transducer mosaic 2).

Transducer mosaic 1 consists of a centrally placed, 3/8-inch diameter, 1.2 megahertz, longitudinally polarized ceramic disc surrounded by a circumferential array of trapezoidal-shaped, .65 megahertz, transversely polarzied shear plates. From the Hooke equations for a transversely isotropic solid it is readily derived that the velocity of a torsional wave propagating in the direction of the axis that is orthogonal to the plane of circular symmetry is acoustically equivalent to shear-wave velocities in the same direction of propagation (See Chapter V for a comprehensive derivation of directional velocities and elastic constants in hexagonally symmetrical

media). Defining a cartesian-coordinate system in which axes 1 and 2 lie in the plane of circular symmetry and axis 3 is orthogonal to this plane,

$$V_{t3} = V_{s32} = V_{s31} = \sqrt{\frac{G_{13}}{\rho}}$$

where V_t and V_s refer to torsional and shear velocities, the first numerical subscript designates the direction of wave propagation, the second numerical subscript represents the direction of particle displacement, G is the modulus of rigidity, and ρ is the sample density. Most of the torsional-wave energy generated by this arrangement of shear transducers travels near the perimeter of the buffer rods and the sample. Thus, the presence of the pore-pressure communication holes drilled axially through the endplugs should have had minimal effect on the energy of first-arrival shear-wave amplitudes (Figure 1). The central positioning of these axial holes also should have had no effect on first-arrival longitudinal-wave energy, since the optical ray paths for longitudenal waves are well focused and, in the case of normal wave incidence to bedding or fissility, are straight lines parallel to the cylindrical axis of the sample/buffer-rod assembly.

A thin coat of waterproof epoxy was applied to all of the transducers to prevent degradation of efficiency with moisture absorption. The outer-surface electrodes of the shear transducers, sputtered gold, were electrically connected by a thin wire loop that was attached to the transducers by small spots of silver-filled epoxy.

Examples of received longitudinal- and torsional-wave signals through the platen-to-platen endplugs and through the Pierre shale and Cotton Valley silty shale are shown in Figure 2.

SAMPLE PREPARATION AND ASSEMBLY

Samples were prepared by coring with high-speed, diamond-tipped core barrels. The Pierre sample was cored in a bath of degassed water to retain saturation and to minimize slaking effects. Shales posed particular problems in sample preparation that were directly related to the effects of clays on the degree of fissility. It was found that the use of kerosene or circulating air as the coolant medium did not improve the yield of usable shale samples, nor did potting the shales in paraffin or plaster.

The ends of each core were surface ground to flatness within ±.00025 inch. The ends were in parallel alignment to within ±.0005 inch, a critical condition for ray-path considerations in acoustical measurements. Axial holes .75 mm in diameter were drilled through the shale cores that had been cut with the cylindrical axis orthogonal to the plane of preferred orientation of the clays. These holes were required in order to take advantage of permeabilities perpendicular to bedding. Without the axial hole, a pore-pressure gradient of 20 bars applied across the length of a core of Pierre shale (14.6 mm) at 10 bars initial differential pressure at the high pore-pressure end did not fully decay to uniform pore pressure over 2 weeks.

All cores except the Pierre shale and the high-porosity, high-permeability sandstones were saturated before being jacketed and mounted in the pressure-vessel assembly. The Pierre sample was sealed at the Williston Basin, North Dakota, wellsite to retain connate brine. Pre-assembly saturation of the low-permeability sandstones, siltstones, and shales was accomplished in a separate saturating vessel. The samples were evacuated for 2 days to 4 weeks at 760 mm Hg vacuum and 40°C. They were then saturated

with degassed, deionized water at a pressure of 250 bars for several days to assure complete saturation. The saturated samples were then jacketed with sections of flexible butyl-rubber bicycle innertubing and quickly mounted into the head assembly of the pressure vessel. The mounted-sample configuration is shown in Figure 1.

PRESSURE AND ELECTRONICS SYSTEMS

Following placement of the mounted samples into the pressure vessel, the samples were resaturated to replace water that may have been lost from the outer regions of the cores during handling. This was the only saturation procedure used for the high-permeability sandstones and the very low-permeability, pre-saturated Pierre shale. The samples were evacuated for 5 minutes and then flooded with degassed, deionized water at 200 bars pore pressure and 10 bars differential pressure (P_c-P_p). A schematic diagram of the pore-pressure and the confining-pressure systems is provided in Figure 3. The confining medium was Dow-Corning 200, a dielectric silicone fluid with 50 centistokes viscosity. Pore pressure and confining pressure were independently controlled. Pore pressure was controlled to ±.25 bar, confining pressure to 1 bar.

In all samples except the shales with axially drilled holes, the dual-conduit pore pressure system was used to monitor the equilibration of applied pore pressure. Pore pressure was applied or decreased at one end only; thus, pore pressure was assumed to be constant throughout the core when both the upper and the lower gauges registered equal pore-pressure values. Pore-pressure equilibration in the axially drilled shales was monitored by two independent means: (1) cessation in rise or fall of both gauge values

and (2) a halt in the change of measured velocity through the sample with time.

Velocities and amplitudes were measured by an ultrasonic-frequency, pulse-transmission technique (e.g., Birch, 1960) which was controlled as diagrammed in Figure 3. A list of the electronic equipment is provided in Figure 4. The oscilloscope was triggered by a signal from a low-power pulse generator. A delayed pulse from the same generator was used to trigger a high-power pulse generator which output to the driver transducer, a 500-volt 10-amp, 5-microsecond duration square wave of 60 to 100 hertz repetition rate. A simultaneous, low-power monitor signal from the high-power pulse generator was used to start the electronic timer. The timer was stopped by an operator-controlled, variably delayed pulse.

VELOCITY AND AMPLITUDE MEASUREMENTS

Velocities were determined from measurements of sample lengths and travel times of transient pulses through the rocks. Sample length was monitored by an axial-displacement transducer configuration (Figure 1) that was capable of detecting length changes as small as 1%. Travel times of first-arrival longitudinal- and shear-wave signals were determined from the onset of the first negative slope in the received waveform (Figure 2). Through careful measurement of sample length and travel time, velocities in the samples could be determined to better than 2% precision.

Received-wave amplitudes for wave incidence normal to bedding were affected primarily by five factors in this experiment: (1) driving-pulse amplitude, (2) coupling coefficient between transducer holders and sample, (3) transmission coefficient between transducer holders and sample, (4)

sample length, and (5) attenuation in the sample. The driving pulse was held constant to within 1%. The coupling force, which varied with differential pressure, changed by a maximum of 4% for compressional-wave amplitudes, A_p, and 17% for shear-wave amplitudes, A_s (Figure 5). These maximum variations in coupling force, determined from amplitude measurements through a stainless steel core placed between the endplugs, substantially overestimated errors expected from more compliant materials such as shales. Corrections to amplitude data at differential pressures lower than 200 bars accounted for this interface-compliance effect. Coupling force was invariant above 200 bars differential pressure for A_p and above 300 bars for A_s. Transmission coefficient, calculated from changes in acoustic impedance between endplugs and sample with increasing differential pressure, changes with density and wave velocity in the sample. The received amplitude is:

$$A = B_o T_1 T_2 = B_o T$$

where B_o is a constant, T_1 is the transmission coefficient at the first sample/endplug interface, T_2 is the transmission coefficient at the second sample/endplug interface, and T is the compounded transmission coefficient for a single observation. To cancel the effect of changes in T with increasing differential pressure, observed amplitudes were multiplied by T_o/T, where T_o is the initial transmission coefficient. For wave incidence normal to sample stratification:

$$T = \frac{2\rho_1 V_1}{\rho_1 V_1 + \rho_2 V_2} \cdot \frac{2\rho_2 V_2}{\rho_2 V_2 + \rho_1 V_1} = \frac{4\rho_1 V_1 \rho_2 V_2}{(\rho_1 V_1 + \rho_2 V_2)^2}$$

where ρ_1 and V_1 are the density and velocity pertaining to the transducer holders/buffer rods, and ρ_2 and V_2 are the density and velocity of the rock sample. Lengths of samples used in amplitude-comparison measurements were equal to better than .5%. After all corrections and sources of error were considered, it was found that received-wave amplitude, controlled primarily by attenuation in the sample, could be determined to within 10%.

REFERENCES

Schreiber, E., 1973, Elastic Constants and Their Measurement, McGraw-Hill Book Co., New York.

Kolsky, H., 1953, Stress Waves in Solids, Clarendon Press, Great Britain.

Plona, T.J., and Tsang, L., 1979, Determination of the average microscopic dimension in granular media using ultrasonic pulses: theory and experiments: Presented at SEG 1979 Annual Convention, New Orleans, LA.

Birch, F., 1960, The velocity of compressional waves in rocks to 10 kb. Part 1: J. Geophys. Res., Vol. 65, p. 1083-1102.

FIGURE CAPTIONS

FIGURE 1. Sample assembly on pressure-vessel head with details of transducer mosaics and pressure and electrical feedthroughs.

FIGURE 2. Samples of received pulses. Vertical amplifications vary. (A), (B): P and S pulses through platen-to-platen endplugs. (C), (D): P and S pulses through dry Pierre shale. (E), (F): P and S pulses through dry Cotton Valley shale.

FIGURE 3. Schematic diagram of pulse-transmission apparatus.

FIGURE 4. List of electronic components used in pulse-transmission measurements.

FIGURE 5. Normalized platen-to-platen measurements of received P- and S-wave amplitudes for computing endplug/sample coupling coefficients.

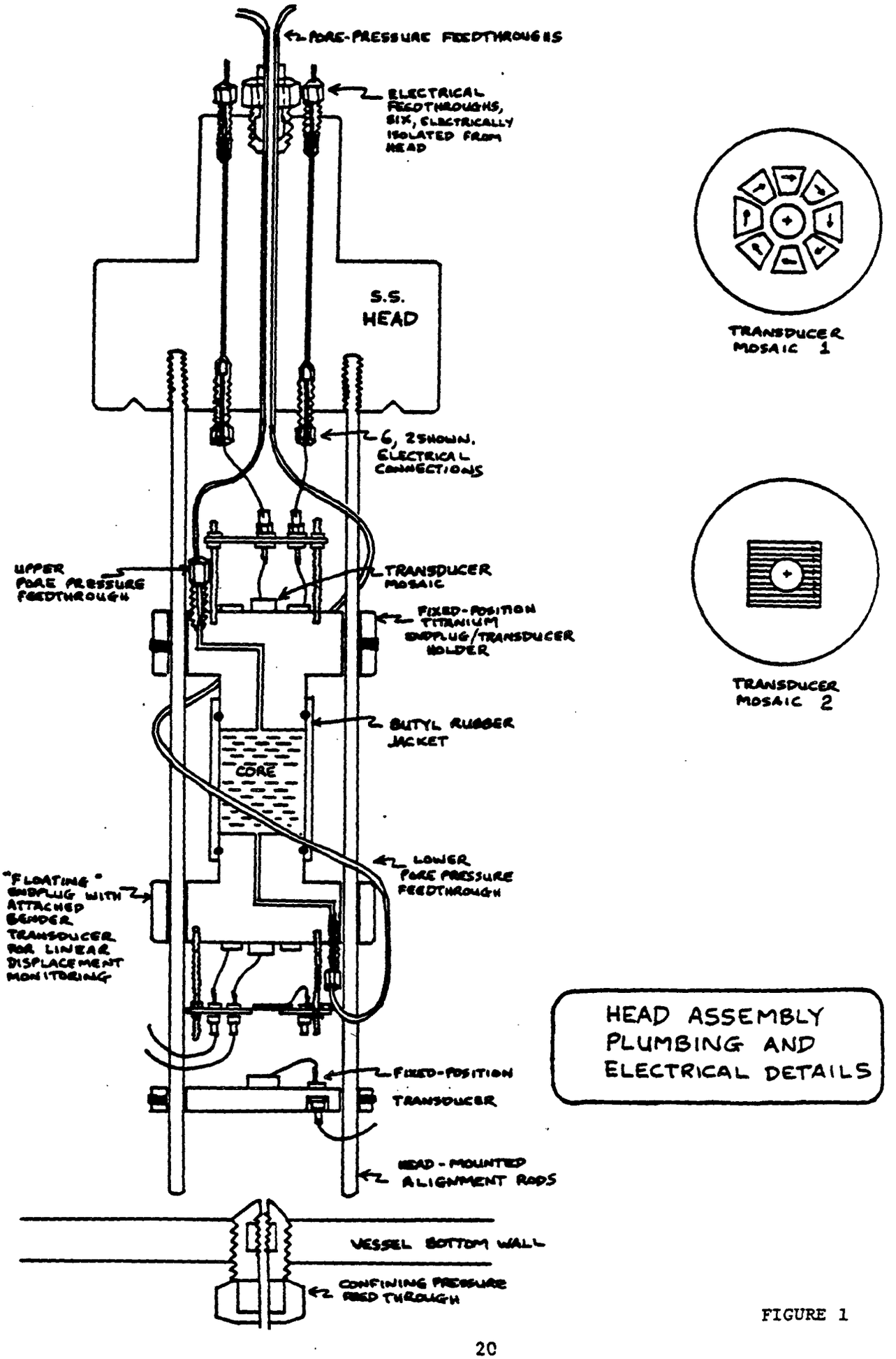

HEAD ASSEMBLY PLUMBING AND ELECTRICAL DETAILS

FIGURE 1

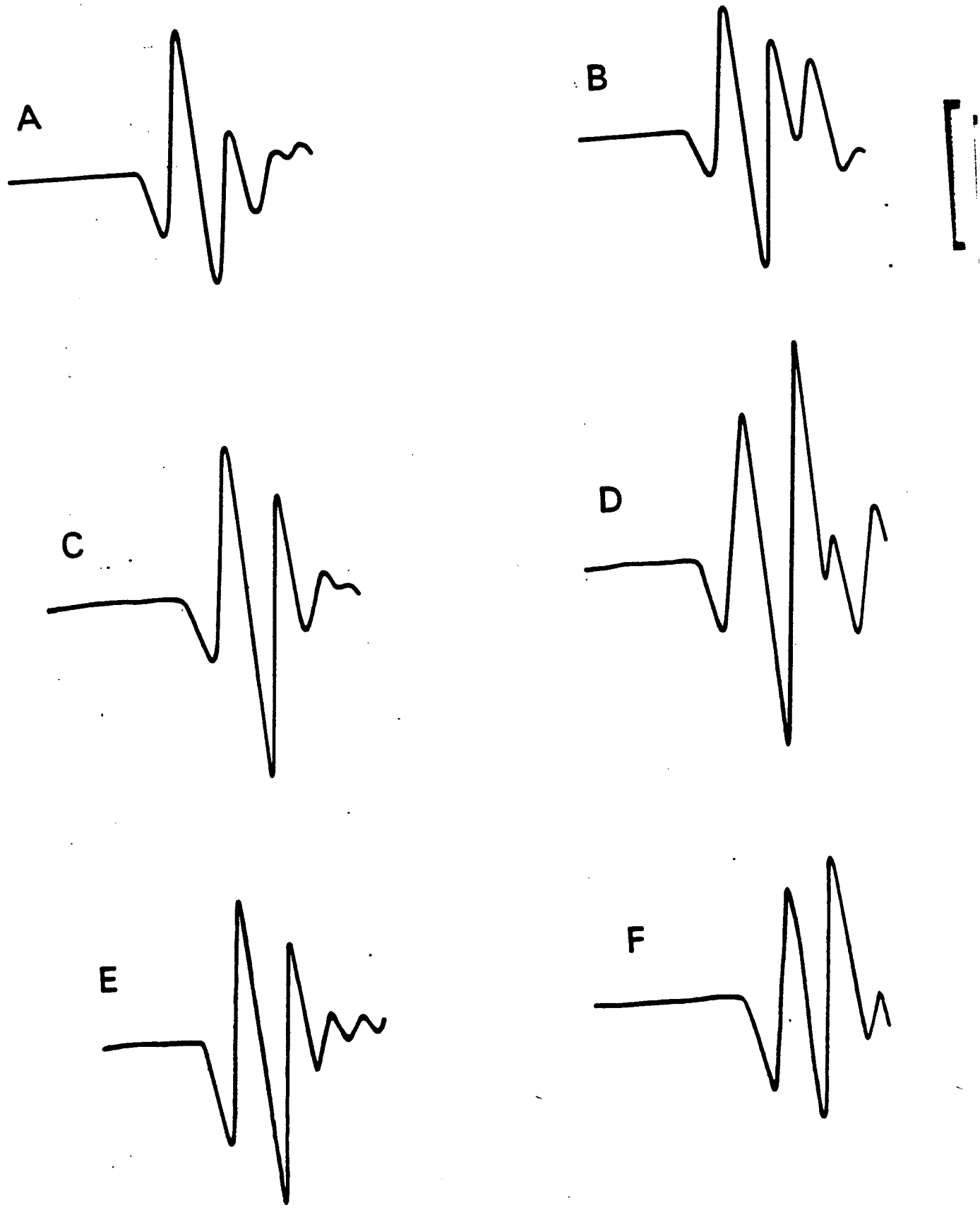

FIGURE 2

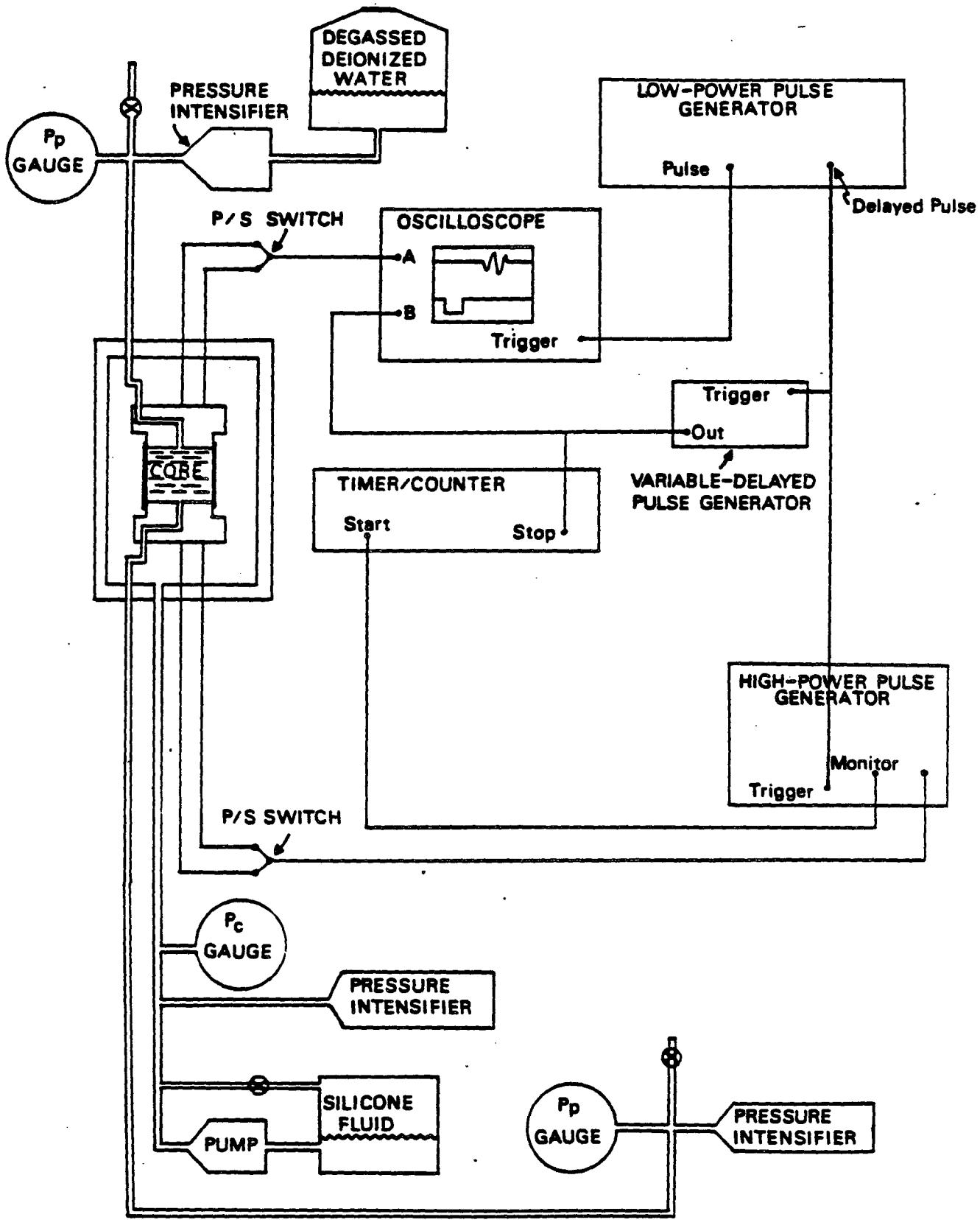

Pulse-Transmission Apparatus

FIGURE 3

LIST OF ELECTRONIC COMPONENTS

1. Lead - Zirconium - Titanate transducer (PZT-5A), Valpey-Fisher, Inc.

2. Hewlett-Packard Model 110 low-power pulse generator

3. Velonex Model high-power pulse and burst generator

4. Racal-Dana Model Timer/Counter

5. Hewlett-Packard Model pre-amplifier

6. Tektronix Model 565 dual-channel, dual-beam oscilloscope

FIGURE 4

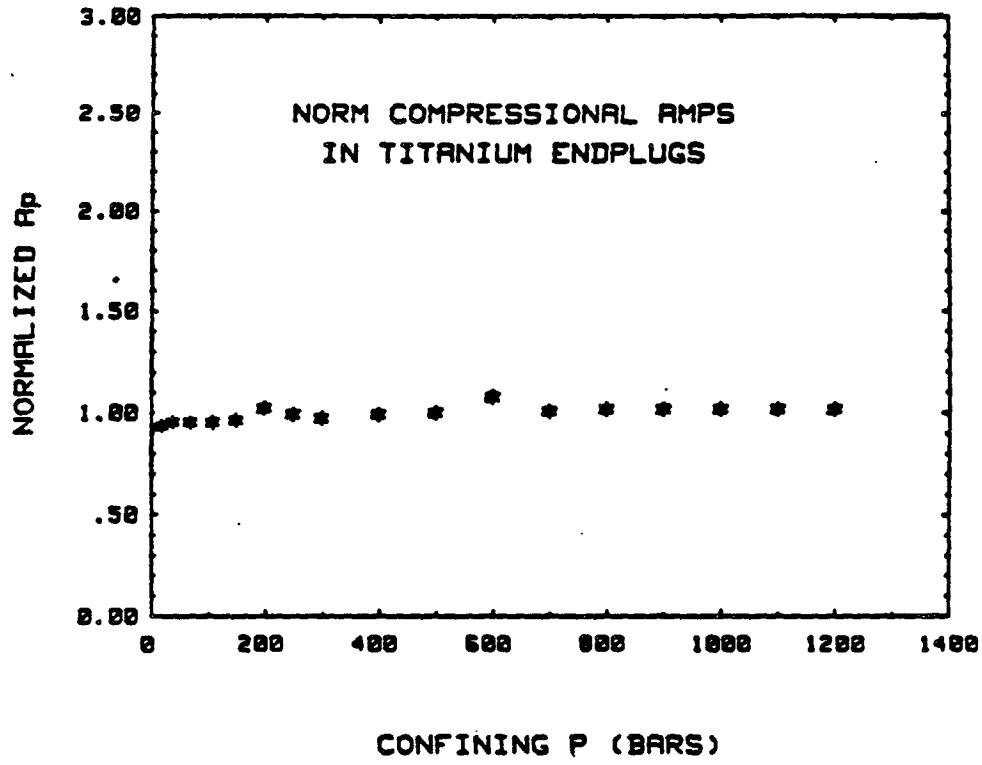
NORM COMPRESSIONAL AMPS
IN TITANIUM ENDPLUGS
NORMALIZED Ap
3.00
2.50
2.00
1.50
1.00
.50
0.00
0
200
400
600
800
1000
1200
1400
CONFINING P (BARS)

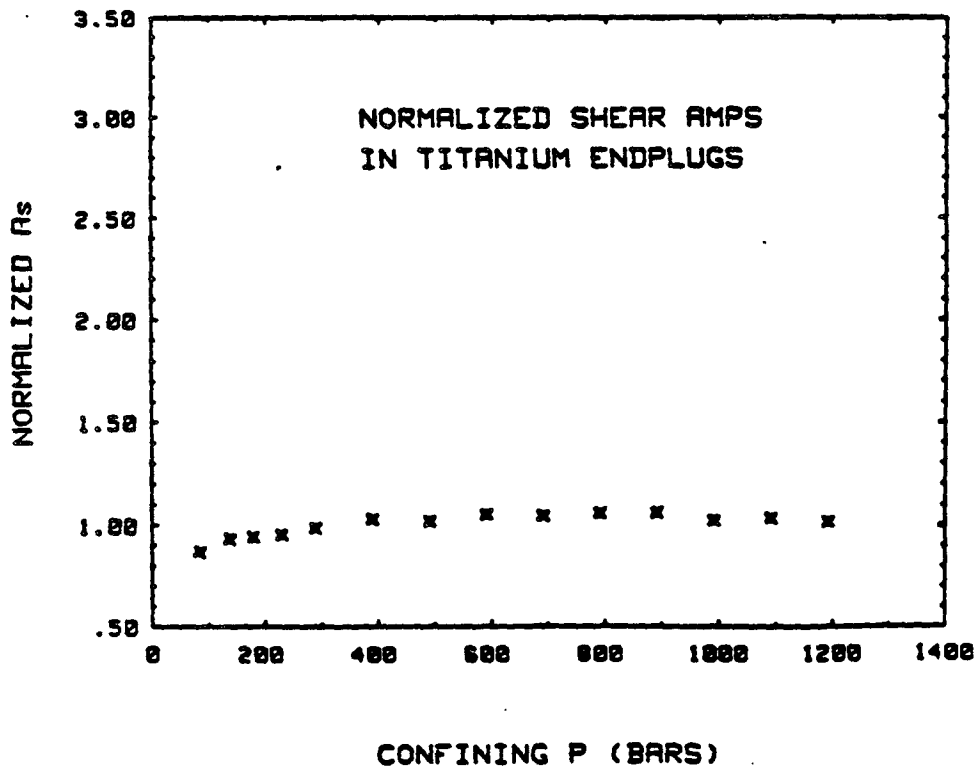
NORMALIZED SHEAR AMPS
IN TITANIUM ENDPLUGS
NORMALIZED As
3.50
3.00
2.50
2.00
1.50
1.00
.50
0
200
400
600
800
1000
1200
1400
CONFINING P (BARS)

FIGURE 5

III. ACOUSTIC IDENTIFICATION AND DETECTION OF ABNORMAL PORE PRESSURES IN SHALE LITHOLOGIES

Presented at the 51st Annual International SEG Meeting October 14, 1981
Submitted to Geophysics, May 1982

ACOUSTIC IDENTIFICATION AND DETECTION OF ABNORMAL PORE PRESSURES IN SHALE LITHOLOGIES

ABSTRACT

Results of an experimental investigation of Pierre Shale, Cotton Valley silty shale, and Berea sandstone at ultrasonic frequencies indicate that compressional and shear velocities together with P and S wave zero-to-peak, first arrival amplitudes are potentially powerful exploration tools not only for the purpose of distinguishing shales from other lithologies, but, equally importantly, for predicting pore pressures in shales.

Velocities alone cannot distinguish silty shales from sandstones. In order to make this distinction, velocity data must be augmented by information about porosity or clay content. However, shales with clay-to-quartz ratios $\geq$ 1:1 and porosities > 10% are readily distinguished from other indurated rock types by their characteristically low velocities.

Velocities in all samples were found to be sensitive to differential pressure but relatively insensitive to pore pressure. Unless velocities can be determined to better than ±1%, the prediction of pore pressures at depth from measured velocities alone is not feasible.

Variations with depth of the transmitted zero-to-peak, first arrival P-wave amplitude, $\left.\frac{\partial A_p}{\partial P_c}\right|_{P_p}$, along with the ratio of P:S amplitudes, $\left.\frac{\partial A_p/A_s}{\partial P_c}\right|_{P_p}$, were found to be the most sensitive acoustic parameters for the delineation of pore pressures in shaly rocks.

Data are presented on pore-volume compressibility plotted against differential pressure for Cotton Valley silty shale and Berea sandstone. At a constant pore pressure of 10 bars, the shale experienced an 18%

reduction in pore volume over a range of differential pressure from 0 to 1160 bars. The pore volume of the sandstone was reduced by 3% under the same pressure conditions.

Velocities and first-arrival amplitudes were measured in jacketed cores under conditions of separately controlled pore pressure and confining pressure. Confining pressure was varied to 1160 bars for pore pressures of 10 bars and 400 bars in order to simulate conditions of abnormally low and abnormally high fluid pressures.

INTRODUCTION

The occurrence of low-permeability, abnormally pressured shales and silty shales in association with sandstone petroleum reservoirs points to the need for exploration tools capable of locating shaly horizons and predicting the pore pressures in those horizons from seismic surveys.

The relationship between low hydraulic permeabilities perpendicular to fissility through shales and the occurrence of abnormal formation pressures is well documented, e.g., Hottmann and Johnson (1965), Magara (1971, 1976), Smith (1973), Gardner, et al., (1974), and Bradley (1975).

Regions of abnormally high fluid pressures in shales are frequently associated with conditions of lithologic undercompaction, abnormally low formation densities, and abnormally high porosities (Rubey and Hubbert (1959), Bishop (1979), Smith (1971), Stuart (1970), and Lewis and Rose (1970)). Indeed, current field techniques for the detection of abnormally high pore pressures in shales, such as those presented by Fertl and Timko (1970) and Hottmann and Johnson (1965), depend on this assumption of undercompaction.

However, this diagnostic criterion of undercompaction is not always valid. Bradley (1979) and Carstens and Dypvik (1980) report on the occurrence of abnormal pore pressures in normally compacted shales. Since the results of this paper demonstrate that P and S velocities show only a weak dependence on pore pressure, it follows that if formation porosity and density are normal, then present techniques for the seismic detection of abnormal pore pressures in these shaly units will be ineffective.

We present results of an ultrasonic frequency experiment that utilizes transmitted zero-to-peak, first-arrival P- and S-wave amplitude trends with depth as measurements of pore pressures in shales. The first matter at hand is to demonstrate that although velocities can reliably identify shale lithologies in which the clay-to-quartz ratio is > 1:1, velocities can neither distinguish a silty shale from a sandstone nor predict pore pressures in shales and silty shales. Next, it must be demonstrated that trends in the P-amplitude data (Figures 11,12) represent measures of attenuation and are not geometric effects due to scattering, diffraction, or reflection from surfaces and regions within the sample cores, the transducer holders, or the sample/endplug interfaces. Then, a mechanism capable of producing the observed amplitude trends will be proposed, the mechanism will be qualitatively corroborated by the results of an independent permeability experiment; and, finally, the implications of these results in terms of a pore-pressure sensitive exploration tool will be discussed.

SAMPLES AND SAMPLE PREPARATION

The vast majority of well-crystallized clays in shales are mixed-layer clays consisting of alternating layers of illite and chlorite or illite and montmorillonite (Blatt et al., 1972). Based on several thousands of analyses of sediments in the United States $\leq$ 600 million years old, Weaver (1967) concluded that more than half the clays, 57%, are illite, 24% are montmorillonite (expandable), 12% are kaolinite, and 7% are chlorite. Furthermore, the ratio of illite to montmonillonite and kaolinite was found to increase with age with a marked increase in illite in pre-Pennsylvanian rocks.

The two shales selected for this velocity and relative-attentuation study, Pierre shale and Cotton Valley silty shale, typify two dominate mineralogical categories of shales as summarized in Figure 1 and Table 1a. Both were collected from Cretaceous shale formations associated with known petroleum reservoirs. Interestingly, although quartz and feldspar constitute significant volume fractions of these shale mineralogies, clay grains dominate the textures of these rocks by completely encapsulating the quartz and feldspar grains, as is clearly visible in the scanning-electron-microscope (SEM) and thin-section photomicrographs of Figure 2 and Figure 3. The 57% volumetric clay fraction in highly fissile, homogeneous Pierre shale, recovered from a depth of 5,000 feet in the Williston Basin, is dominated by mixed-layer illite-montmorillonite with small amounts of kaolinite and chlorite (Table 1a). Its microtexture is controlled by the extreme anisotropy resulting from preferred orientation of clay platelets parallel to bedding (Figure 2). Pore shapes and distributions are also controlled by the alignment of clay grains. Average grain and pore

thicknesses measured perpendicular to bedding are $\leq .3\mu$. No feature perpendicular to bedding was observed by SEM to be $> 10\mu$.

The 36% volumetric clay fraction of the homogeneous Cotton Valley silty shale, recovered from a depth of 9,629 feet in eastern Texas, is principally illite with minor chlorite and kaolinite. Average grain and pore thicknesses measured perpendicular to bedding are $\leq 2\mu$, with all observed features $< 20\mu$. Parallel to foliation, the Cotton Valley shale reveals occasional concentrations of eryanite, euhedral potassium-silicate zeolite prisms, secondary mineralizations indicative of hydrothermal alteration.

For purposes of lithologic and textural comparison, Berea sandstone was selected as the third sample. Figures 1 - 3 and Tables 1 - 2 reveal the characteristic texture and bulk mineralogy of the sandstone in contrast to the mineralogies and textures of the shales.

Sample dimensions of the cores were small (2.5 cm diameter, 1.4 cm length) in order to minimize pore-pressure equilibration times throughout the shales. In addition, the maximum length of the Pierre sample was limited by its high fissility. All cores were cut to the length of the Pierre sample to allow direct comparisons of the transmitted - amplitude data.

All cores were cut with the cylindrical axis perpendicular to bedding; thus, wave incidence was always normal to bedding. The ends of all cores were flat and parallel to within $\pm$ .0005 in.

Pore fluid in the Pierre shale was connate brine. Pore fluid in the Cotton Valley and Berea samples was deionized water. Water and brine permeabilities normal to bedding in the shales were found to be nearly nonexistent: a pore pressure gradient of 20 bars applied across a saturated

core of Pierre shale at Pc - Pp = 10 bars did not fully decay to uniform pressure within 2 weeks. Axial holes .75 mm in diameter drilled through the shales allowed us to take advantage of significantly higher permeabilities parallel to bedding.

All cores were jacketed with sections of flexible butyl rubber tubing. The confining medium was Dow Corning fluid of 50 centistokes viscosity.

EXPERIMENT

Travel times and transmitted amplitudes through the cores are measured by a pulse-transmission technique (e.g., Birch, 1961). A piezoelectric ceramic, lead-zirconium-titanate, is the material used to generate compressional and torsional signals for both driving and receiving transducers. The transducer arrays and the transducer/endplug/sample geometry are described in Tosaya (1982). The transducers are affixed to titanium endplugs with a thin film of silver-conductive epoxy.

Optimal pulse-source frequencies were calculated to minimize scattering of the transmitted pulse and to maximize definition of the first arrival.

Pulse Generator: Voltage onput is in the form of rectangular pulses (rise time 7 ns), 5 μs pulse width, 60 repetitions per second, 500 volts amplitude at 10 amps.

Pulses in Samples: Compressional pulses received from the sample to the receiver-transducer endplug measure 2.3 - 4.8 mm per cycle; torsional pulses measure 2.2 - 5.0 mm per cycle, corresponding to P and S peak frequencies of 1.0 MHz and .6 MHz, respectively.

In order to minimize wave dispersion, the ratio of the sample diameter to the pulse wavelength, $d:\lambda$, should be greater than 5. P- and S-wave $d:\lambda$ ratios are a minimum of 5.3 and 5.1, respectively. To assure that the measured velocity is characteristic of the whole sample rather than a few singularities, the ratio of the travel distance through the sample to the length of the wavepath through any inhomogeneity, $L = \ell$, must be greater than 10. Our samples contain no inhomogeneities larger than the scale of the grain and the pore sizes.

Scattering effects and waveform distortion are minimized for ratios of wavelength-to-pore diameter and wavelength-to-grain diameter greater than 3 (Plona and Tsang, 1979). This parameter for the Pierre, Cotton Valley, and Berea samples is at least 1.5×10^3, 7.8×10^2, and 5.0×10^1, respectively. The length-to-diameter ratio, L:d, for each sample is less than 5; thus, first-arrival amplitudes are not diminished by sidewall reflections of wave energy. Planarity of the wavefront is checked by varying the lengths of samples by +100% and -30% to note any velocity dispersions with varying length.

Pore pressure and confining pressure were separately controlled. Confining pressure was varied to 1200 bars for pore pressures of 10 bars and 400 bars. These pore pressures were selected to simulate conditions of abnormally low and abnormally high pore pressure in the Pierre sample. In situ normal pore pressures are 160 and 310 bars for Pierre shale and Cotton Valley shale, respectively.

The Pierre sample was preserved at the well site to retain connate brine. The Cotton Valley and Berea samples were initially room dry. All samples were evacuated then fully saturated before jacketing at 200 bars pressure with deionized water. The Pierre shale was evaculated for two minutes, then resaturated at 200 bars with deionized water to assure full saturation.

As a result of the low permeabilities of the Pierre and the Cotton Valley samples, pore pressure took up to 2.5 weeks to equilibrate at high differential pressures. Pore-pressure equilibration was monitored by two independent means: a halt in the rise of gauge pressure and a cessation in the increase of velocities with time.

Velocities were straightforwardly calculated from travel times and sample lengths. Changes in sample length under differential pressure were monitored with an axial-displacement transducer configuration.

Transmitted amplitudes were corrected for two effects: (1) changes in transmission coefficients at the two sample endplug interfaces due to changes in acoustic impedance with increasing differential pressure and (2) changes in endplug-to-sample coupling with increasing differential pressure. Tosaya (1982a) contains a discussion of transmission coefficient corrections for normal wave incidence, as well as calibration curves for endplug-to-sample coupling coefficients.

RESULTS AND DISCUSSION I: VELOCITIES

P and S velocities measured in Pierre shale, Cotton Valley silty shale, and Berea sandstone are presented in Figures 4 - 6. Measurements were made at room temperature with confining pressure varied to 1160 bars for the following pore-fluid conditions: (1) vacuum dry; (2) fully saturated, low pore pressure (10 bars); and (3) saturated, high pore pressure (400 bars). Velocities could be determined to within 2%.

Examination of Figure 8 reveals that the shapes of the velocity curves for Pierre and Cotton Valley differ fundamentally from those of three sandstones: St. Peter, Bandera, and Berea. The sandstone curves flatten with increasing confining pressure; indeed, St. Peter shows a zero slope above 400 bars. In contrast, the velocity profiles of the shales continue with high positive slopes to 1160 bars, the maximum confining pressure attainable with our apparatus. Jones and Wang (1981) demonstrate that velocities in undrained samples of Pierre shale show a strong linear response to confining pressures up to 4 kilobars.

The contrasting velocity responses of sandstones and shales to increasing confining pressures, $\left.\frac{\partial V_{p,s}}{\partial P_c}\right|_{P_p}$, is due in part to variations of frame compliance with lithologic type, resulting from contrasts in induration, assuming that pore-fluid compressibility is constant for all samples. Examination of Figure 2 reveals the textural detail of shales and sandstones. The St. Peter sandstone is characterized by well cemented, well rounded, well sorted quartz grains and by pores with aspect ratios close to 1. At the opposite textural extreme is Pierre shale, characterized by a high degree of preferred orientation of low aspect-ratio pores and grains (10^{-2} - 10^{-4}). Clay is the cement in this rock.

Induration in sandstones is marked by intergranular cementation, generally by quartz or calcite, and stiff saw-toothed pressure-solution contacts. Induration in shales, however, consists principally of cohesion both between clay grains and between sheet-silicate layers within individual clay grains arising from van der Waals attraction, cation linkages, hydrogen bonds, and other mechanisms (Mitchell, 1960). These weak, electrical interlayer bonds (Figure 14) present little layer-parallel shearing resistance.

Velocity response to increasing confining pressure may be due to variations in frame compliance resulting from contrasts in distributions of grain-contact geometries as well as to differences resulting from contrasts in induration type. The schematic grain contact of Figure 9a, in which the contact radius, a, is much smaller than the mean grain radius, R, such that $\frac{a}{R} << 1$, is highly compressible compared to a grain contact characterized by $\frac{a}{R} \approx 1$, as shown in Figure 9b.

Applying these observations of grain/pore shapes and frame compliances to the shapes of the velocity curves (Figure 8), we see that after initial closure of low aspect-ratio cracks and pores at low confining pressures, St. Peter sandstone becomes incompressible above 400 bars confining pressure. Dynamic bulk compressibility is related to the measured velocities by the relation $\beta = (\rho(V_p^2 - \frac{4}{3}V_s^2))^{-1}$ in the direction of isotropy. Framework and intergranular contact geometries are invariant with pressure until the fracture strength of the rock is reached.

The relatively high slopes of the shale velocity curves (Figures 4, 5, and 8) reflect continuous closure of pores and cracks with pressure as well as increased alignment of clay grains in the plane of low shear resistance. The result is increased development of the degree of preferred orientation

of clay grains with increasing differential pressure (P_c-P_p). The implication of this analysis is significant: physical and acoustical anisotropy of shales should increase with depth or differential pressure until the intrinisic anisotropy of the statistically weighted volume fraction of the dominant clay mineral is reached. The clays in the Pierre and the Cotton Valley samples are dominantly illitic in structure (Figure 9). Data are not available for the intrinsic elastic anisotropy of illite. However, the crystallographic structure of illite is similar to that of muscovite. Computed from directional compressional velocities in Simmons and Wang (1971), muscovite yields an anisotropy of $\frac{V_{p33}-V_{p11}}{V_{p33}}$ = 80%, where V_{p33} and V_{p11} are the compressional velocities measured normal to layering and in the plane of layering, respectively. Jones and Wang (1982) found that the velocity anisotropy of Pierre shale recovered from a depth of 5000 feet in the Williston Basin was higher than the anisotropy of a sample recovered from a depth of 3000 feet. Kaarsberg (1959) found that anisotropy increased with compaction in natural and artificial argillaceous aggregates. Tosaya (1982b) determined experimentally that the acoustical anisotropy of saturated Cotton Valley shale increases with increasing differential pressure.

The ultrasonic velocity data for Pierre shale, presented in Figure 4, show that the velocity differences between the low pore pressure and high pore pressure curves decrease from 13% to 1% through the range of confining pressure increase from 460 to 1160 bars. An estimated velocity curve for normal <u>in situ</u> pore pressure is included with measured data in Figures 4 and 5. Within the errors of seismic exploration data, it is evident that velocities alone are poor predictors of pore pressure in shales at moderate or high differential pressures.

The "DRY" curves in Figures 4 and 5 were obtained from cores of Pierre and Cotton Valley that were dried for 2 months at 760 mm Hg vacuum, 50°C. During velocity measurements, the pore pressure line was open to atmosphere of relative humidity 35% to 60%.

As shown in Figure 7, to a first approximation velocity is simply a function of differential pressure. Thus, the effective pressure may be expressed roughly by $P_{eff} = P_c - \alpha P_p$, with $\alpha = 1$ (Nur and Byerlee, 1971; Hubbert and Rubey, 1959). The deviations in this expression are well within the errors of field exploration techniques, but indicate that effective pressure in shales is actually related to pore pressure in a more complicated manner which may be related to the structure of water in and on the clays with increasing pore pressure.

As demonstrated in Figure 10 and supported by the results of Tosaya and Nur (1982), velocity data supplemented by information about either clay content or porosity comprise a powerful tool for distinguishing shale lithologies from other rock types. Velocity data alone cannot reliably distinguish shales from other lithologies: Cotton Valley shale is indistinguishable from sandstones on the basis of its measured velocities.

RESULTS AND DISCUSSION II: PORE-VOLUME COMPRESSIBILITY

The reduction in pore volume with increasing confining pressure and low, constant pore pressure (50 bars) is shown in Figure 10 for Berea sandstone and Cotton Valley silty shale. Pore volumes are measurable to ± .0042 cc. Both rocks experience a drop in porosity, $\phi_f - \phi_i$, of .75% with increasing confining pressure to 1160 bars. The initial porosity of the Berea sample at room temperature and pressure was 18.22%. Thus, the percentage of initial porosity lost by Berea, $\frac{\phi_f - \phi_i}{\phi_i}$, is 3.57%. However, the Cotton Valley sample had an intial porosity of only 4.20%, and, therefore, experienced an 18.33% pore-volume reduction.

RESULTS AND DISCUSSION III: ZERO-TO-PEAK AMPLITUDES OF P AND S FIRST ARRIVALS AS MEASURES OF PORE PRESSURE AND ATTENUATION

Normalized first-arrival P-wave amplitudes plotted against confining pressure for all samples are presented in Figures 12a,b,c. All amplitudes have been corrected for contrasts in acoustic impedance between the sample and endplugs and for endplug coupling effects (Tosaya, 1982a). Voltage, pulse width, and repetition rate of the input signal were held constant for all measurements.

Figure 12a is a plot of the normalized, transmitted P-wave amplitude, $\frac{\partial A_p}{\partial P_c}\Big|_{P_p}$, for three separate runs of Pierre shale. The trends in the dry and the high pore-pressure runs are similar to each other but significantly different from the low pore-pressure curve. Since the received amplitude is inversely related to attenuation through the sample, there is evidently a fundamental difference in the Q response of a shale under conditions of full brine saturation at low pore pressure compared to conditions of either vacuum dryness or full brine saturation at high pore pressure.

DRY: The degree of dryness of a shale is complicated by the water-sorption properties (absorption and adsorption) of constituent clay minerals. Consideration must be directed to clay chemistry, fluid chemistry, clay size distribution, high specific surface area, and fluid permeability through indurated shales as a function of these physical and chemical parameters. Our samples were dried for 2 months at 760 mm Hg vacuum, 40°C. The degree of core dryness was monitored by change in weight with time. At the end of the drying period, the Cotton Valley sample showed no weight loss with time, measured in units of .01 gram/week. The Pierre sample was still losing a small amount of water at the end of 2 months, evidenced by a .01 gram/week drop during the final week.

The geometry of the pore network in shales is dictated by the high degree of preferred orientation of the sheet silicate minerals, a causal relationship that is clearly visible in the SEM photos of Figure 2a,b and the data of Table 2.

Due primarily to clay/fluid chemical interactions and to the low permeabilities characteristic of shales, it is possible that a metastable layer of hydroxyl and metal-cation surface adsorbates remains on the surfaces of the clay grains in our "dry" cores, as depicted in Figure 14. It is even more likely that adsorbates with a high degree of crystallographic ordering remain electrochemically bound to the clays in the tightly constricted grain contact regions. The existence of these grain-contact adsorbates provides a viable mechanism for the observed strong dependence of P amplitude on confining pressure in dry detrital rocks (Figure 12a,b,c). As an oscillatory wave disturbance passes through the grain-contact region, wave energy is dissipated due to the work that goes into breaking surface-adsorbate bonds. This mechanism for energy loss was first described and tested by Spencer (1981) and is depicted in Figure 14a.

Frictional dissipation may also be responsible, wholly or in part, for the observed amplitude attenuation behavior. This mechanism has been treated extensively in the literature. Johnston, et al., (1979) comprehensively review the contributions to this subject.

In addition, it is possible, although not likely, that water "pendants" remain in grain-contact regions of the "dry" shales due to extremely low permeabilities and high capillary pressures, as shown in Figure 14b. As the volume of water in the contact region is reduced by heat and evacuation, the radius of curvature of the water-pendant/vapor

interface, R, is reduced, thus increasing the capillary pressure, P, since P is related to R by the expression $P = \gamma_{LV}/R$, where γ_{LV} is the surface tension of the liquid/vapor interface. In this case, energy is dissipated as the wave disturbance passes through the contact region due to spatial displacements of the water pendant, a mechanism detailed by Mavko and Nur (1979) and Palmer and Traviolia (1980).

There is an observed decrease in amplitude attenuation with pressure in dry rocks (Figure 12a,b,c), due primarily to stiffening of grain contacts with increasing confining pressure. Applying the Mavko model of tapered-crack compressibility (1978) to pore closure in shales (Figure 14c), we see that a pore described by the function $y = b\left[1-\left(\frac{x}{c}\right)^2\right]^m$, where $m > \frac{1}{2}$, b is a constant, and c is half the semi-major axis, begins to close quickly with the application of low confining pressure and then stiffens with increasing confining pressure. The result is attenuation behavior that is nonlinear with confining pressure, as is seen in the progressive change in slope in the dry curves of Figure 12a,b to 500 bars. At confining pressures greater than 500 bars the shale curves become linear, an effect perhaps due to deformation of the clay grains and intergranular contacts.

LOW PORE PRESSURE: Under conditions of full brine saturation at low constant pore pressure, the transmitted P-wave amplitude through Pierre shale shows no dependence on confining pressure (Figure 12a). Although this effect has not been observed before, it is highly plausible in light of the complex nature of clay-brine interactions.

Consider a physiochemical clay-brine interaction involving absorption and adsorption of metal cations and hydroxyl anions. If the shale is fully brine saturated, not only are all clay surfaces wetted, but

montmorillonitic and mixed-layer illitic-montmorillonitic clays can swell to the limits of the available pore space by accommodating several layers of ordered water molecules between each pair of structural gibbsite sheets (Figure 15a,b) (Lambe and Whitman, 1969). Under these conditions, the shale does not consist of two distinct phases, clay and pore fluid, but, rather, becomes a single, continuous, water-clay phase with mechanical properties similar to those of a gel: the material can sustain shear stresses but has approximately constant compressibility with increasing confining pressure (Figure 14a).

Since the slope of the low pore pressure P-amplitude curve for Pierre shale is not in qualitative agreement with the slope of the low pore pressure P-velocity curve (Figure 4), it is evident that the velocities and the first arrival P-wave amplitudes are sensitive to different bulk rock parameters. It is well-established that velocity depends on the real part of the elastic moduli, $V^2 \sim \frac{1}{Re}$, while the inverse of attenuation is related to the ratio of the real to the imaginary parts, $Q \sim \frac{Re}{Im}$ (Geertsma and Smit, 1961). In physical terms, velocities show a strong dependence on the internal structure of the granular framework, on the effects of fluids on the mechanical response of the granular framework, and on the mechanical properties of the bulk fluid (Brown and Korringa, 1976; Walsh and Grosenbaugh, 1979; Mavko and Nur, 1977, Gassman, 1950; Biot, 1956), but appear to be insensitive to electrochemical interactions between the granular framework and the pore fluid. First arrival P-wave amplitudes, however, display a strong dependence on the electrochemically determined spatial broadening of solid/liquid phase boundaries. This effect is seen to increase systematically with increasing clay content, as is demonstrated clearly in Figure 13 (refer to Tables 1 and 2 for clay contents and

specific surface areas). The slope of the normalized, first-arrival P amplitude with depth flattens with increasing clay content at low pore pressure. This effect is expected to be highly sensitive to the volume fraction of expandable clays (i.e., clay chemistry), to the chemistry of the fluid saturant, and to the specific surface area of the sample. The effect is not significant in rocks containing small amounts of nonexpandable clay: the P-amplitude curves for Berea andstone (Figure 12c) are qualitatively similar to the velocity curves of Figure 6.

When clay content is held constant, e.g., Figure 12a, we see that the angular dispersion between P-amplitude curves is a sensitive measure of pore pressure. This dispersion is maximized for high clay contents: the strong dispersion shown by Pierre shale (Figure 12a) appears weaker in Cotton Valley silty shale (Figure 12b) and is not present in Berea sandstone (Figure 12c).

With further examination of Figure 12a, we see that, in addition to the independence of the low pore pressure P-amplitude response in Pierre shale to confining pressure, the curve is consistently high relative to the high pore pressure and the dry curves, an effect that is contrary to the behavior observed in sandstones, e.g., Figure 12c (Johnston, et al., 1979). Since transmitted first-arrival amplitudes are inversely related to attenuation through the sample, the high amplitude response of Pierre shale at low pore pressure corresponds to a high value of Q (low attenuation) relative to the dry and the high pore pressure runs. This observation follows logically from an argument of acoustic-impedance contrasts. The density and the acoustic impedance (ρV) of water-swelled clays are higher than those of either air or water and thus provide a lower impedance contrast with the quartzitic and feldspathic components of the rock frame

(Figure 3). In a shale such as the Pierre sample used in these experiments, with 14% average porosity and 57% expandable illite-montmonillonite by volume, the impedance consideration is significant, and may account for the relatively high P-wave amplitude of the low pore-pressure run.

HIGH PORE PRESSURE: Under conditions of full brine saturation at high pore pressures, P-wave amplitude attenuation through Pierre shale behaves in a similar manner to the dry shale, showing a strong dependence on confining pressure and relatively high attenuation at low confining pressures. Further discussion of the nature of clay-water interactions provides a plausible explanation for the observed behavior. Specifically, we need to address the process by which high-impedance, watered clays at low pore pressures become low-impedance, watered clays at high pore pressures.

As discussed in Mitchell (1960), components of total pressure in fluid-saturated clays include not only lithostatic and hydrostatic pressures but also physiochemical components, principally osmotic pressure and adsorption pressure. While there are presently no means to quantify the pore-pressure contributions from each of these components, several fundamental concepts concerning the nature of interactive clay-water behavior emerge when considered on a purely qualitative basis.

Osmotic pressure arises from spatial variations in ionic concentrations approximated for dilute solutions by the Van't Hoff equation

$$\pi = RT(\Sigma c_2 - \Sigma c_1) \quad ,$$

where R = universal gas constant, T = absolute temperature, and Σc_1 and Σc_2 = sums of concentrations of ionic constituents at points 1 and 2. This equation assumes that ionic force fields do not interact — an oversimplification for all but dilute solutions.

Adsorption pressure arises from the attractive interaction of water molecules with clay surfaces. A net electrical charge on clay particles results from vacancies and unbalanced ionic substitutions in the crystal structure and from the adorsption potential associated with unsatisfied electrochemical bonds at the free surfaces. Charges on the particles are balanced by counter ions in the surrounding solution. the concentration of counter ions dimishes with increasing distance from the particle surface. This counter-charged field, known as the electrical double layer, is composed of two parts. The inner layer, referred to as the compact or the Stern layer, consists of 1-2 molecular layers (10-30 Å) of relatively immobile, rigidly held ions. The outer layer, known as the diffuse part of the doubler layer, contains relatively mobile, weakly bound ions. The extent of the double layer is affected by the density of charge on the surface of the clay particle, valency of the ions, concentration of the electrolytic solution, the dielectric properties of the medium, and temperature. Short-range (< 40 Å) adsorptive force-field effects include local ionic interactions, hydrogen bonds, and van der Waals forces. Long-range (> 40 Å) forces are comprised of interactions of water dipoles with the electrostatic field originating in the charged clay surface. Long-range forces may be approximated by means of theories of the electrical double layer such as those of Gouy-Chapman, Helmholtz, Stern, and Donnan (e.g., Lambe and Whitman, 1969). Adequate theories describing short-range forces have not yet been developed.

An additional pressure component not accounted for by existing effective-stress theories may exist due to the very small interparticle spacings characteristic of shales. The structured water adsorbed onto surfaces of these small, very thin pores (1 - 40 Å openings) is known to differ in physical properties from bulk liquid water to distances of at least 10 Å (Martin, 1960; Van Olphen, 1977; Gillott, 1968).

These interactive forces that are known to exist between clay particles undoubtedly exert some influence on local fluid-phase pressures. Our experimental results suggest that, as pore pressure increases, the water absorption-adsorption properties of the hyper-expanded illitic and montmorillonitic clays may be modified (Figure 16). At low pore pressures the Stern layer evidently dominates the attenuation properties of the saturated shale. However, at high pore pressures the relatively strong relationship between amplitude attenuation and confining pressure suggests the presence of either a free-water phase in the pores or, more likely, modification of the doubler layer by increasing pore pressure such that the diffuse outer layer becomes an important factor in the attenuation behavior. It appears that the water-expanded clays become slightly compressed by increasing pore pressure perhaps by reduction of interparticle Stern-layer thicknesses and/or by compaction or expulsion of intraparticle, interlayer water molecules. Since the diffuse part of the double layer is likely to behave mechanically in a manner that is more similar to free pore water than to the rigidly held Stern layer, the result of increasing pore pressure is apparently to transform the single-phase clay-water shale into a two-phase clay-water system. With respect to the impedance contrast against the nonexpandable-mineral fraction of the rock frame, this higher impedance-contrast two-phase clay system is now similar to the two-phase

air and dry-clay system of the dry shale in terms of its bulk mechanical response.

Independent corroboration of this hypothesis is obtained from Nur, et al., (1980). The results of their permeability measurements in clay-bearing sandstones demonstrate that effective permeability in brine-saturated sandstones increases with increasing pore pressure (Figure 17). This increase in permeability is strongly a function of clay content, with clay-free St. Peter Sandstone showing no effect.

Shear-wave amplitude data from these samples are not as informative as compressional-wave data. However, the ratio of P-to-S amplitudes $\frac{\partial(A_p/A_s)}{\partial P_c}\Big|_{P_p}$ (Figure 18a,b,c), can be used in the same manner as the P-amplitude curves to yield information on pore pressure and clay content in rocks.

CONCLUSIONS

The velocity data of Figures 4 and 5 are of limited value in determining the pore pressures of shale formations at depth that are well indurated in light of the degree of accuracy of current seismic exploration techniques. The precision of sonic-logging and vertical seismic-profiling methods may be adequate, but since both are downhole techniques, the prognostic value of determining pore pressures before drilling is lost. It must be noted that the pressure dependence of velocities in shales that are significantly undercompacted may greatly enhance the value of velocity measurements in determining pore pressures in shales.

P- and S-wave velocities cannot unambiguously distinguish silty shales from sandstones (Figure 8) unless information about either porosity or total clay content by volume is available (Figure 9, Tosaya and Nur, 1982). However, our results suggest that P- and S-wave velocities coupled with information about the manner in which the first-arrival P-wave amplitudes and P:S amplitude ratios vary with depth should yield data on clay content and pore pressure in subsurface shaly lithologies. If the lithologic composition is known, then P-amplitude and P:S amplitude-ratio variations with depth should unambiguously determine the fluid pressure in clay-rich rocks. The use of slopes of curves, $\left.\frac{\partial A_p}{\partial P_c}\right|_{P_p}$ and $\left.\frac{\partial (A_p/A_s)}{\partial P_c}\right|_{P_p}$, and angular divergence between curves rather than absolute amplitudes eliminates scaling problems.

REFERENCES

Aylmore, L.A.G., and Quirk, J.P., 1960, The structural status of clay systems, in Swineford, ed., Clays and Clay Minerals, Vol. 9, p. 104-130.

Biot, M.A., 1956, Theory of propagation of elastic waves in fluid-saturated porous solid: Parts I and II: J. Acousti. Soc. Am., Vol. 28, p. 168-191.

_____, 1955, Theory of elasticity and consolidation for a porous anisotropic solid: J. Appl. Phys., Vol. 26, p. 182-185.

Birch, F., 1960, The velocity of compressional waves in rocks to 10 kilobars, Part 1: J. Geophys. Research, Vol. 65, p. 1083-1102.

Bishop, R.S., 1979, Calculated compaction states of thick abnormally pressured shales: Amer. Assoc. of Petroleum Geol. Bull., Vol. 63, p. 918-933.

Blatt, H., Middleton, G., and Murray, R., 1972, Origin of Sedimentary Rocks, Prentice-Hall, New Jersey, 634 pp.

Bradley, J.S., 1975, Abnormal formation pressure: Amer. Assoc. Petroleum Geol. Bull., Vol. 59, p. 957-973.

Brown, R.J.S., and Korringa, J., 1975, On the dependence of the elastic properties of a porous rock on the compressibility of the pore fluid: Geophysics, Vol. 40, p. 608-616.

Carstens, H., and Dypvik, H., 1981, Abnormal formation pressure and shale porosity: Amer. Assoc. Petroleum Geol. Bull., Vol. 65, p. 344-350.

Fertl, W.H., and Timko, D.J., 1970, Overpressured formations - II: Oil and Gas Jour., Vol. 68, p. 97-108.

Gardner, G.H.F., Gardner, L.W., and Gregory, A.R., 1974, Formation velocity and density - the diagnostic basics for stratigraphic traps: Geophysics, Vol. 39, p. 770-780.

Gassman, F., 1951, Elastic waves through a packing of spheres: Geophysics, Vol. 16, p. 673-685.

Gillott, J.E., 1968, Clay in Engineering Geology, Elsevier Publishing Co., Amerstdam, the Netherlands, 296 pp.

Hottmann, C.E., and Johnson, R.K., 1965, Estimation of formation pressures from log-derived shale properties: Jour. Petroleum Tech., Vol. 17, p. 717-722.

Hubbert, M.K., and Rubey, W.W., 1959, Role of fluid pressure in mechanics of overthrust faulting I: Geol. Soc. Amer. Bull., Vol. 70, p. 115-166.

Johnston, D.H., Toksoz, M.N., and Timur, A., 1979, Attenuation of seismic waves in dry and saturated rocks: II. Mechanisms: Geophysics, Vol. 44, p. 691-711.

Jones, L.E.A., and Wang, H.F., 1981, Ultrasonic velocities in Cretaceous shales from the Williston basin: Geophysics, Vol. 46, p. 288-297.

Kaarsberg, E.A., 1959, Introductory studies of natural and artificial argillaceous aggregates by sound-propagation and x-ray diffraction methods: J. Geol., Vol. 67, p. 447-472.

Lambe, T.W., and Whitman, R.V., 1969, Soil Mechanics, John Wiley and Sons, New York, 553 pp.

Lewis, C.R., and Rose, S.C., 1970, A theory relating high temperatures and overpressures: Jour. Petroleum Tech., Vol. 22, p. 11-16.

Magara, K., 1971, Permeability considerations in generation of abnormal pressures: Soc. Petroleum Engr. J., September, p. 236-242.

_____, 1976, Water expulsion from clastic sediments during compaction - direction and volumes: Amer. Assoc. Petroleum Geol. Bull., Vol. 60, p. 543-553.

Martin, R.T., 1960, Adsorbed water on clay: a review, in Swineford, ed., Clays and Clay Minerals, Vol. 9, p. 28-70.

Mavko, G.M., and Nur, A.M., (1979), Wave attenuation in partially saturated rocks: Geophysics, Vol. 44, p. 161-178.

_____, 1978, The effect of nonelliptical cracks on the compressibility of rocks: J. Geophys. Res., Vol. 83, p. 4459-4468.

Mitchell, J.K., 1960, Components of pore water pressure and their engineering significance, in Swineford, ed., Clays and Clay Minerals, Vol. 9, p. 162-184.

Nur, A., and Byerlee, J., 1971, An exact effective stress law for elastic deformation of rocks with fluids: J. Geophys. Research, Vol. 76.

Nur, A., Walls, J., Winkler, K., and DeVilbiss, J., 1980, Effects of fluid saturation on waves in porous rocks and relations to hydraulic permeability: Soc. Pet. Engr. Jour., December, p. 450-458.

Palmer, I.D., and Traviolia, M.L., 1980, Attenuation by squirt flow in under-saturated gas sands: Geophysics, Vol. 45, p. 1780-1792.

Plona, T.J., and Tsang, L., 1979, Determination of the average microscopic dimension in granular media using ultrasonic pulses: Theory and experiments, Presented at the Society of Exploration Geophysicists 1979 Annual Convention, New Orleans, LA, USA.

Rubey, W.W., and Hubbert, M.K., 1959, Role of fluid pressure in mechanics of overthrust faulting, II: Geol. Soc. Amer. Bull., Vol. 70, p. 167-206.

Simmons, G., and Wang, H., 1971, Single Crystal Elastic Constants and calculated aggregate properties: A handbook, Second Edition, MIT Press, Cambridge, MA, 370 pp.

Smith, J.E., 1971, The dynamics of shale compaction and the evolution of pore fluid pressures: J. Inter. Assoc. Math. Geol., Vol. 3, p. 239-263.

_____, 1973, Shale compaction: Soc. Petroleum Engr. J., Vol. 13, p. 12-22.

Spencer, J.W., Jr., 1981, Stress relaxations at low frequencies in fluid-saturated rocks: attenuation and modulus dispersion: Jour. Geophys. Res., Vol. 86, B3, p. 1803-1812.

Stuart, C.A., 1970, Geopressures, 2nd Symposium on Abnormal Subsurface Pressures Proc., p. 121.

Tosaya, C.A., 1982a, Acoustical properties of clay-bearing rocks, Ph.D. Thesis Geophysics Department, Stanford University.

Tosaya, C.A., 1982b, Acoustical anisotropy of Cotton Valley shale: submitted to Geophysics.

Van Olphen, H., 1977, An introduction to clay colloid chemistry, 2nd Edition, Wiley Interscience Publication, New York, 301 pp.

Walsh, J.B., and Grosenbaugh, M.A., 1979, A new model for analyzing the effect of fractures on compressibility: J. Geophys. Res., Vol. 84, p. 3532-3536.

Weaver, C., 1967, The significance of clay minerals in sediments, in Nagy and Colombo, eds., Fundamental Aspects of Petroleum Geochemistry, Elsevier Publ. Co., New York, p. 37-76.

FIGURE CAPTIONS

FIGURE 1: Ratios of clay to quartz and feldspar for Berea sandstone, Cotton Valley silty shale, and Pierre shale.

FIGURE 2: Scanning-electron-microscope photomicrographs of (A) Pierre shale, (B) Cotton Valley silty shale, (C) Berea sandstone, (D) St. Peter sandstone.

FIGURE 3: Thin-section photomicrographs of (A) Pierre shale, (B) Cotton Valley shale, (C) Berea sandstone in plane-polarized, transmitted light. Horizontal distance across each photo is 2.5 mm. Black areas are predominantly clays, white areas are quartz and feldspar.

FIGURE 4: Compressional and shear velocities measured perpendicular to bedding in Pierre shale. Dashed curves represent estimated *in situ* velocities at normal pressure conditions.

FIGURE 5: Compressional and shear velocities measured perpendicular to bedding in Cotton Valley silty shale. Dashed curves represent estimated *in situ* velocities at normal pressure conditions.

FIGURE 6: Compressional and shear velocities measured perpendicular to bedding in Berea sandstone.

FIGURE 7: P and S velocities plotted against differential pressure for (A) Pierre, (B) Cotton Valley, and (C) Berea. Note the dependence of velocity on pore pressure in the shales, shown by the divergence of the low pore pressure (solid diamonds) and high pore pressure (circles) curves.

FIGURE 8: Compressional velocity versus confining pressure in brine- or water-saturated sandstones and shales at 10 bars constant pore pressure. Note the relatively high slopes of the shale velocity curves throughout the confining pressure range.

FIGURE 9: Grain-contact compressibility. (A) compressible contact, (B) incompressible contact.

FIGURE 10: P velocities plotted against volumetric clay content for 18 sandstones, siltstones, and shales at P_c-P_p = 400 bars, brine saturation. Diagonal lines are iso-porosities. Dashed lines separate sandstone, siltstone-shale, and shale fields. (From Tosaya and Nur, 1982).

FIGURE 11: Pore-volume compressibility of Berea sandstone and Cotton Valley shale, water saturated, P_p = 10 bars.

FIGURE 12: Normalized, first-arrival, transmitted P-wave amplitudes through (a) Pierre shale, (B) Cotton Valley silty shale, and (C) Berea sandstone measured normal to bedding in dry and saturated samples at high and low pore pressures.

FIGURE 13: Normalized, first-arrival P-wave amplitudes at P_p = 10 bars through Pierre shale, Cotton Valley shale, and Berea sandstone. Each curve is normalized.

FIGURE 14: Attenuation mechanisms operating in "dry" shale. (A) Bond breakage of surface adsorbates at grain contacts as wave disturbance passes through. (B) Spatial displacement of water pendants at grain contacts as wave passes (Palmer and Traviolia, 1980). (C) Tapered-crack model (Mavko and Nur, 1978) applied to description of pore geometry in shales describes decrease in bulk compressibility (and decrease in attenuation) with increasing confining pressure.

FIGURE 15: Structure of a brine-saturated shale at low pore pressure. Clays expand by absorption and adsorption to produce a rock of zero effective porosity. (A) Crystallographic structure of illite, showing relative positions of gibbsite and silicate sheets and positions of interlayer cations, K^+. (B) Schematic of illite crystal structure. (C) Specific surface areas of clays relative to sands and silts.

FIGURE 16: Attenuation mechanisms operating in brine saturated shale at high pore pressures. (A) Biot pressure-gradient and viscous shear mechanisms (from Johnston et al, 1979). (B) Mavko "squirt" mechanism (from Mavko and Nur, 1979). (C) Mavko tapered crack model describing compressibility behavior of high P_p shale with increasing confining pressure.

FIGURE 17: Normalized permeability plotted against pore pressure in brine-saturated sandstones with clay contents of 0% (St. Peter), 4% (Berea), and 20% (Bandera). Permeability of clay-rich Bandera shows a strong dependence on pore pressure that is consistent with acoustical P-amplitude data (from Nur et al, 1980).

FIGURE 18: Variations in normalized P:S amplitude ratios with confining pressure, $\left.\frac{\partial(A_p/A_s)}{\partial P_c}\right|_{P_p}$. (A), (B) Angular dispersion between P_p = 10 bars and P_p = 400 bars curves appears to be a useful measure of pore pressure in shaly rocks. (C) Low-clay Berea sandstone shows little dispersion with pore pressure.

TABLE CAPTIONS

TABLE 1: (A) Bulk mineralogies of samples. (B) Porosities and dry and saturated densities of samples.

TABLE 2: Specific surface areas (from NMR) and average particle sizes (from SEM) of shale samples.

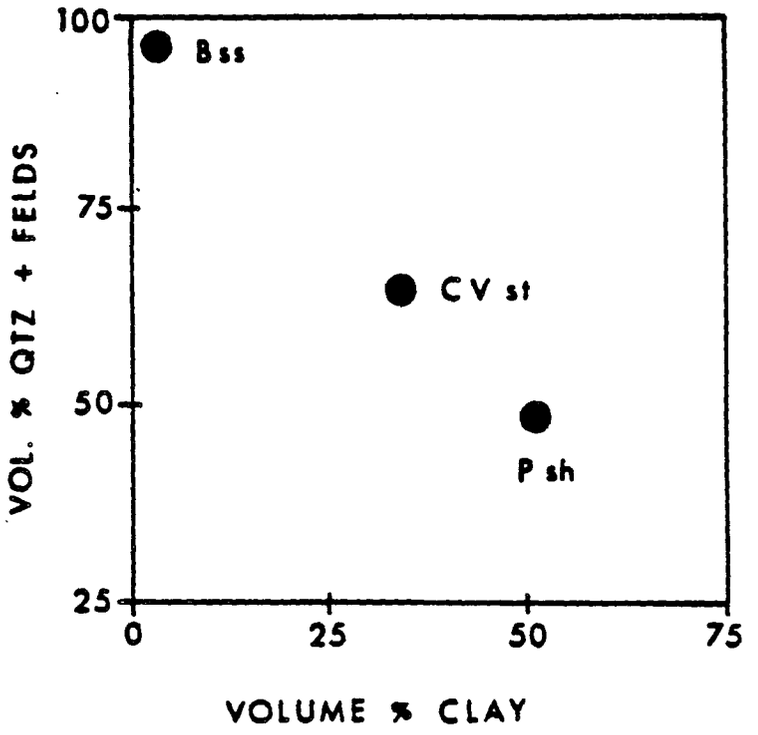

FIGURE 1

Figure 2

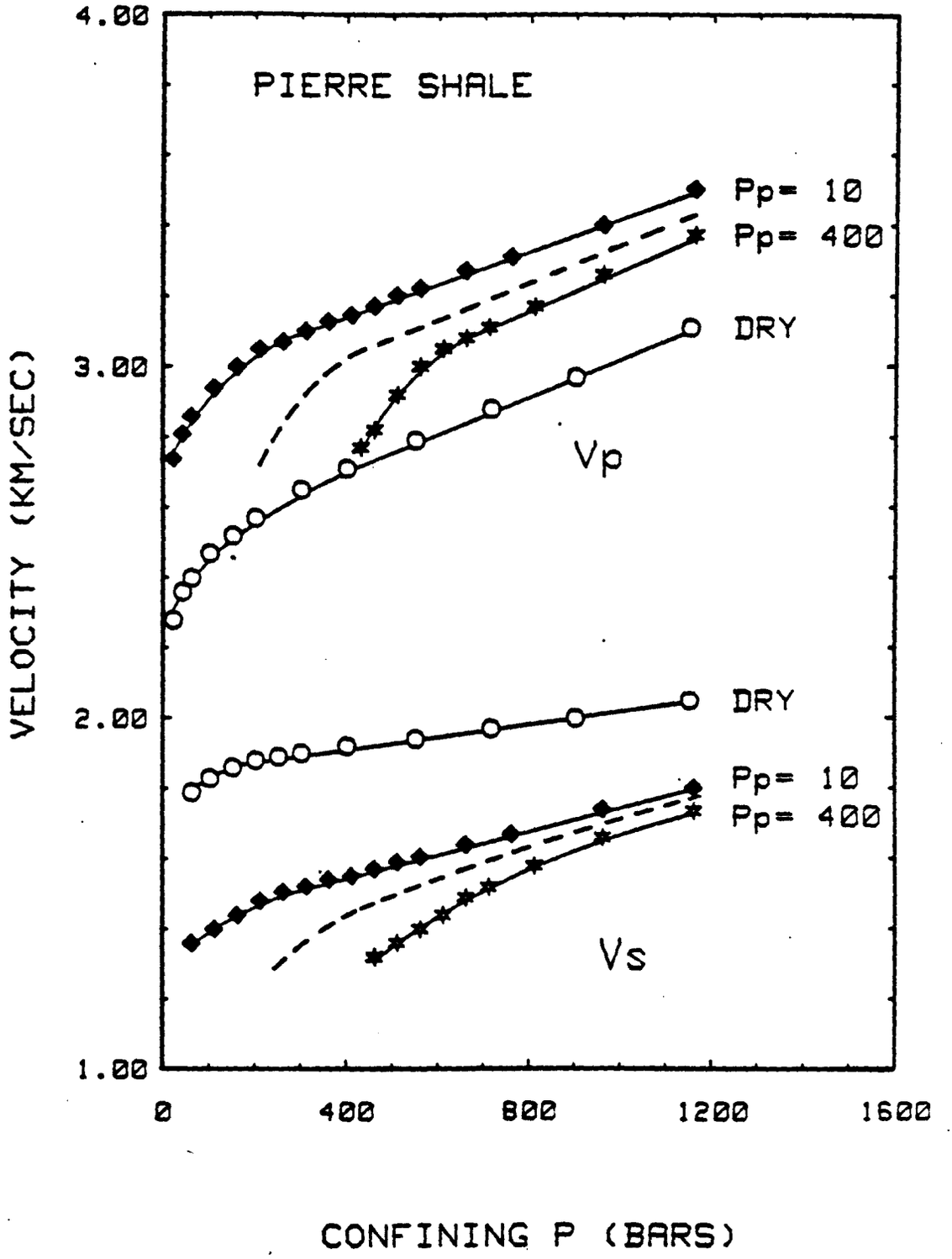
PIERRE SHALE
4.00
3.00
2.00
1.00
VELOCITY (KM/SEC)
Pp= 10
Pp= 400
DRY
Vp
DRY
Pp= 10
Pp= 400
Vs
0
400
800
1200
1600
CONFINING P (BARS)

FIGURE 4

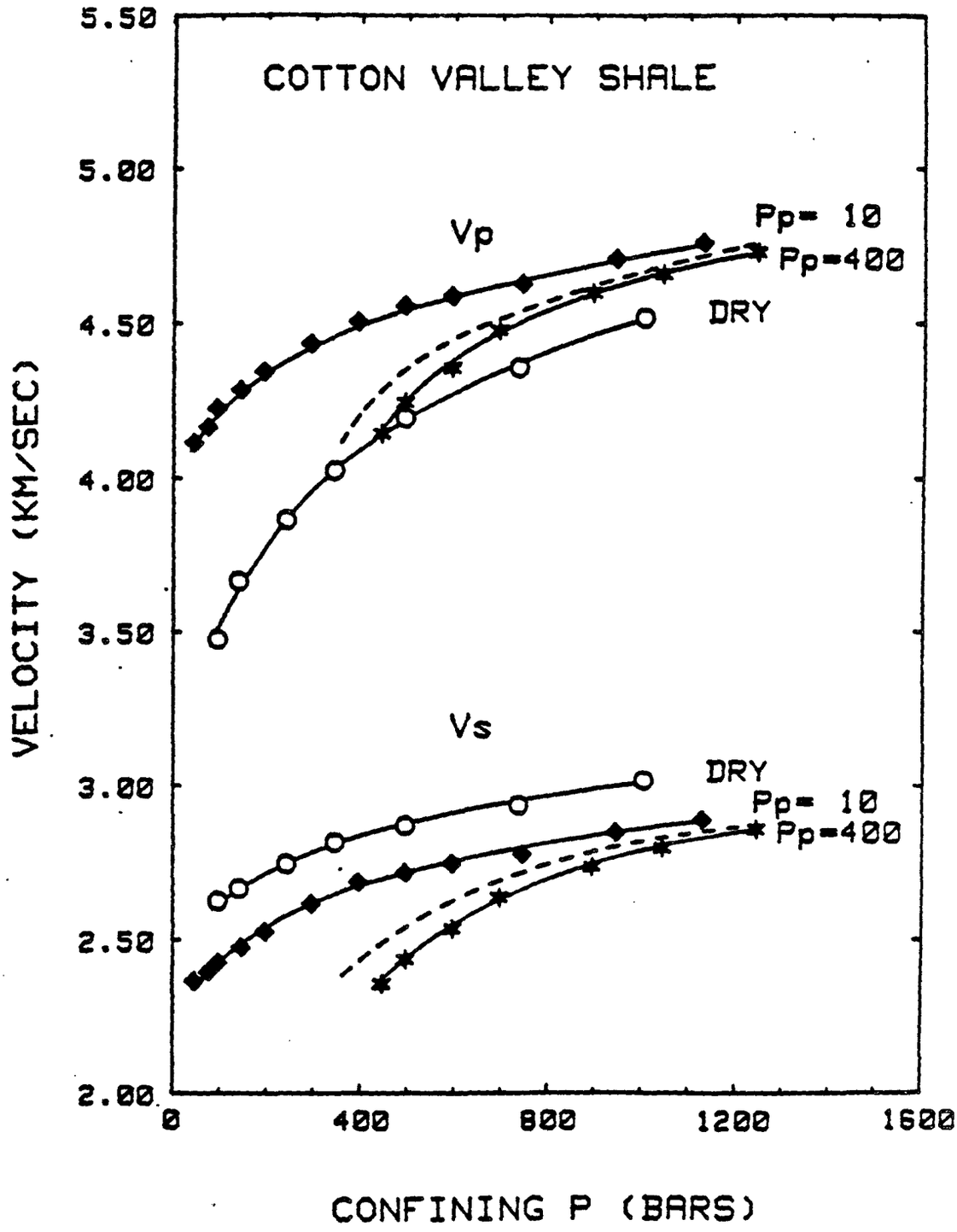
COTTON VALLEY SHALE
Vp
Pp= 10
Pp=400
DRY
Vs
DRY
Pp= 10
Pp=400
VELOCITY (KM/SEC)
5.50
5.00
4.50
4.00
3.50
3.00
2.50
2.00
0
400
800
1200
1600
CONFINING P (BARS)

FIGURE 5

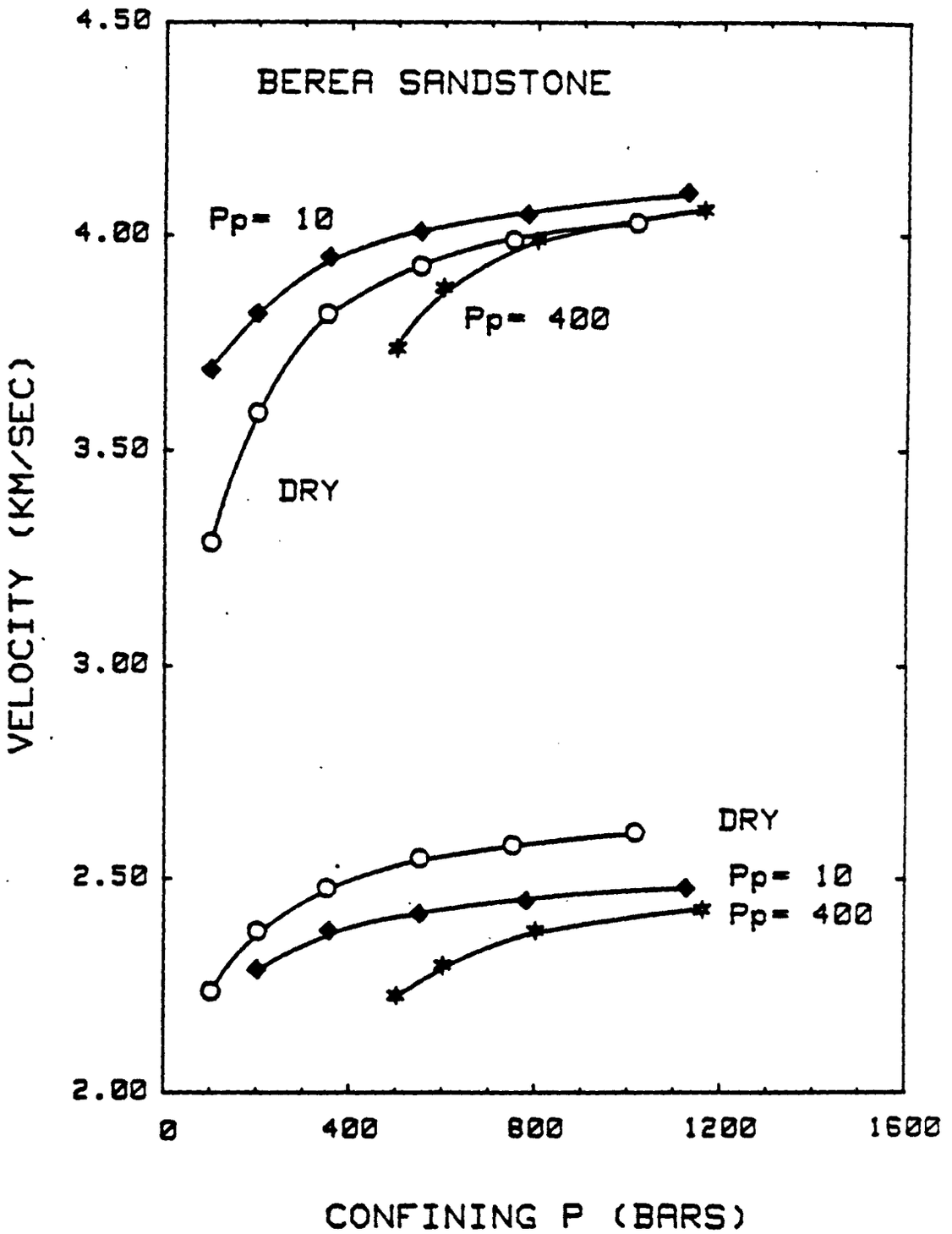
BEREA SANDSTONE
Pp= 10
Pp= 400
DRY
DRY
Pp= 10
Pp= 400
4.50
4.00
3.50
3.00
2.50
2.00
0
400
800
1200
1600
VELOCITY (KM/SEC)
CONFINING P (BARS)

FIGURE 6

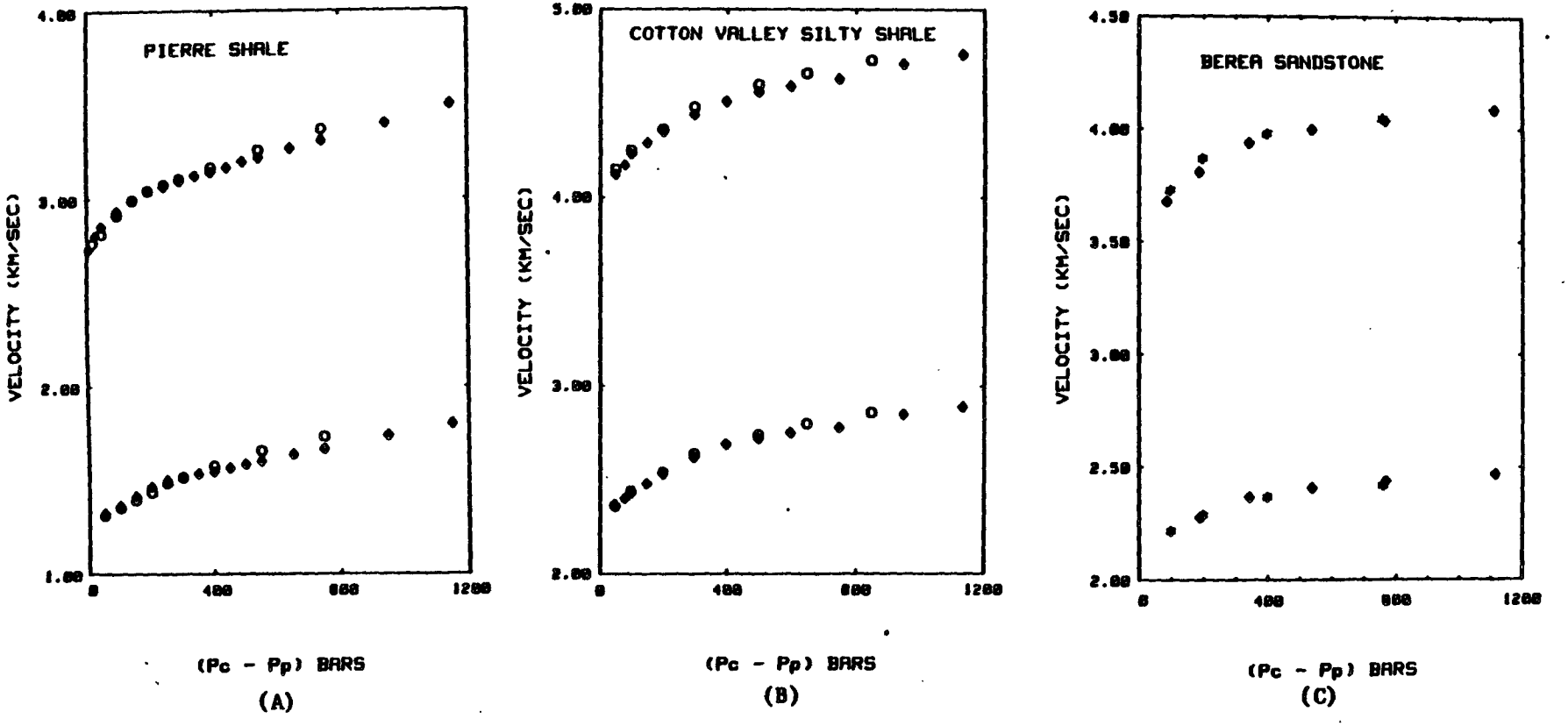
PIERRE SHALE
VELOCITY (KM/SEC)
4.00
3.00
2.00
1.00
0
400
800
1200
(Pc - Pp) BARS
(A)
COTTON VALLEY SILTY SHALE
VELOCITY (KM/SEC)
5.00
4.00
3.00
2.00
0
400
800
1200
(Pc - Pp) BARS
(B)
BEREA SANDSTONE
VELOCITY (KM/SEC)
4.50
4.00
3.50
3.00
2.50
2.00
0
400
800
1200
(Pc - Pp) BARS
(C)

FIGURE 7

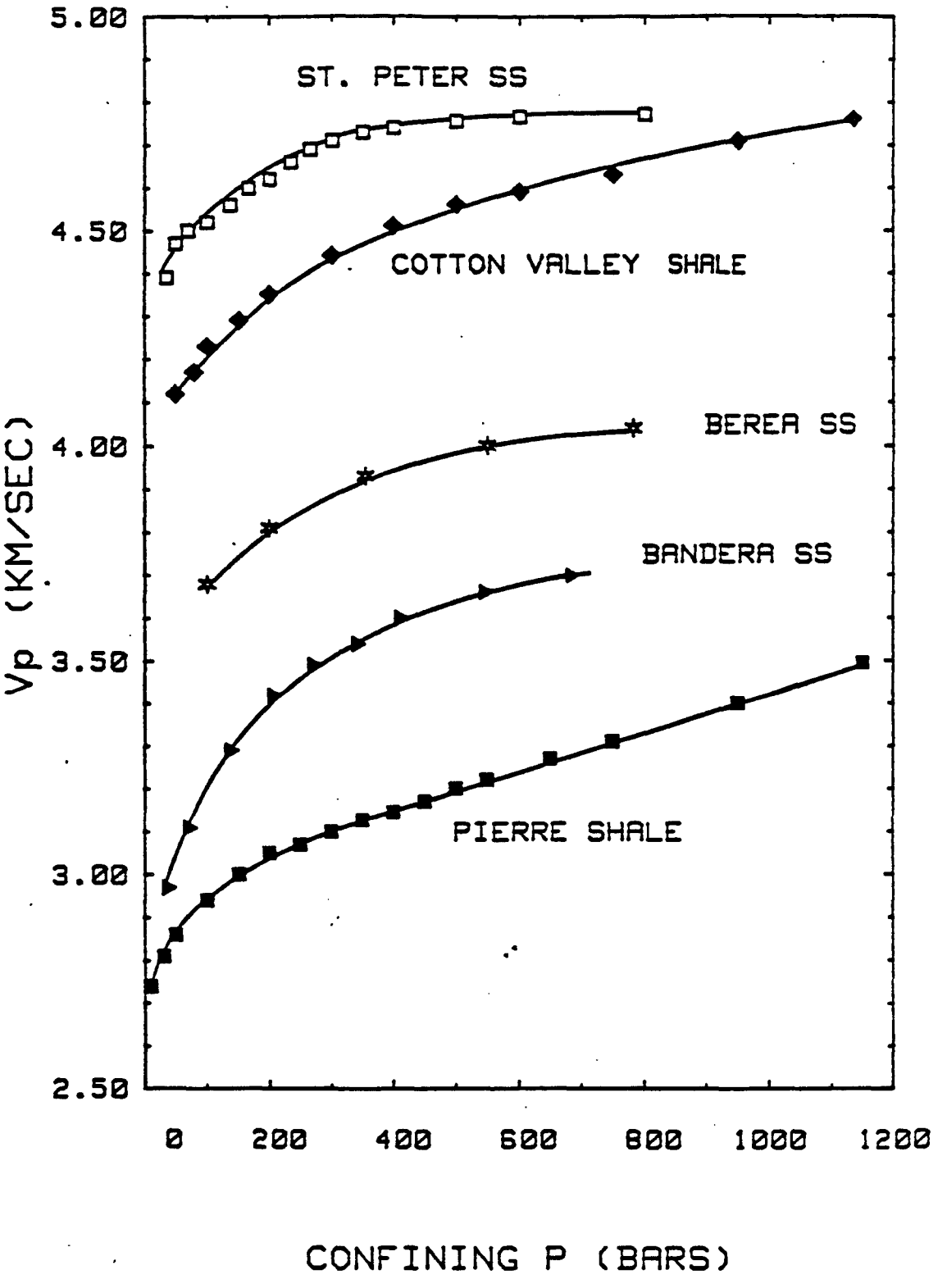
5.00
4.50
4.00
3.50
3.00
2.50
Vp (KM/SEC)
ST. PETER SS
COTTON VALLEY SHALE
BEREA SS
BANDERA SS
PIERRE SHALE
0
200
400
600
800
1000
1200
CONFINING P (BARS)

FIGURE 8

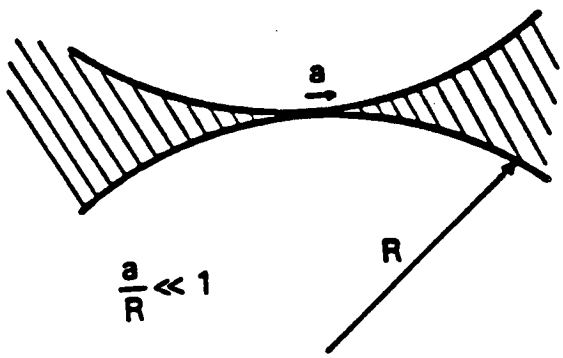

Ⓐ

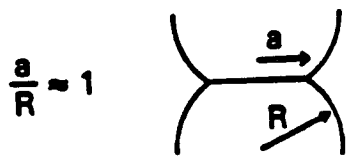

Ⓑ

FIGURE 9

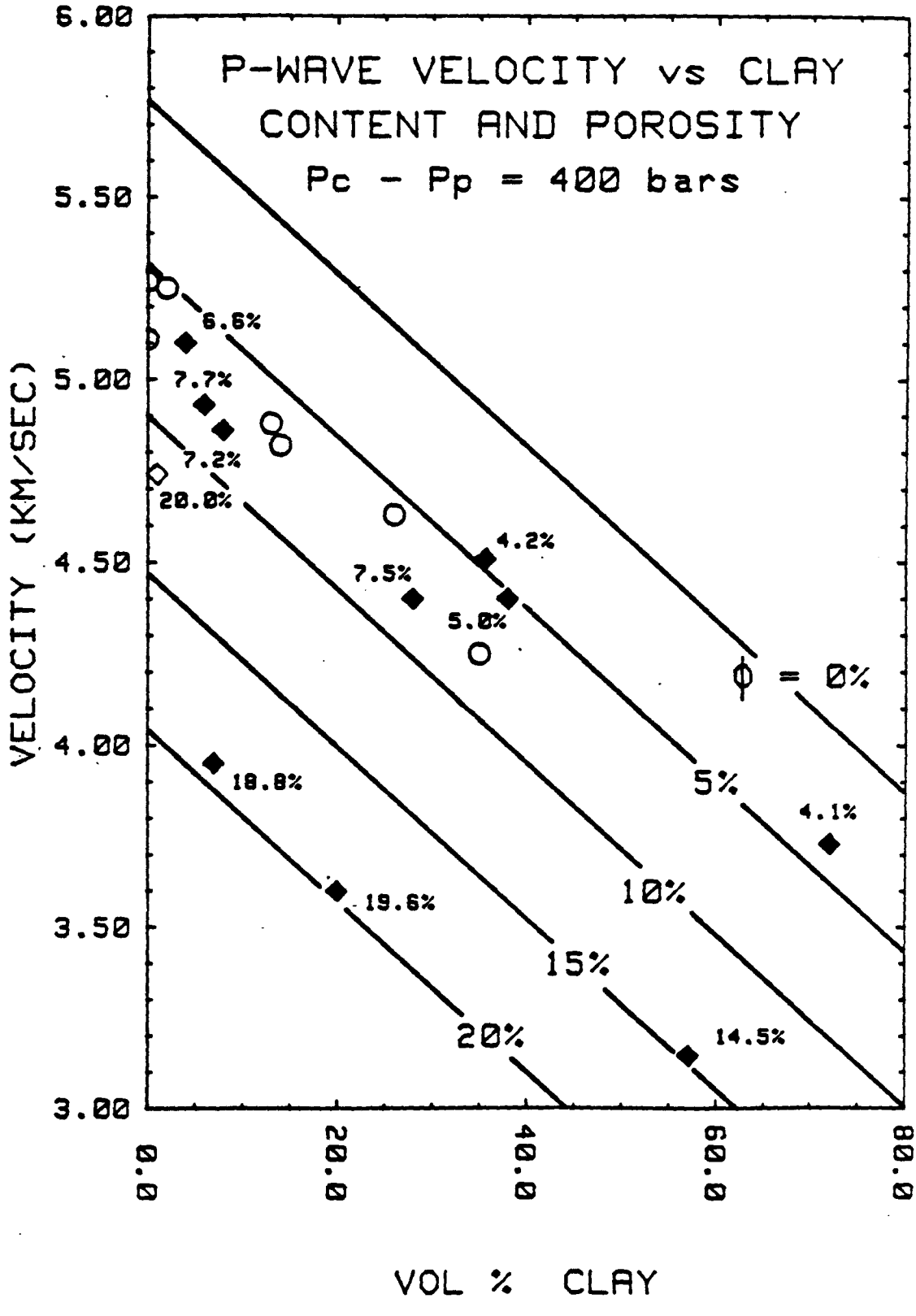
P-WAVE VELOCITY vs CLAY CONTENT AND POROSITY
Pc - Pp = 400 bars
VELOCITY (KM/SEC)
6.00
5.50
5.00
4.50
4.00
3.50
3.00
0.0
0.02
0.04
0.06
0.08
VOL % CLAY
ϕ = 0%
5%
10%
15%
20%
6.6%
7.7%
7.2%
20.0%
4.2%
7.5%
5.0%
18.8%
19.6%
4.1%
14.5%

FIGURE 10

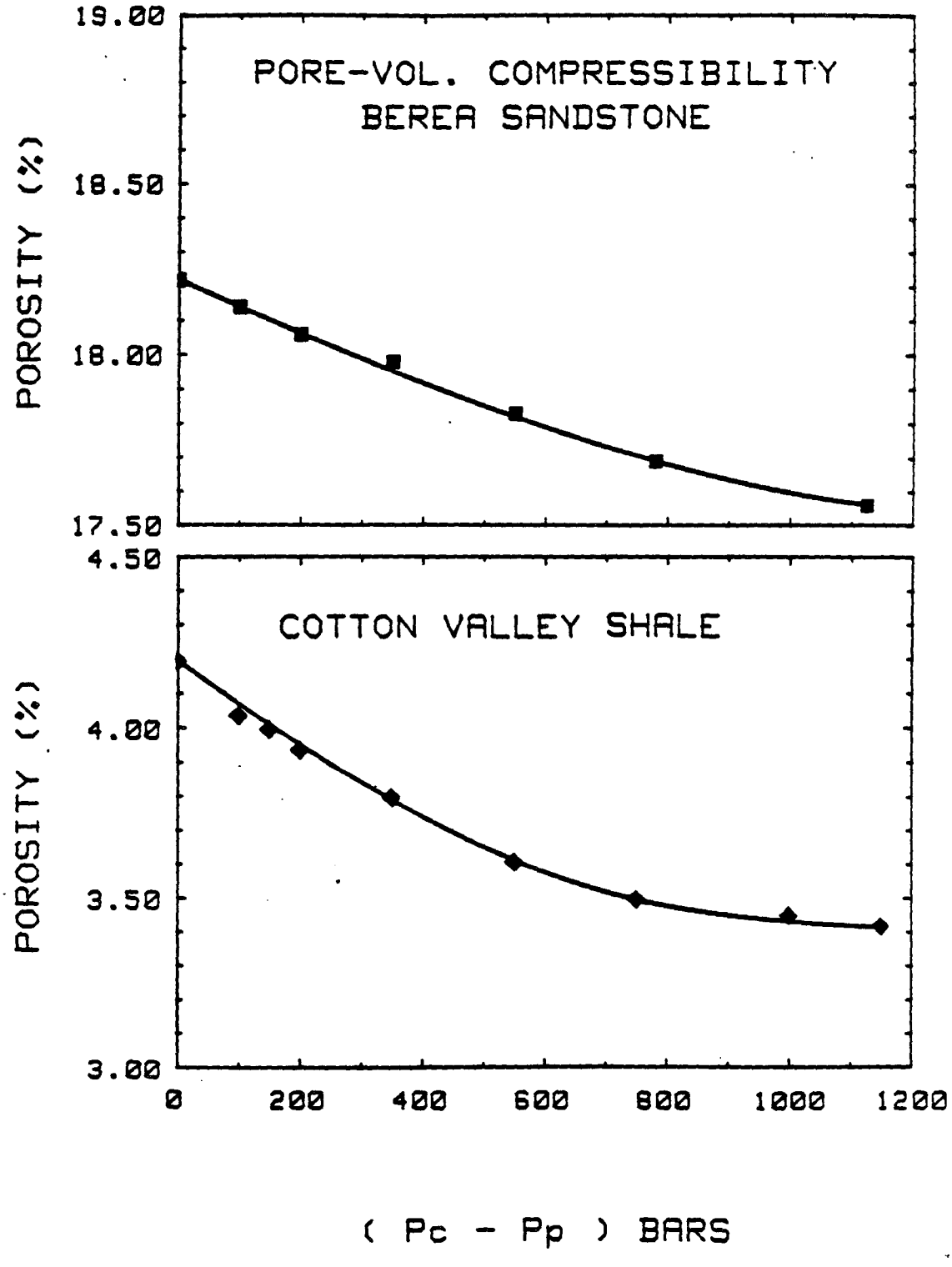
PORE-VOL. COMPRESSIBILITY
BEREA SANDSTONE
POROSITY (%)
19.00
18.50
18.00
17.50
COTTON VALLEY SHALE
POROSITY (%)
4.50
4.00
3.50
3.00
0
200
400
600
800
1000
1200
(Pc - Pp) BARS

FIGURE 11

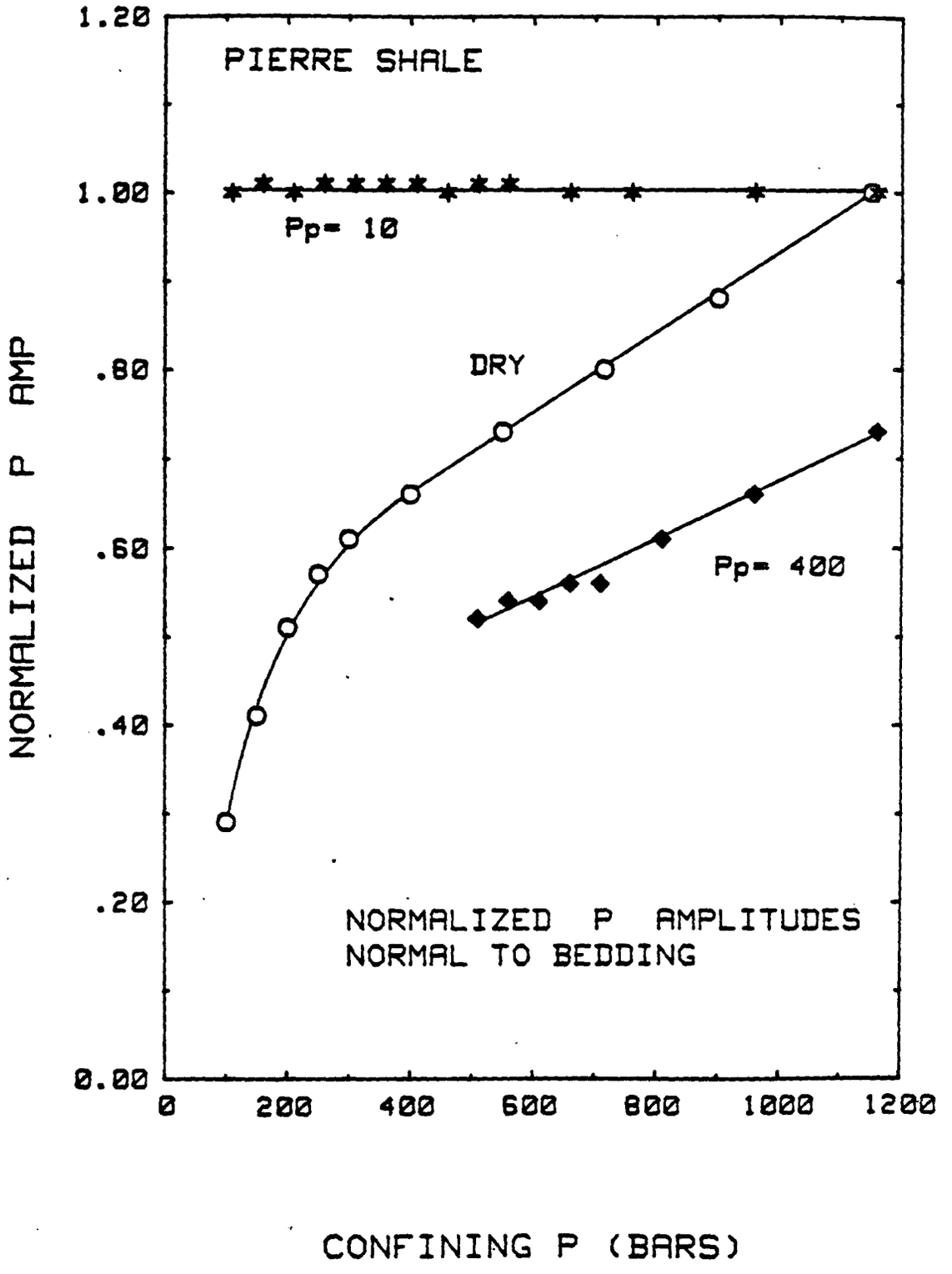
PIERRE SHALE
Pp= 10
DRY
Pp= 400
NORMALIZED P AMPLITUDES
NORMAL TO BEDDING
NORMALIZED P AMP
1.20
1.00
.80
.60
.40
.20
0.00
0
200
400
600
800
1000
1200
CONFINING P (BARS)

FIGURE 12a

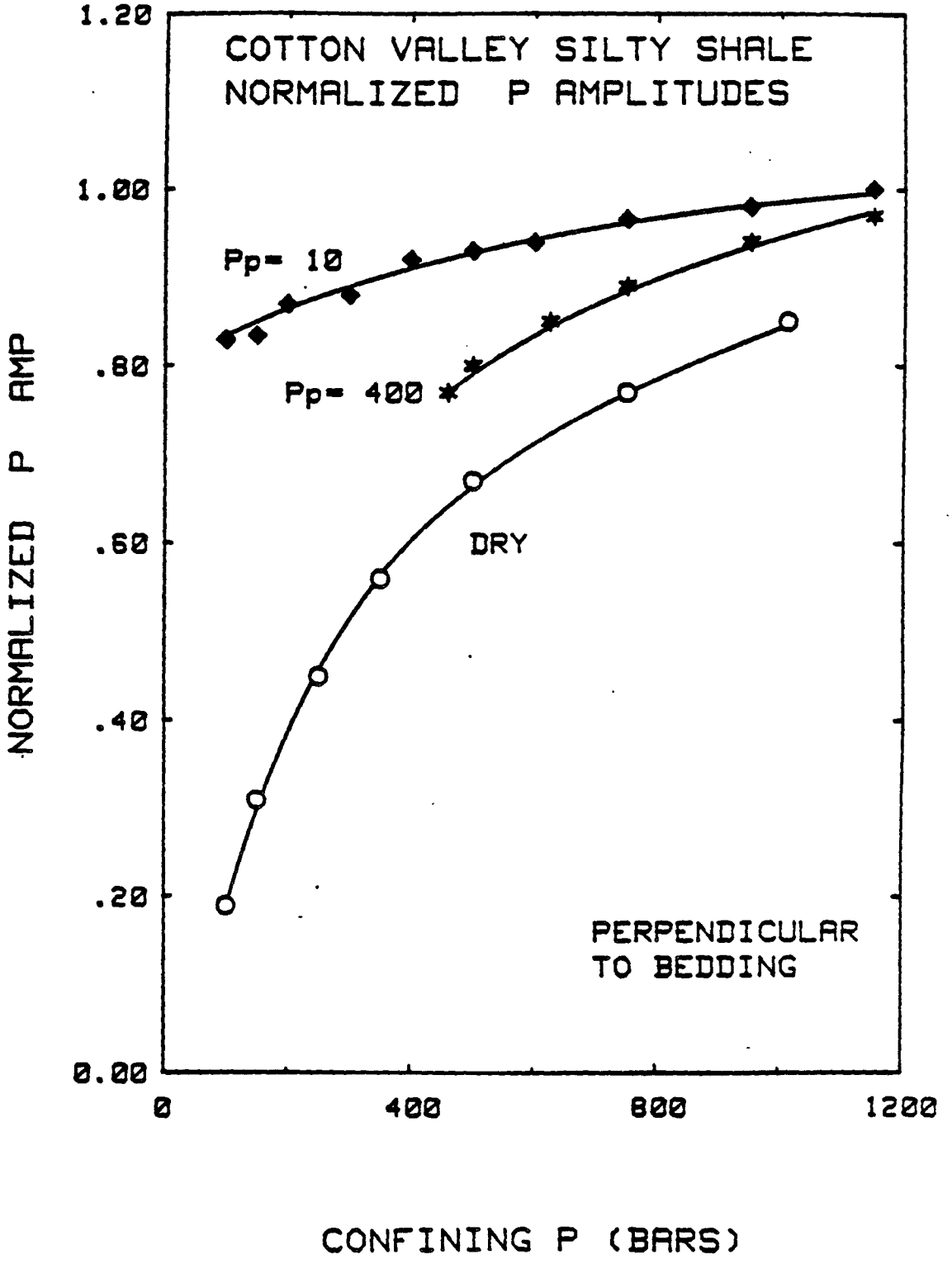
COTTON VALLEY SILTY SHALE
NORMALIZED P AMPLITUDES
Pp= 10
Pp= 400
DRY
PERPENDICULAR
TO BEDDING
NORMALIZED P AMP
1.20
1.00
.80
.60
.40
.20
0.00
0
400
800
1200
CONFINING P (BARS)

FIGURE 12b

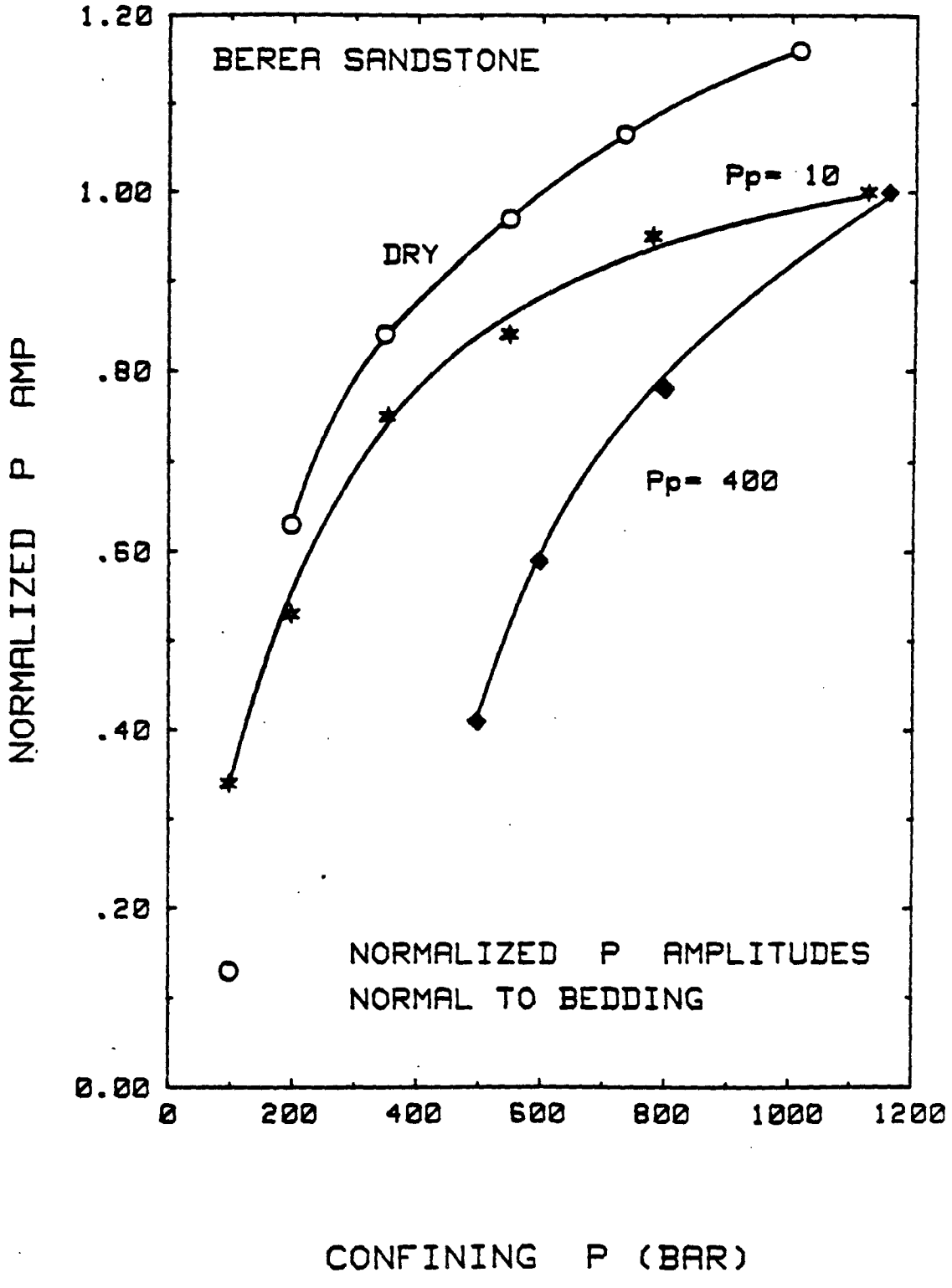
BEREA SANDSTONE
Pp= 10
DRY
Pp= 400
NORMALIZED P AMPLITUDES
NORMAL TO BEDDING
NORMALIZED P AMP
1.20
1.00
.80
.60
.40
.20
0.00
0
200
400
600
800
1000
1200
CONFINING P (BAR)

FIGURE 12c

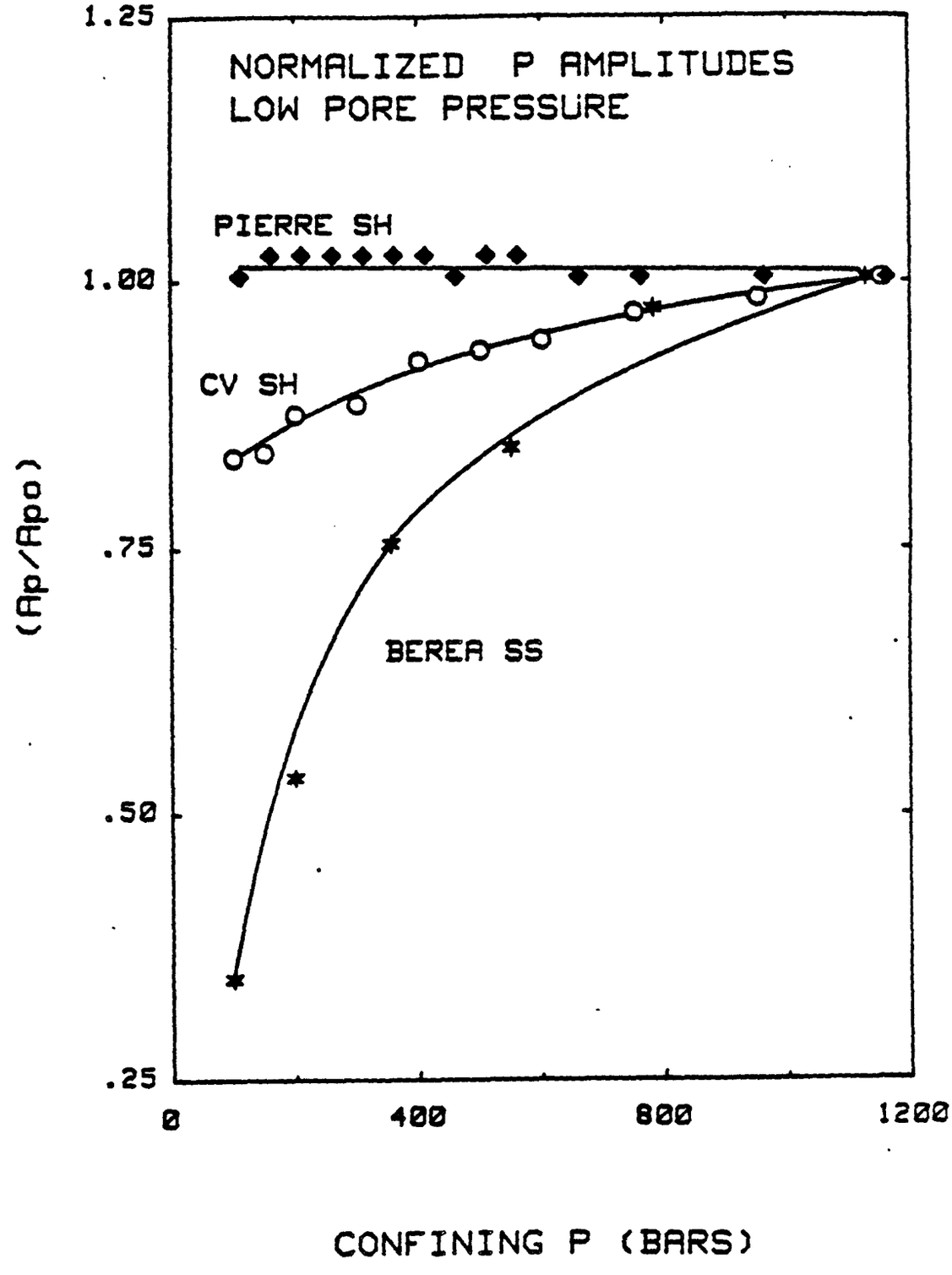
NORMALIZED P AMPLITUDES
LOW PORE PRESSURE
PIERRE SH
CV SH
BEREA SS
1.25
1.00
.75
.50
.25
(Ap/Apo)
0
400
800
1200
CONFINING P (BARS)

FIGURE 13

"DRY"

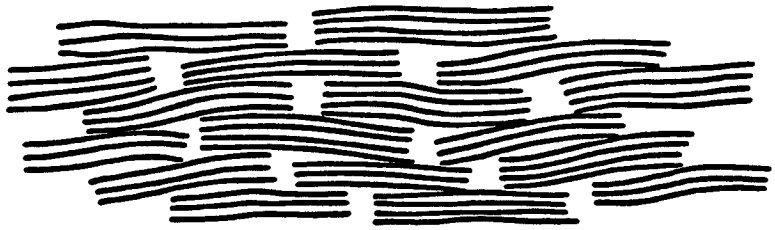

Ⓐ

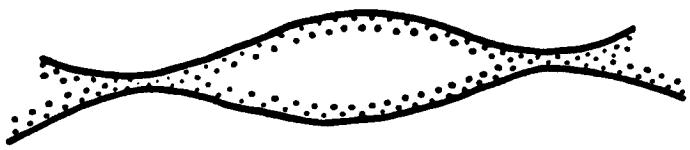

SURFACE ADSORBATES LINING PORES

Ⓑ

WATER IN CONTACTS BY CAPILLARY PRESSURE

Ⓒ

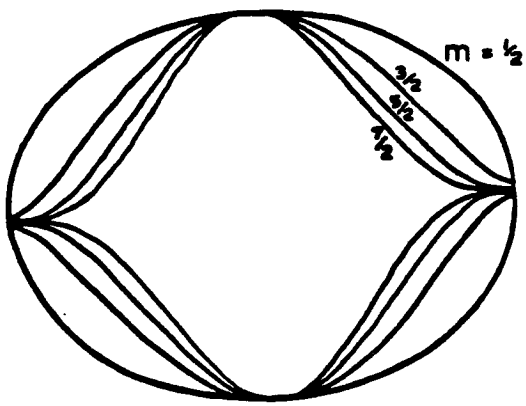

$$y = b\left[1-\left(\frac{x}{c}\right)^2\right]^m$$

FIGURE 14

LOW PORE PRESSURE

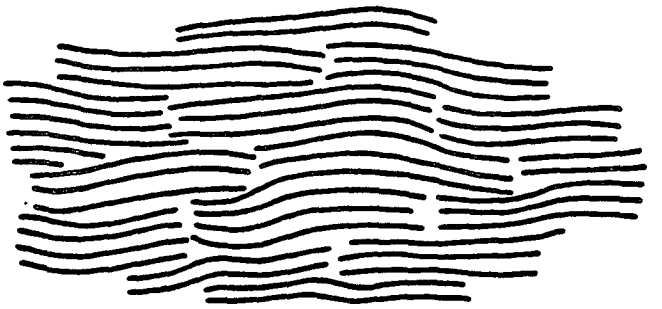

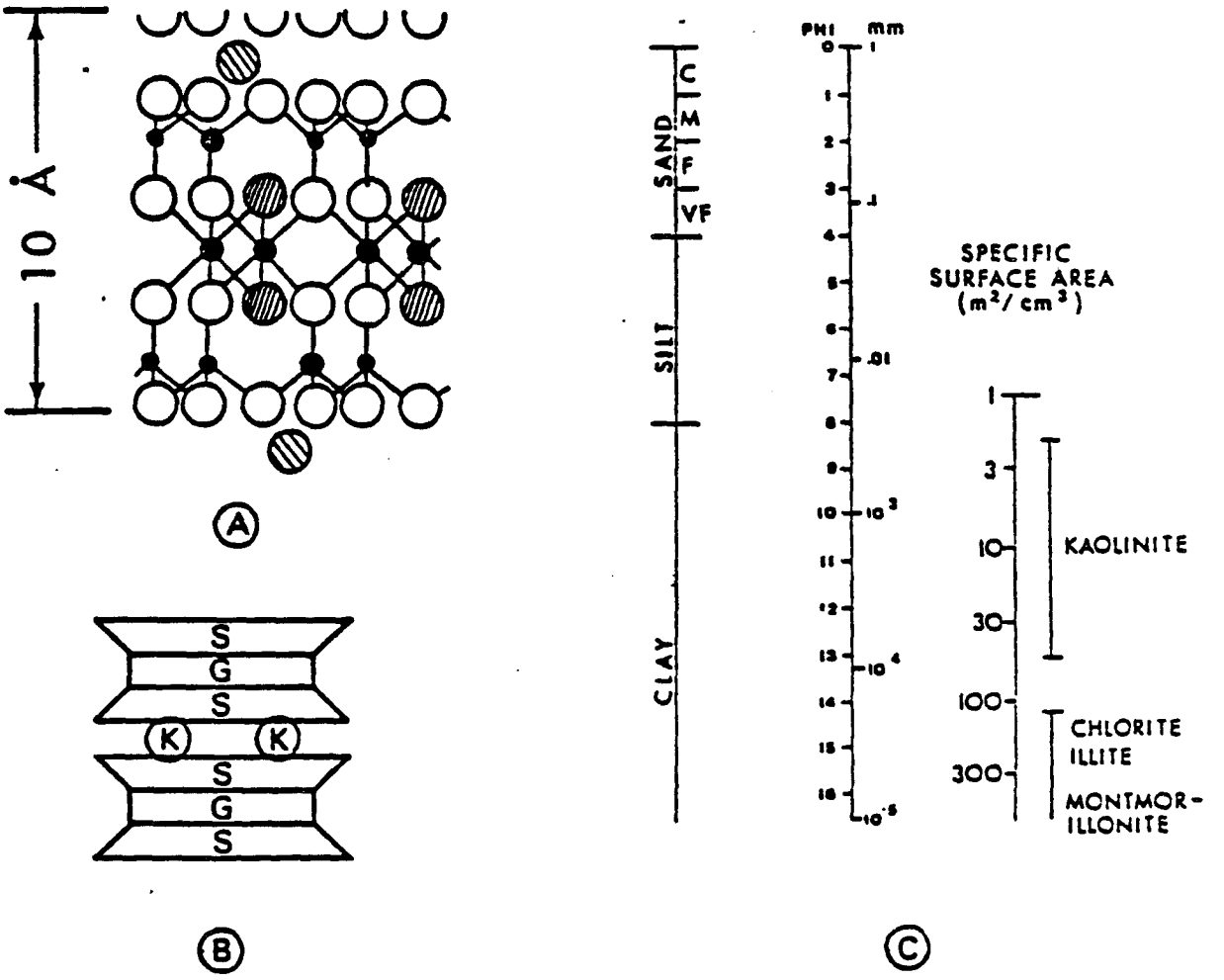

FIGURE 15

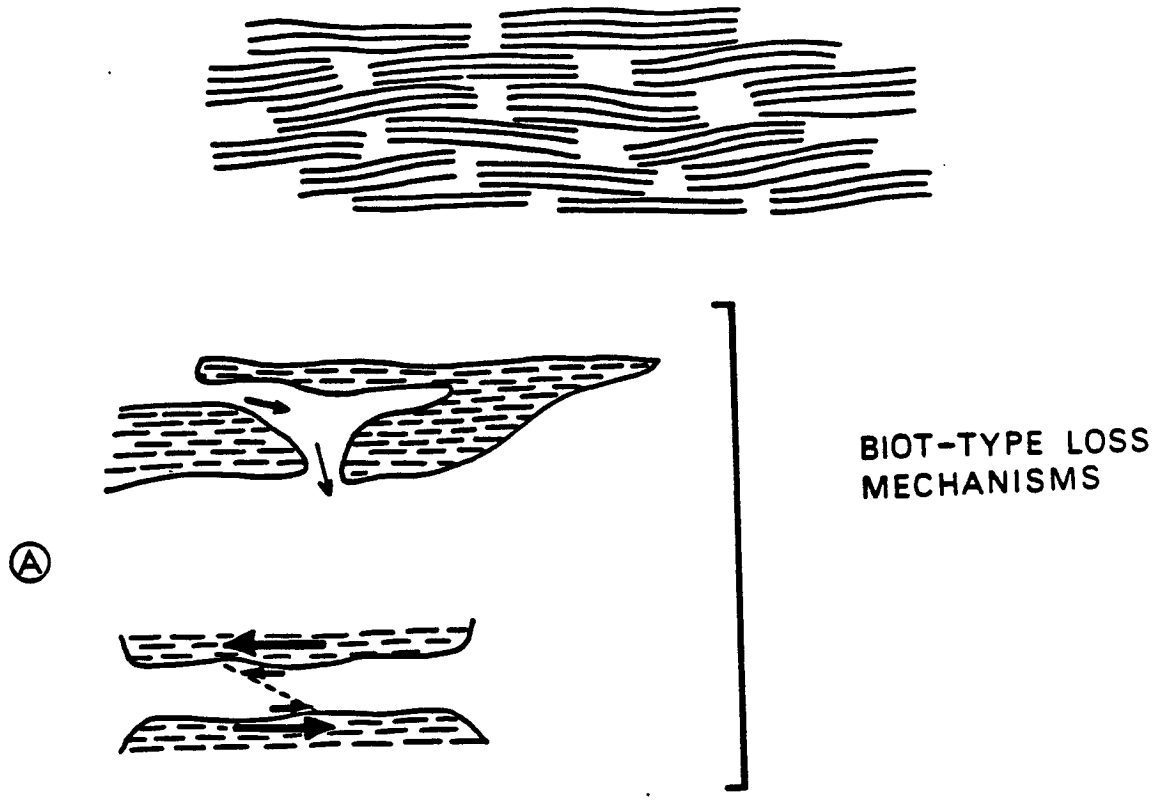
HIGH PORE PRESSURE
BIOT-TYPE LOSS MECHANISMS
Ⓐ
MAVKO LOSS MECHANISM
Ⓑ
m = ½
3/2
5/2
7/2
Ⓒ
$y = b\left[1-\left(\frac{x}{c}\right)^2\right]^m$

FIGURE 16

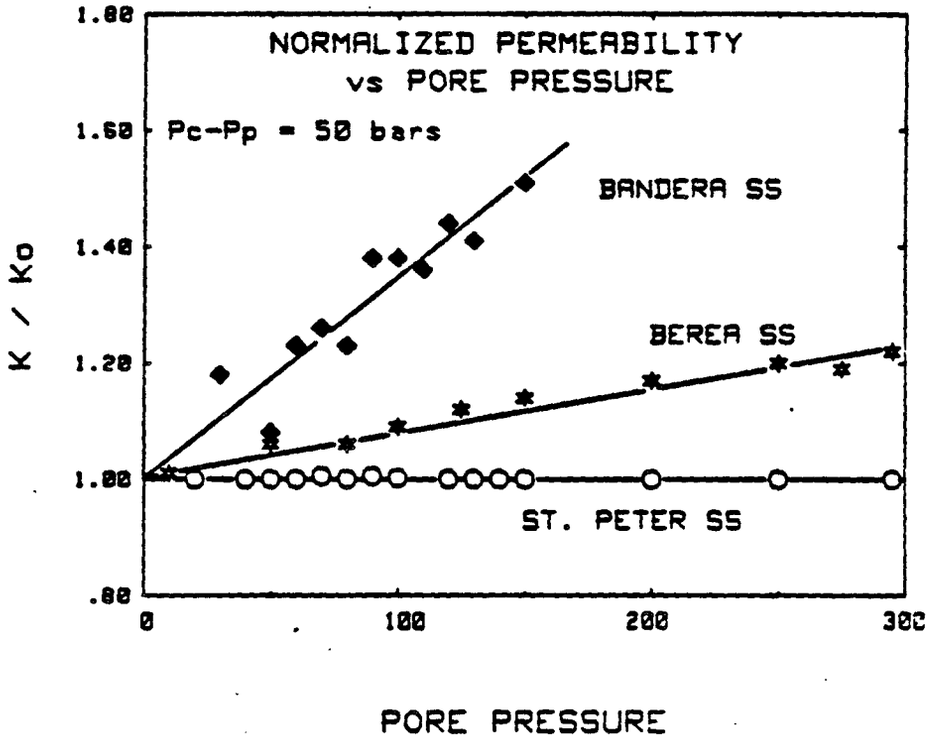
NORMALIZED PERMEABILITY
vs PORE PRESSURE
Pc-Pp = 50 bars
BANDERA SS
BEREA SS
ST. PETER SS
K / Ko
1.80
1.60
1.40
1.20
1.00
.80
0
100
200
300
PORE PRESSURE

FIGURE 17

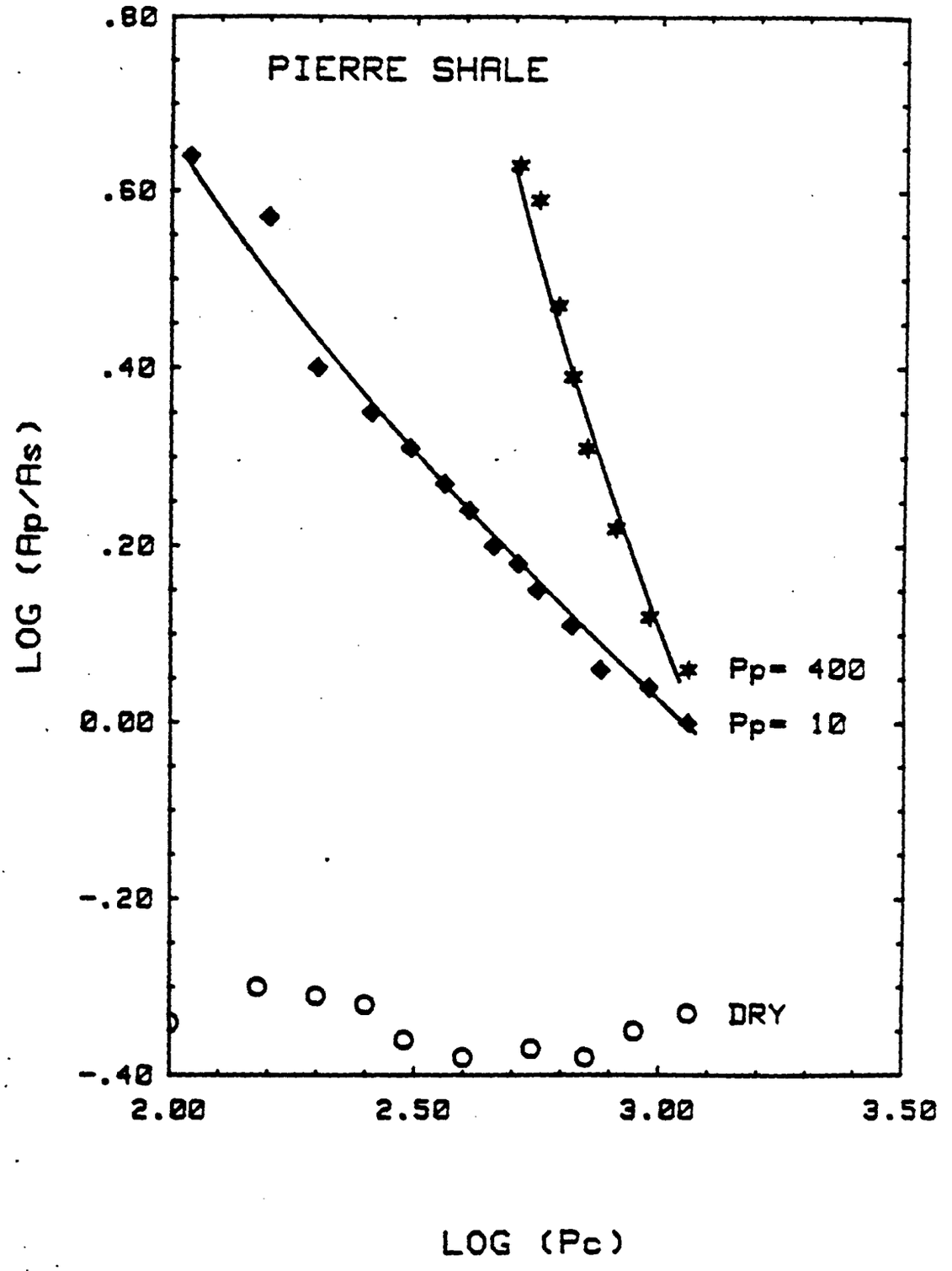
PIERRE SHALE
.80
.60
.40
.20
0.00
-.20
-.40
LOG (Ap/As)
2.00
2.50
3.00
3.50
LOG (Pc)
Pp= 400
Pp= 10
DRY

FIGURE 18a

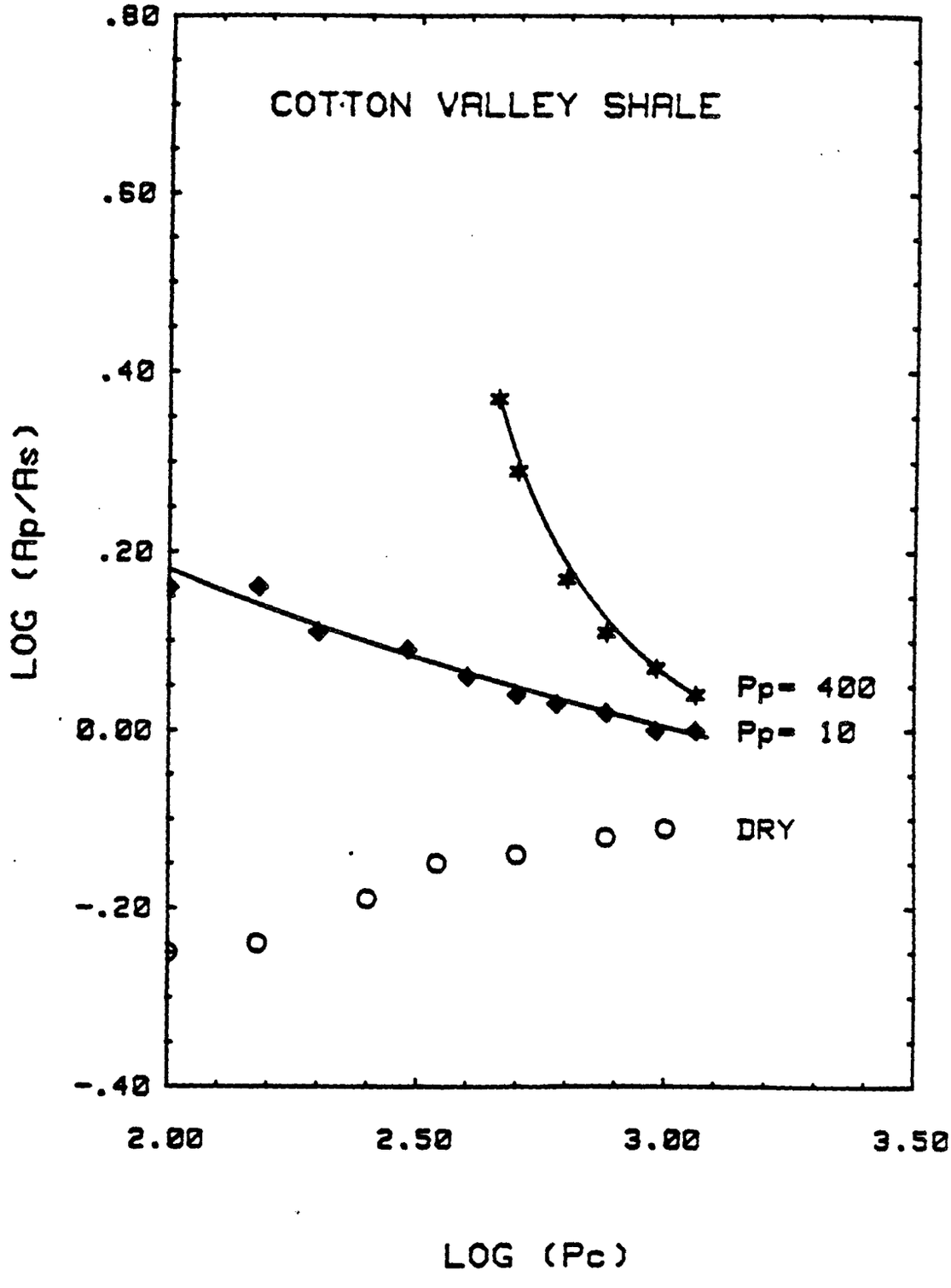
COTTON VALLEY SHALE
.80
.60
.40
.20
0.00
-.20
-.40
2.00
2.50
3.00
3.50
LOG (Ap/As)
LOG (Pc)
Pp= 400
Pp= 10
DRY

FIGURE 18b

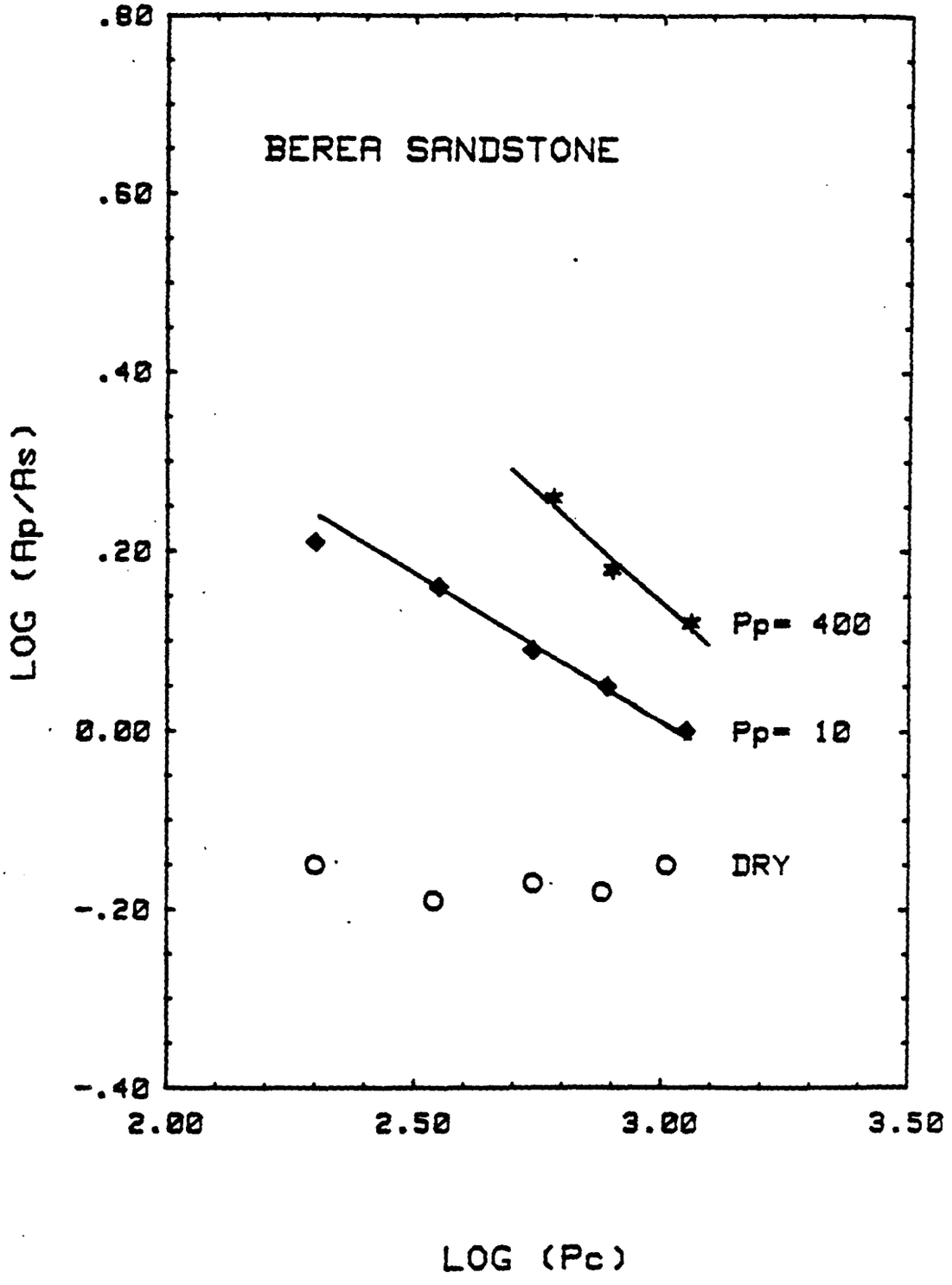
BEREA SANDSTONE
.80
.60
.40
.20
0.00
-.20
-.40
2.00
2.50
3.00
3.50
LOG (Ap/As)
LOG (Pc)
Pp= 400
Pp= 10
DRY

FIGURE 18c

PIERRE SHALE:	qtz: 18%	
	felds: 3%	
	pyrite: 1%	
	amorphous silica: 21%	
	clay: 57%:	illite: 15%
		illite-mont.: 37.5%
		chlorite: 3.5%
		kaolinite: 14%
		amorphous clay: 30%
COTTON VALLEY SHALE:	qtz: 49%	
	felds: 9.5%	
	calcite: 3%	
	siderite: 2%	
	pyrite: .5%	
	clay: 36%:	illite: 35%
		chlorite: 6%
		kaolinite: 18%
		amorphous clay: 41%
BEREA SANDSTONE:	qtz: 91%	
	felds: 7%	
	clay: 2%:	illite
		kaolinite

TABLE 1a

SAMPLE	POROSITY	DENSITY (g/cm^3)
PIERRE SHALE	14.5 %	dry: 2.29 sat.: 2.34
COTTON VALLEY SHALE	4.2 %	dry: 2.60 sat.: 2.64
BEREA SANDSTONE	18.2 %	dry: 2.12 sat.: 2.30

TABLE 1b

IV. AN EXPERIMENTAL INVESTIGATION OF THE EFFECTS OF DIAGENESIS AND CLAYS ON COMPRESSIONAL AND SHEAR VELOCITIES IN ROCKS

Published in Geophysical Research Letters, Vol. 9, pp. 5-8, January 1982.

Presented at the American Geophysical Union, Fall Meeting, December 1981.

SAMPLE	SPECIFIC SURFACE AREA (m^2/cm^3)	AVERAGE PARTICLE SIZE (μ)	AVERAGE PORE RADIUS NORMAL TO FISSILITY
PIERRE SHALE	248 m^2/cm^3	3 μ diameter .3 μ thickness	.15 μ = 15 Å
COTTON VALLEY SHALE	73 m^2/cm^3	7 μ diameter .5 μ thickness	.25 μ = 25 Å

TABLE 2

AN EXPERIMENTAL INVESTIGATION OF THE EFFECTS OF DIAGENESIS AND CLAYS ON COMPRESSIONAL AND SHEAR VELOCITIES IN ROCKS

ABSTRACT

Experimental results at ultrasonic frequencies in brine- or water-saturated samples cut perpendicular to bedding demonstrate that compressional and shear velocities vary linearly with porosity and volume-fraction clay in detrital silicate rocks characterized by pores with low aspect ratios. Velocities are more sensitive to porosity than to clay content, obeying the empirically derived expressions $V_p = -2.4C - 8.6\phi + 5.8$ and $V_s = -2.1C - 6.3\phi + 3.7$ at 800 bars confining pressure and 400 bars pore pressure, where the units of V_p and V_s are kilometers per second, ϕ is the volume fraction pores, and C is the volume fraction clay. Deviations from this equation are less than ±2% with the exception of the high pore aspect ratio St. Peter sandstone, which has a compressional velocity that is 17% higher than the predicted value and a shear velocity that is high by 23%. Within the compositional and textural limits represented by the test samples, the equations are insensitive to the chemical composition of the dominant clay mineral and apparently insensitive to the location of the clay grains with respect to the mineral framework, e.g., in free pore space or in contact zones between mineral grains of lower compressibilities.

INTRODUCTION

Exploratory detection of porosity and clay content in sedimentary reservoir rocks and in rocks associated with potential reservoirs is of importance in the estimation of reservoir volumes and in the determination of pore-fluid flow patterns for recovery. The effects of porosity on the elastic and the acoustic properties of rocks has been a subject of great interest. Wyllie, et al., (1958) proposed an empirically derived time-average equation that relates propagation velocity to porosity:

$$1/V_M = \phi/V_F + (1-\phi)/V_R$$

where V_M is the measured velocity, V_F is the velocity in the fluid saturant, V_R is the velocity in the rock solid, and ϕ is the volumetric pore fraction. The relation appeared to give acceptable results (± a few percent) for clay-free sandstones under conditions of high differential pressures, but significantly overestimated velocities in rocks with crack-shaped pores or isolated, vugular porosity such as shales, limestones, and dolomites. More accurate relationships between propagation velocity and porosity can be obtained by taking into consideration pore shapes and the nature of the framework. Based on Biot's continuum theory, Geertsma (1961) derived a relation between velocity and porosity in consolidated, clean sandstones that was based on deformation characteristics of the rock. Coefficients that depend on grain cementing material and pore geometry were taken into account in a relation between bulk compressibility and porosity. Paterson (1956) reviewed the various theories with respect to the degree of coupling between the pore filler and the framework material. Toksöz, et al., (1976),

Mavko and Nur (1978), O'Connell and Budiansky (1974), Walsh and Grosenbaugh (1979) and Cheng and Toksöz (1979) considered the effects of distributions of elliptical and tapered pore shapes on the bulk elastic and acoustic behavior of rocks.

In contrast, the effects of clay minerals on rock velocities are poorly understood. Investigators, e.g., Toksöz, et al. (1976) and King (1966), have only alluded to interactions between pore fluids and clays as processes that lower matrix rigidity. Indeed, results of the measurements presented in this paper suggest that framework clays do lower bulk and shear moduli in a systematic manner. DeMartini, et al., (1976) published data on compressional velocities and clay contents in a suite of sandstones with porosities close to 5% from the Ardmore Basin, Oklahoma. Their data are included with ours in Figures 2 and 3 and in Table 1.

EXPERIMENTAL PROCEDURE

This study was initiated to investigate the nature of the dependence of compressional and shear velocities in detrital silicate rocks on porosity, pore geometry, volume fraction clay and clay mineralogy. Porosities in the selected suite of 18 samples ranged from 4.2% to 20.0%; total clay content by volume varied from less than 1% to 72%. All cores were cut with the cylindrical axis perpendicular to bedding. Velocities were measured in low-salinity brine- and water-saturated samples at ultrasonic frequencies (~1 MHz) by a pulse-transmission technique. Velocities are precise to ±1%; porosities are reproducible to ±2%. Confining pressures and pore pressures were separately applied and controlled. Clay contents were obtained from thin-section microscopy, X-ray diffraction and elemental analysis. Table 1 is a compilation of pertinent sample information.

RESULTS AND DISCUSSION

Velocity profiles with increasing confining pressure are presented in Figure 1 for several sandstones and shales. It is apparent from close examination of Figure 1 and Table 1 that compressional velocity is not solely a function of lithology, clay content, or porosity. There is no evident dependence of velocity on porosity: St. Peter, Berea, and Bandera sandstones have approximately equal porosities close to 19% yet display a wide variation in measured velocities. Plotted in their midst is the velocity profile for Cotton Valley silty shale, which has porosity of only 4.2%.

The volumetric clay fraction appears to more systematically influence measured velocities: clay content tends to decrease downward in Figure 1. The notable exception is Cotton Valley shale, with 35% clay, which is indistinguishable from sandstones with clay contents of 0 - 7% on the basis of its velocity behavior with increasing confining pressure.

The implication of these results is that a seismic reflection profile would correctly identify the Pierre sample as a shale but would incorrectly label the Cotton Valley sample as a sandstone. However, it is of critical importance to be able to identify the Cotton Valley sample as a silty shale. Problematic characteristics of clay-rich shales, particularly low-permeability properties associated with regions of abnormal pore pressures, apply equally to fissile, silty shales. The thin-section photomicrograph of Figure 5b shows the complete envelopment of quartz grains by the predominantly illitic matrix material in this silty shale. Clearly, then, a set of criteria capable of unambiguously distinguishing shales from sandstones has widespread applications value.

Figure 2a,b presents the compressional and shear velocity data, respectively, at a single value of confining pressure (800 bars) and pore pressure (400 bars). Although data are sparse in some regions of the plots, the trends are clear. Both P and S velocities vary linearly with porosity and clay content.

Compressional velocities in the rocks included in this study are more sensitive to porosity than clay content by a factor of approximately 4:

$$V_p = -2.4C - 8.6\phi + 5.8 \quad , \qquad (1)$$

where ϕ is the volume fraction pores, C is the volume fraction clay, and the units of V are kilometers per second.

Shear velocities obey the expression:

$$V_s = -2.1C - 6.3\phi + 3.7 \quad . \qquad (2)$$

Equations (1) and (2) are strictly valid only at a confining pressure of 800 bars and a pore pressure of 400 bars, the approximate in situ lithostatic and hydrostatic pressures of the Cotton Valley and Ardmore Basin sandstones, siltstones, and silty shales used in this study. Presumably, similar equations would be valid at other differential pressures.

The only datum not in agreement with Figures 2 and 3 is the point represented by St. Peter sandstone (<1% clay, 20% porosity) which has a compressional velocity that is 17% higher and a shear velocity that is 23% higher than expected from the behavior of the other data. However, examination of Figure 4 reveals that the pore geometery of St. Peter sandstone deviates significantly from that of the shales and the other sandstones. The St. Peter sandstone is characterized by a large fraction of high aspect-

ratio pores which are clearly visible in Figure 4e. This deviation in velocity and pore structure suggests that porosity may not be the proper parameter for characterization of pore geometry in equations (1) and (2). A parameter such as $\frac{\phi}{S}$, where ϕ is porosity and S is specific surface area measured by BET (for clean, porous sandstones) or NMR (for low-porosity, highly presolved sandstones and fine-grained rocks), may more appropriately account for both total porosity and pore and contact geometries. It must be noted, however, that St. Peter sandstone is neither a petroleum reservoir rock nor typical in textural characteristics to reservoir rocks. Porosity is an adequate variable for describing the velocity behavior of the reservoir rocks and reservoir-associated rocks included in this study.

Relative qualitative pore aspect-ratio distributions may be derived from the slopes of velocity curves as a function of confining pressure if a single pore geometry is assumed constant for all rocks, as shown in Figure 1. All of the velocity curves display large slopes at confining presures below 350 bars, representing closure of very low aspect-ratio discontinuities. At confining pressures greater than 350 bars, all curves except that of the St. Peter sandstone continue with a positive slope reflecting continuous closure of pores with increasingly larger aspect ratios.

Pore aspect ratios are related to the degree of diagenetic porosity reduction resulting from pressure solution and the precipitation of new intergramular phases such as authigenic clays as well as to the degrees of sorting and roundness of constituent allogenic grains. Pressure solution tends to modify intergramular discontinuities toward lower aspect ratios, as a comparison of the crack-like pores in low-porosity, highly presolved Cotton Valley sandstone (Figure 4c) with the very low-grade diagenetic texture of St. Peter sandstone (Figure 4e) clearly shows.

Clays, regardless of their mineralogy (Table 1) and apparently regardless of whether they are authigenic or allogenic in origin, affect compressional velocities in the same manner in brine- or water-saturated samples over the range of clay compositions used in this study. Detailed examination of the distribution of clays in Berea sandstone, Bandera sandstone, and Cotton Valley silty shale (Figure 5b,c,d) suggests that the distribution of clays in rocks is not of primary importance to acoustic behavior. However, clays situated in grain contacts were expected to have a significantly larger effect on lowering bulk rigidities and stiffnesses than clays occupying free pore space. Indeed, the spatial distribution of clays in Berea sandstone contrasts sharply with the distribution of clays in the shales. The detrital (allogenic) clays of the shale samples completely encapsulate all other detrital minerals (Figure 5a,b) such that the quartz grains appear to be suspended in a clay matrix and there are few quartz-quartz contacts. The scanning electron photomicrographs (Figure 4b,f) verify the dominance of platy clay minerals in controlling the geometries of grain contacts in these rocks. The grain-to-grain contacts in Berea sandstone (Figure 4e, Figure 5d), however, are predominantly clay free, with authigenic illite and kaolinite tending to occupy free pore space. Bandera sandstone (Figure 4a, Figure 5c) is intermediate to the two textural extremes, exhibiting a preponderance of both quartz-quartz and quartz-clay contacts.

Within the range of rock textures and mineralogies represented by the samples in this study, it is probable that the amount of clay in grain contacts is proportional to the total amount of clay in a given rock, as estimates from examination of Figures 4 and 5 suggest. From Table 1, it is clear that rocks with clay listed in "contacts" have the highest clay volume

fractions, while those with clay in "pores" have the lowest volume fractions. Therefore, velocity may depend strongly upon where the clay resides, but it appears that the proportionate location of the clays in contacts:pores may be conveniently characterized simply by the total volumetric clay fraction.

Clays with chemistries consistent with relatively large metal-cationic and water-sorption characteristics, e.g., montmorillonite and mixed-layer illite-montmorillonite, were expected to exhibit a stronger influence on lowering bulk shear moduli and raising bulk compressibilities that nonexpansive, massive clay minerals such as kaolinite. However, the lack of dependence of compressional velocity on the chemical compositions of the clays in our samples suggests that the difference between the wet moduli of quartz and clays is much larger than the difference in moduli between clays of different mineralogies such that the latter do not show a first-order effect on compressional velocities. It must be noted, however, that kaolinite (kandite) is not the sole clay mineral in any of the study rocks. All of the clay-bearing rocks contain significant clay fractions that consist of illite, chlorite, or mixed-layer illite-montmorillomite.

Figure 3a,b demonstrates that there are three major divisions of detrital silicate rocks in terms of volumetric clay content: (1) sandstones, 0 - 25%; (2) silty shales and shaly siltstones, which differ texturally only by the presence or absence of fissility, 25 - 50%; and (3) shales, 50 - 100%. There are no constraints on porosity, which can evidently vary from 3 - 20% within each rock type.

CONCLUSIONS

In summary:

(1) P-wave velocity depends on porosity more strongly than on clay content by a factor of 3.6 according to the expression $V_p = -2.4C - 8.6\phi + 5.8$ in fully saturated rocks with crack-like pores at an effective pressure of 400 bars. The ranges of porosity and volume-fraction clay for which the equation is valid are 4 - 20% and 0 - 72%, respectively.

(2) S-wave velocity depends on porosity more strongly than on clay content by a factor of 3.0 according to the expression $V_s = -2.1C - 6.3\phi + 3.7$ under the same conditions specified above.

(3) The equations do not require specification of the location of clays within the rock or specification of mineralogic compositions of the clays.

(4) The large deviations of compressional and shear velocities in St. Peter sandstone from their predicted values suggest that observational and statistical data on pore shapes in rocks may be an important refinement to the results presented here.

The results of this study are preliminary and, thus, require confirmation and refinement by a larger number and spread of data. It is believed that the results from the range of compositions represented by the measurements presented here, including two suites of known petroleum reservoir rocks (Cotton Valley sandstones and Ardmore Basin sandstones), shed new light on the variation of compressional and shear velocities with porosity and clay content, and that the results therefore constitute a useful tool for both seismic exploration and well logging applications.

REFERENCES

Cheng, C.H., and Toksöz, M.N., 1979, Inversion of seismic velocities for the pore aspect ratio spectrum of a rock: J. Geophys. Res., Vol. 84, p. 7533-7543.

DeMartini, D.C., Beard, D.C., Danburg, J.S., and Robinson, J.H., 1976, Variations of seismic velocities in sandstones and limestones with lithology and pore fluid at simulated in situ conditions: Proc. E.G.P.C. Exploration Seminar (Nov. 15-17, 1976).

Eshelby, J.D., 1957, The determination of the elastic field of an ellipsoidal inclusion, and related problems: Proc. Roy. Soc., Ser. A., Vol. 241, p. 376.

Geertsma, J., 1961, Velocity-log interpretation; the effect of rock bulk compressibility: Soc. Petroleum Engr. Jour., p. 235-248.

King, M., 1966, Wave velocities in rocks as a function of changes in overburden pressure and pore fluid saturants: Geophysics, Vol. 21, p. 50-73.

Kuster, G.T., and Toksöz, M.N., 1974, Velocity and attenuation of seismic waves in two-phase media, I: Theoretical formulations: Geophysics, Vol. 39, p. 587.

Mavko, G.M., and Nur, A.M., 1978, The effect of nonelliptical cracks on the compressibility of rocks: J. Geophys. Res., Vol. 83, p. 4459-4468.

O'Connell, R.J. and Budiansky, B., 1974, Seismic velocities in dry and saturated cracked solids: J. Geophys. Res., Vol. 79, p. 5412-5426.

Paterson, N.R., 1956, Seismic wave propagation in porous granular media: Geophysics, Vol. 21, p. 691-714.

Toksöz, M.N., Cheng, C.H., and Timur, A., 1976, Velocities of seismic waves in porous rocks: Geophysics, Vol. 41, p. 621-645.

Walsh, J.B., and Grosenbaugh, M.A., 1979, A new model for analyzing the effect of fractures on compressibility: J. Geophys. Res., Vol. 84, p. 3532-3536.

Wyllie, M.R.J., Gregory, A.R., and Gardner, G.H.F., 1958, An experimental investigation of factors affecting elastic wave velocities in porous media: Geophysics, Vol. 23, p. 459-493.

FIGURE AND TABLE CAPTIONS

FIGURE 1. Compressional velocities as a function of confining pressure in fully brine- or water-saturated samples. Note the flattening of the St. Peter sandstone curve above 350 bars.

FIGURE 2. (A) Compressional, (B) Shear velocity as a function of clay content and porosity at P_c = 800 bars, P_p = 400 bars in brine- or water-saturated samples. Solid diamonds represent new data; open diamond is St. Peter sandstone; open circles are the data of DeMartini, et al., (1976).

FIGURE 3. Regions of sandstones, siltstones-silty shales, and shales defined for (A) compressional, and (B) shear velocity plots of Figure 1.

FIGURE 4. Scanning electron photomicrographs showing pore shapes and clay textures: (A) Bandera sandstone; (B) Cotton Valley silty shale #3; (C) Cotton Valley sandstone #3; (D) Berea sandstone; (E) St. Peter sandstone; (F) Beth Elkhorn Pike shale.

FIGURE 5. Thin-section photomicrographs in plane-polarized light. Long dimension of photographs is 2.5 mm. Black areas are predominantly clay. (A) Pierre shale; (B) Cotton Valley siltstone #2; (C) Bandera sandstone; (D) Berea sandstone.

TABLE 1. Sample descriptions: Cores 1-11 were fully saturated, degassed water or 2N NaCl brine. Pierre shale was recovered saturated with connate fluid. Descriptions of the Ardmore Basin sandstones and siltstones are from DeMartini, et al., (1976). Locations of clay grains in the rock frameworks were determined from textures of minerals in SEM photographs. Clays which occupy free pore space are defined by us to be authigenic in origin; those which occupy framework contact zones are allogenic.

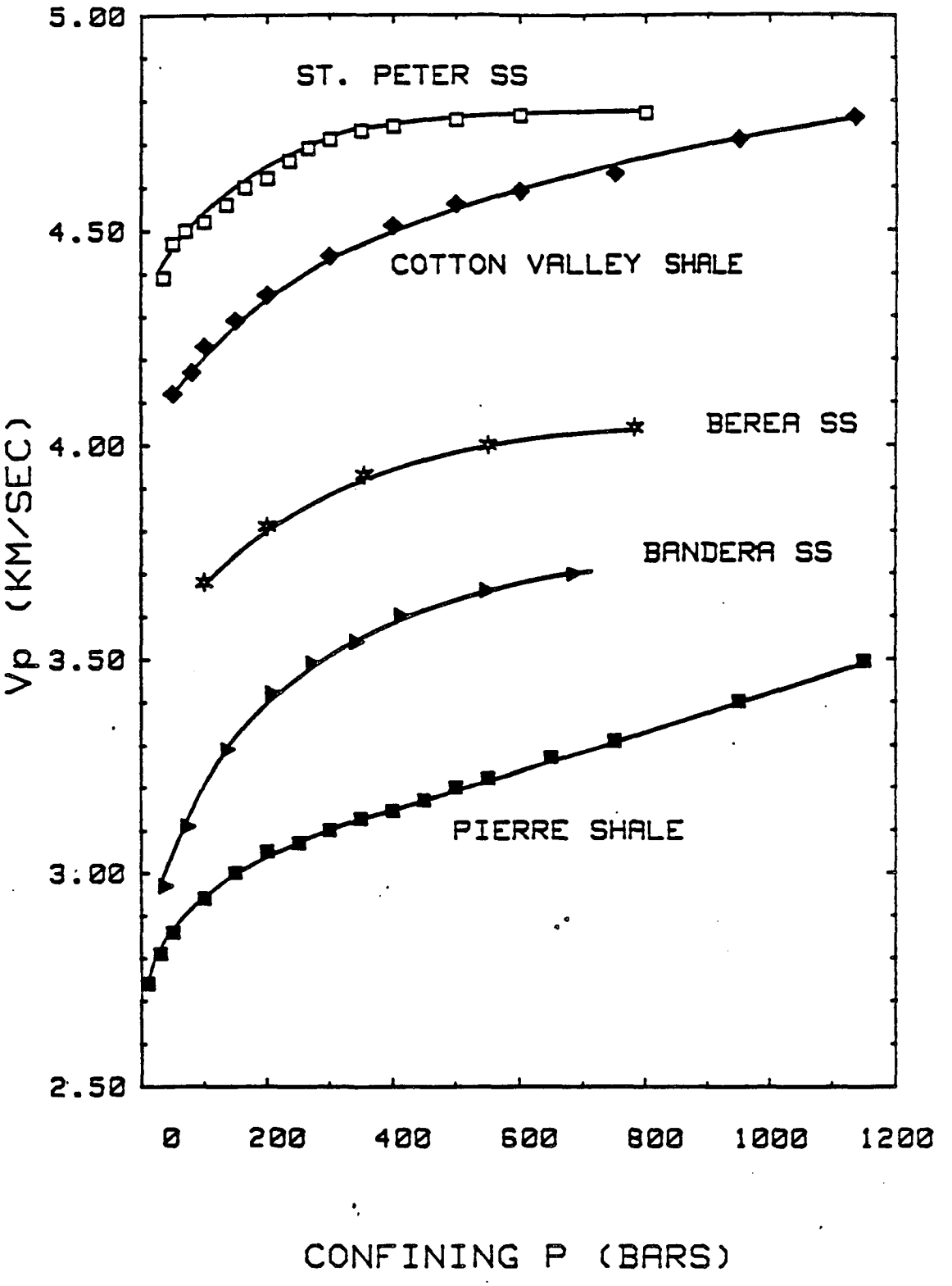
5.00
4.50
4.00
3.50
3.00
2.50
Vp (KM/SEC)
ST. PETER SS
COTTON VALLEY SHALE
BEREA SS
BANDERA SS
PIERRE SHALE
0
200
400
600
800
1000
1200
CONFINING P (BARS)

FIGURE 1

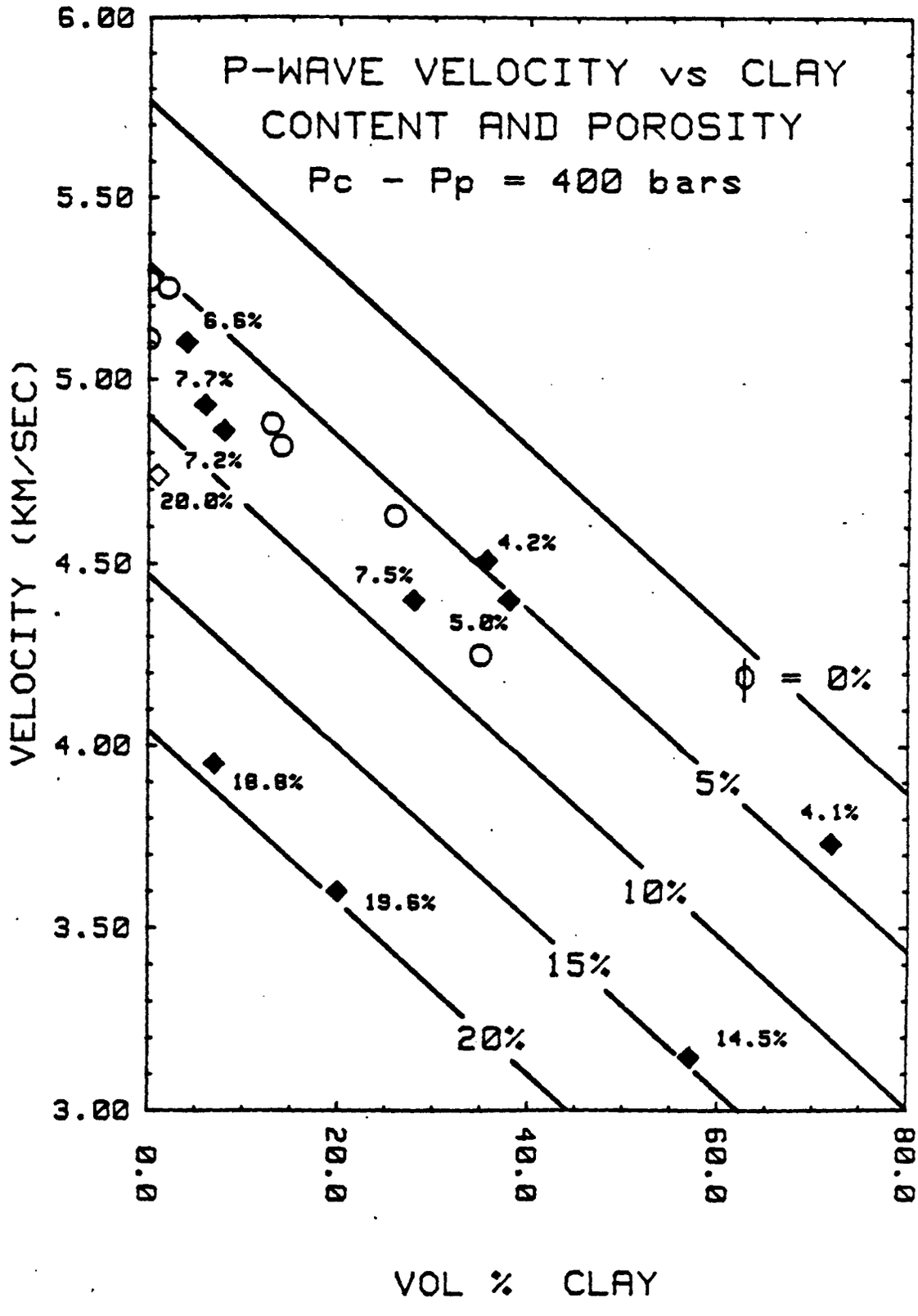
P-WAVE VELOCITY vs CLAY CONTENT AND POROSITY
Pc - Pp = 400 bars
VELOCITY (KM/SEC)
6.00
5.50
5.00
4.50
4.00
3.50
3.00
0.0
20.0
40.0
60.0
80.0
VOL % CLAY
6.6%
7.7%
7.2%
20.0%
4.2%
7.5%
5.0%
18.8%
19.6%
4.1%
14.5%
ϕ = 0%
5%
10%
15%
20%

FIGURE 2a

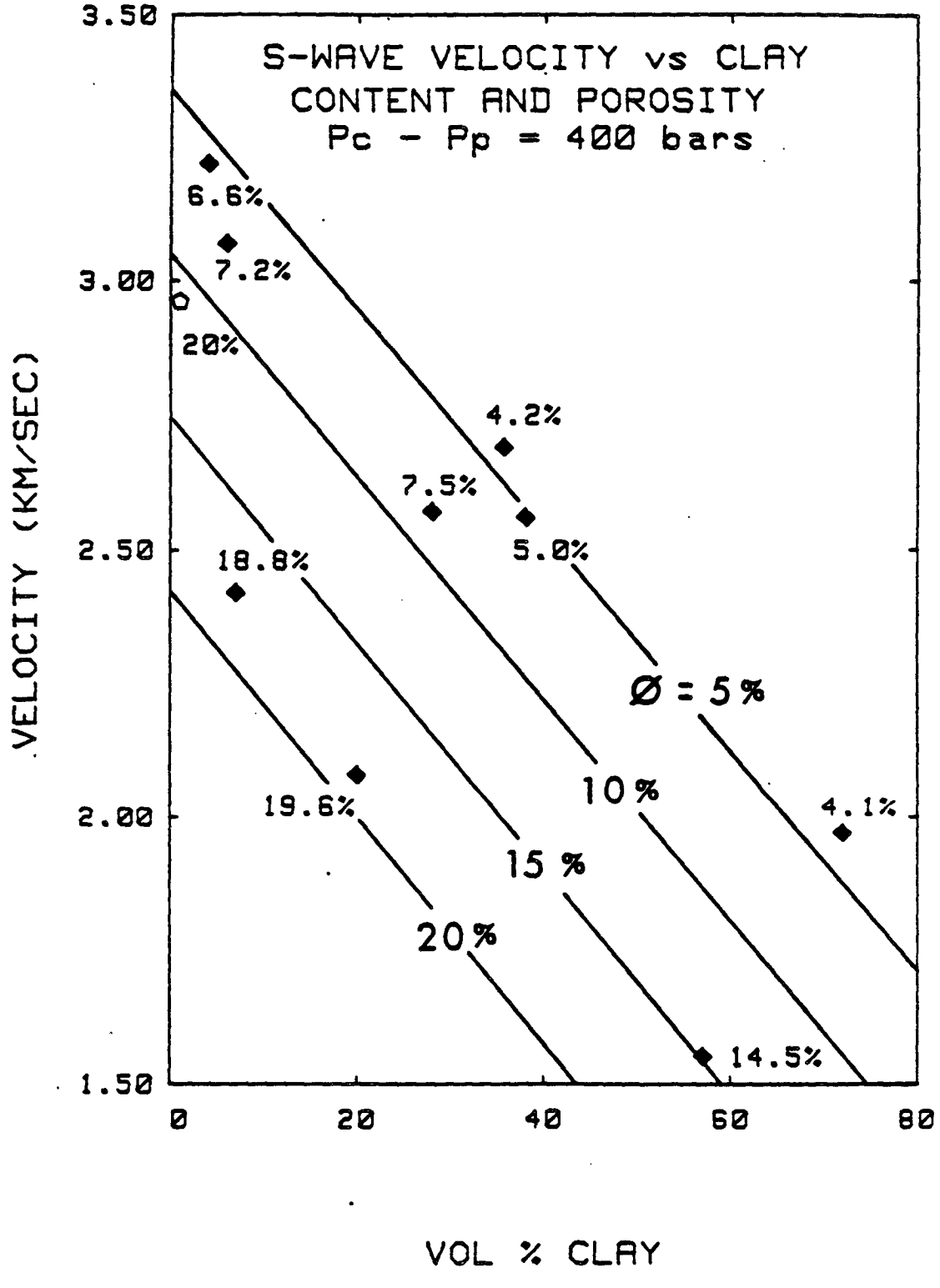
S-WAVE VELOCITY vs CLAY
CONTENT AND POROSITY
Pc - Pp = 400 bars
3.50
3.00
2.50
2.00
1.50
VELOCITY (KM/SEC)
0
20
40
60
80
VOL % CLAY
6.6%
7.2%
20%
4.2%
7.5%
5.0%
18.8%
19.6%
4.1%
14.5%
Ø = 5%
10%
15%
20%

FIGURE 2b

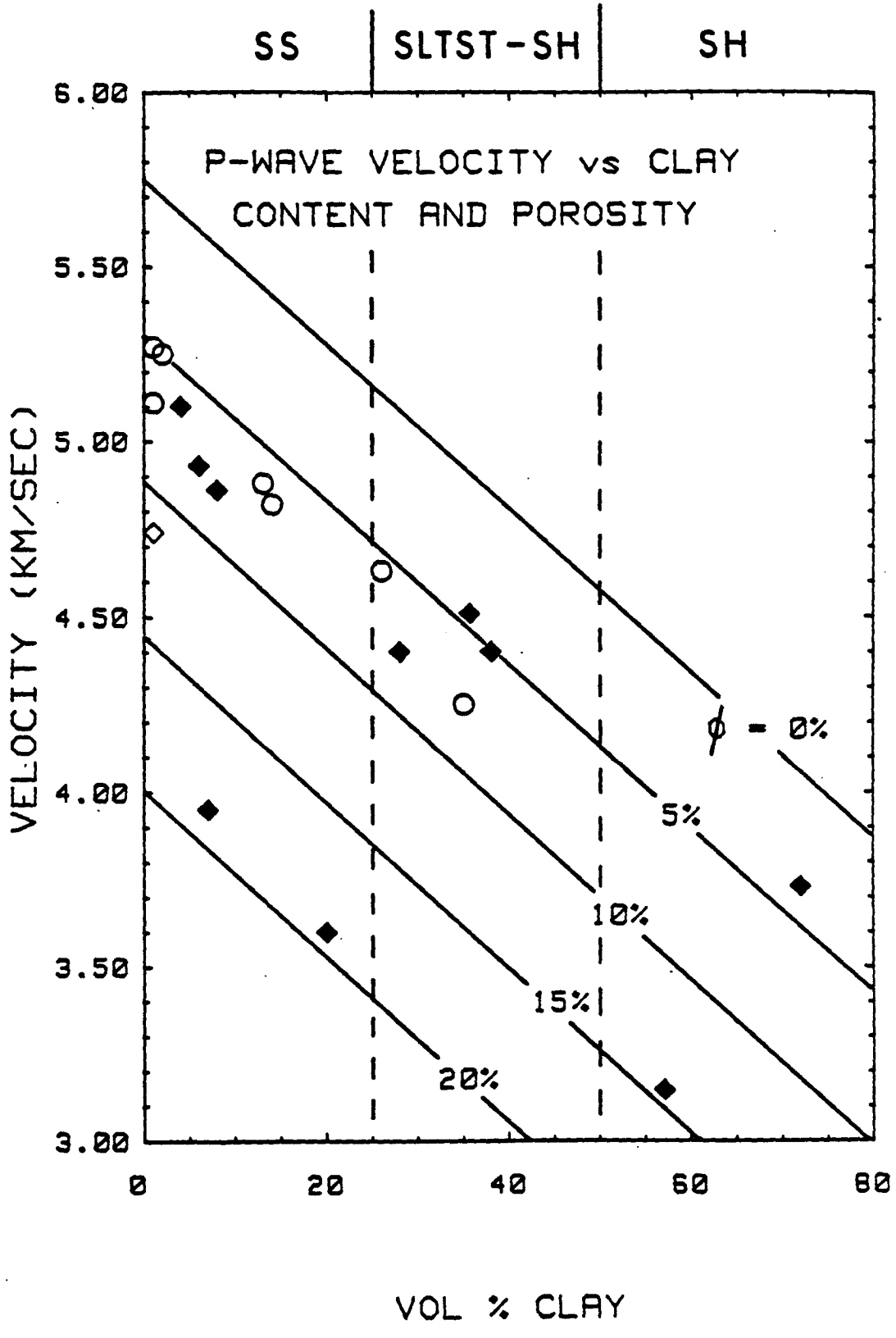
SS
SLTST-SH
SH
P-WAVE VELOCITY vs CLAY
CONTENT AND POROSITY
VELOCITY (KM/SEC)
6.00
5.50
5.00
4.50
4.00
3.50
3.00
0
20
40
60
80
ϕ = 0%
5%
10%
15%
20%
VOL % CLAY

FIGURE 3a

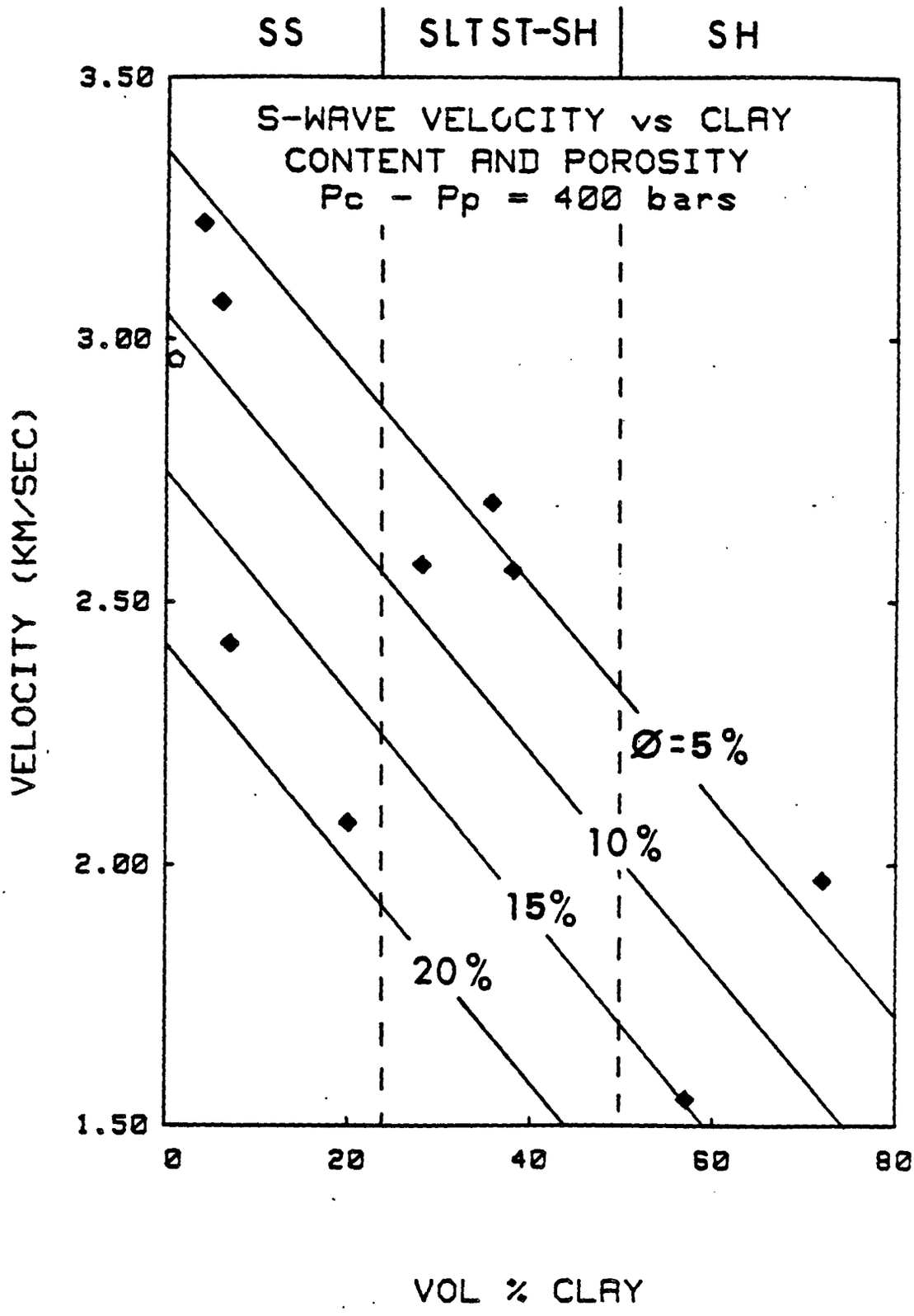
SS
SLTST-SH
SH
S-WAVE VELOCITY vs CLAY CONTENT AND POROSITY
Pc - Pp = 400 bars
3.50
3.00
2.50
2.00
1.50
VELOCITY (KM/SEC)
Ø=5%
10%
15%
20%
0
20
40
60
80
VOL % CLAY

FIGURE 3b

Figure 4

Page 95

Figure 5

SAMPLE NUMBER	ROCK NAME	VOLUME FRACTION PORES	VOLUME FRACTION CLAY	P-WAVE VELOCITY AT P_c = 800 BARS P_p = 400 BARS (KM/SEC)	DOMINANT CLAY MINERAL	LOCATION OF CLAY GRAINS	SATURANT
1	Berea Sandstone	.188	.07	3.95	Illite	Pores	Water
2	Bandera Sandstone	.196	.20	3.60	Kaolinite	Pores + Contacts	2N NaCl Brine
3	St. Peter Sandstone	.200	<.01	4.74			Water
4	Cotton Valley Sandstone #1	.066	.04	5.10	Illite	Pores	Water
5	Cotton Valley Sandstone #2	.077	.06	4.93	Illite	Pores	Water
6	Cotton Valley Sandstone #3	.072	.08	4.86	Illite	Pores	Water
7	Cotton Valley Silty Shale #1	.075	.28	4.40	Illite	Contacts	Water
8	Cotton Valley Silty Shale #2	.042	.357	4.51	Illite	Contacts	Water
9	Cotton Valley Silty Shale #3	.050	.38	4.40	Illite	Contacts	Water
10	Pierre Shale	.145	.57	3.14	Mixed-Layer Illite-Montmorillonite	Contacts	Connate Brine
11	Beth Elkhorn Shale	.041	.72	3.73	Illite and Chlorite	Contacts	Water
12	Ardmore Basin Sandstone #1		0	5.27		Unknown	Brine
13	Ardmore Basin Sandstone #2		.02	5.25	Unknown	Unknown	Brine
14	Ardmore Basin Sandstone #3		0	5.11	Unknown	Unknown	Brine
15	Ardmore Basin Sandstone #4	~ .05	.13	4.88	Unknown	Unknown	Brine
16	Ardmore Basin Sandstone #5		.14	4.82	Unknown	Unknown	Brine
17	Ardmore Basin Siltstone #1		.26	4.63	Unknown	Unknown	Brine
18	Ardmore Basin Siltstone #2		.35	4.25	Unknown	Unknown	Brine

TABLE 1

V. ACOUSTICAL ANISOTROPY OF COTTON VALLEY SHALE

To be presented at the Society of Petroleum Engineers International Meeting, New Orleans, September 1982.

To be submitted to Geophysics.

ABSTRACT

The dynamic elastic stiffnesses of transversely isotropic Cotton Valley silty shale were computed from ultrasonic-frequency compressional- and shear-wave velocity measurements. The measurements were made in three oriented right cylinders of fully water-saturated shale. Confining pressure was varied to 1100 bars for a constant pore pressure of 50 bars.

All velocities and corresponding elastic stiffnesses increased with differential pressure in a manner that suggested continuous closure of pores and cracks and increasing alignment of platy clay particles with pressure. In addition, elastic anisotropy was found to increase with stress level, evidently approaching the intrinsic anisotropy of the zero-porosity, statistically weighted, aggregated volume fraction of the dominant clay mineral.

Expressions for the elastic stiffnesses were derived for the boundary-value problem of plane strain, the conditions for which are approximated by wave-propagation measurements using an ultrasonic-frequency, pulse-transmission technique.

INTRODUCTION

In recent years seismologists have become increasingly interested in the acoustical properties of clay-bearing rocks. The continued development of high-resolution seismic-processing techniques for locating and evaluating petroleum reservoirs and subsurface stratigraphy has necessitated detailed, accurate knowledge about the response of rocks to acoustic-wave disturbances. Particular interest has focused on the evaluation of elastic coefficients of anisotropic rocks in order to correct for tilted formations or horizontally bounded, intrinsically anisotropic units.

It is well documented that treatment of the earth's crust as an elastically isotropic medium yields results that are erroneous in the evaluation of media that are not isotropic on the wavelength scales of seismic or sonic exploration tools. Descriptions of elastic-wave propagation in transversely isotropic media based on periodic layering of isotropic media range from the zero-porosity models of Voigt and Reuss (Dieter, 1961) to various long-wavelength, grossly homogeneous, anisotropic-equivalent, lamellae-stacking theories including those of Postma (1955), Rytov (1956), Helbig (1981), Backus (1962), Anderson (1961), Uhrig and Van Melle (1955), and Love (1934). Although these models of long-wave equivalents to horizontally layered isotropic media adequately describe observed crustal anisotropies due to layering of isotropic materials, large errors result when they are applied to intrinsically anisotropic materials such as shales.

Strict control of significant parameters in laboratory studies provides a highly useful means of assessing the influence of subsurface environmental conditions on the physical properties of rocks. Direct measurement of directional elastic-wave propagation properties in shales is the most

accurate non-destructive method of determining the elastic coefficients of intrinsically anisotropic media. Data from studies of this kind provide widely applicable, realistic values of acoustical anisotropy over a range of simulated in situ conditions.

The sample selected for this study is well consolidated, fissile, homogeneous, silty Cotton Valley shale. Mineralogically, it is composed of 50% quartz, 10% feldspar, 36% clay — predominantly illite — and minor amounts of calcite, siderite, and pyrite. It was recovered from a depth of 9630 feet in eastern Texas.

The validity of treating well-consolidated shales as elastic bodies is justified by the in situ measurements of McDonal, et al., (1958). Attenuation measurements on Pierre shale near Limon, Colorado, indicated that at depths of 350 to 750 feet the Cretaceous shale behaved elastically rather than visco-elastically as had been suggested by Ricker (1953) in a previous study.

STRESS-STRAIN RELATIONS FOR GENERALIZED ANISOTROPIC MEDIA

The generalized form of Hooke's law for continuous anisotropic bodies may be written

$$\sigma_{ij} = c_{ijkl}\,\varepsilon_{kl} \tag{1}$$

where the c_{ijkl} are components of a fourth-rank elastic stiffness tensor that linearly relate each component of homogeneous stress, σ_{ij}, to all components of homogeneous strain, ε_{kl}, and the subscripts i, j, k, l refer to coordinate areas X_1, X_2, X_3. Therefore, (1) represents nine equations, each with nine terms on the right-hand side, and there are 81 coefficients in c_{ijkl}.

Alternatively, the strains may be expressed in terms of the stresses:

$$\varepsilon_{ij} = s_{ijkl}\,\sigma_{kl} \tag{2}$$

where the s_{ijkl} are 81 components of the elastic compliance tensor. The s_{ijkl} and the c_{ijkl} have different physical meanings in the expressions of the generalized Hooke's law and apply to different boundary-value conditions. Displacement constraints consistent with the criteria for generalized plane strain require solutions for non-vanishing components of the stress tensor in the form of Equations (1). Stress constraints that conform to the criteria for generalized plane stress lead to solutions for non-vanishing components of the strain tensor in the form of Equations (2). However, as far as the governing equations are concerned, plane strain differs from plane stress only in the values of the constant coefficients: symmetry arguments that apply to the c_{ijkl} apply equally to the s_{ijkl}. Since it is easier to

visualize the physical nature of equations (2), symmetry arguments that will reduce the number of independent elastic compliances and stiffnesses will be developed for these relations.

If a shear stress, σ_{ij}, $i \neq j$, is applied to a body, the requirement that body torques not exist dictates that σ_{ij} cannot be applied without σ_{ji}. Therefore, the components

$$s_{ijkl} = s_{klij} \tag{3}$$

must be set equal. If a uniaxial tension is applied parallel to coordinate axis X_3, two particular components of strain are given by

$$\varepsilon_{12} = s_{1233}\,\sigma_{33} \text{ and } \varepsilon_{21} = s_{2133}\,\sigma_{33} \,. \tag{4}$$

However, since $\varepsilon_{12} = \varepsilon_{21}$ it follows that $s_{1233} = s_{2133}$ and, generalizing,

$$s_{ijkl} = s_{jilk} \tag{5}$$

Similarly,

$$c_{ijkl} = c_{jilk} \tag{6}$$

Thus, from relations (3) and (5), only 36 of the 81 components of s_{ijkl} and c_{ijkl} are independent. Similar developments can be found in Lekhnitskii (1963), Nye (1972), Leipholz (1974), Sokolnikoff (1956), Boas and Mackenzie (1950), Hearmon (1961), and Jaeger (1962).

Symmetry of the first two and the last two suffixes of the c_{ijkl} and the s_{ijkl} allows a reduction in the number of subscripts through replacement of tensor notation by matrix notation. (1) and (2) take the forms

$$\sigma_i = c_{ij}\,\varepsilon_j \tag{7}$$

$$\varepsilon_i = s_{ij}\,\sigma_j \tag{8}$$

where i, j = 1,2,3,...6 according to the substitutions

$$\begin{bmatrix} \sigma_{11} & \sigma_{12} & \sigma_{13} \\ \sigma_{21} & \sigma_{22} & \sigma_{23} \\ \sigma_{31} & \sigma_{32} & \sigma_{33} \end{bmatrix} \rightarrow \begin{bmatrix} \sigma_1 & \sigma_6 & \sigma_5 \\ \sigma_6 & \sigma_2 & \sigma_4 \\ \sigma_5 & \sigma_4 & \sigma_3 \end{bmatrix}$$

$$\begin{bmatrix} \varepsilon_{11} & \varepsilon_{12} & \varepsilon_{13} \\ \varepsilon_{21} & \varepsilon_{22} & \varepsilon_{23} \\ \varepsilon_{31} & \varepsilon_{32} & \varepsilon_{33} \end{bmatrix} \rightarrow \begin{bmatrix} \varepsilon_1 & \tfrac{1}{2}\varepsilon_6 & \tfrac{1}{2}\varepsilon_5 \\ \tfrac{1}{2}\varepsilon_6 & \varepsilon_2 & \tfrac{1}{2}\varepsilon_4 \\ \tfrac{1}{2}\varepsilon_5 & \tfrac{1}{2}\varepsilon_4 & \varepsilon_3 \end{bmatrix} \tag{9}$$

Also, $s_{ij} = s_{mnop}$ if i and j = 1,2,3

$s_{ij} = 2\,s_{mnop}$ if i or j = 4,5,6

$s_{ij} = 4\,s_{mnop}$ if i and j = 4,5,6

in order to avoid the appearance of 2's and 4's in (8). Thus, the 36 components of the s_{ij} and the c_{ij} arrays are written out

$$\begin{pmatrix} s_{11} & s_{12} & s_{13} & s_{14} & s_{15} & s_{16} \\ s_{21} & s_{22} & s_{23} & s_{24} & s_{25} & s_{26} \\ s_{31} & s_{32} & s_{33} & s_{34} & s_{35} & s_{36} \\ s_{41} & s_{42} & s_{43} & s_{44} & s_{45} & s_{46} \\ s_{51} & s_{52} & s_{53} & s_{54} & s_{55} & s_{56} \\ s_{61} & s_{62} & s_{63} & s_{64} & s_{65} & s_{66} \end{pmatrix} \tag{10a}$$

$$\begin{pmatrix} c_{11} & c_{12} & c_{13} & c_{14} & c_{15} & c_{16} \\ c_{21} & c_{22} & c_{23} & c_{24} & c_{25} & c_{26} \\ c_{31} & c_{32} & c_{33} & c_{34} & c_{35} & c_{36} \\ c_{41} & c_{42} & c_{43} & c_{44} & c_{45} & c_{46} \\ c_{51} & c_{52} & c_{53} & c_{54} & c_{55} & c_{56} \\ c_{61} & c_{62} & c_{63} & c_{64} & c_{65} & c_{66} \end{pmatrix} .$$

Further reduction in the number of independent elastic constants for the most general case of elastic anisotropy comes from a consideration of potential strain energy under reversible isothermal or adiabatic conditions such that work done by stress components σ_i acting on the cube faces of a unit cube subjected to infinitesimal homogeneous strains with components $d\varepsilon_i$ is equal to the increase in free energy per unit volume, $d\Psi$:

$$d\Psi = dW = \sigma_i d\varepsilon_i \quad i = 1,2,\ldots 6 \ . \tag{11}$$

In tensor notation the corresponding equation is:

$$dW = \sigma_{ij} d\varepsilon_{ij} \qquad i,j = 1,2,3 \ . \tag{12}$$

If Hooke's law (7) governs the behavior, then

$$d\Psi = c_{ij}\varepsilon_j d\varepsilon_j \tag{13}$$

and $$\frac{\partial \Psi}{\partial \varepsilon_j} = c_{ij}\varepsilon_j \ . \tag{14}$$

Differentiating both sides with respect to ε_j yields

$$\frac{\partial}{\partial \varepsilon_j}\left(\frac{\partial \Psi}{\partial \varepsilon_i}\right) = c_{ij} \ . \tag{15}$$

Since Ψ is a single valued function of the components of the strain tensor, the order of differentiation of the left side of equation (15) is symmetrical with respect to i and j:

$$c_{ij} = c_{ji} \tag{16}$$

$$s_{ij} = s_{ji} \ . \tag{17}$$

The arrays (10) are symmetrical about the leading diagonal reducing the number of independent elastic coefficients to 21. Following the equilibrium arguments of Nye (1972), the elastic strain energy, obtained by integrating (13) and using the equality (16), is

$$\tfrac{1}{2}\, c_{ij}\varepsilon_i\varepsilon_j \tag{18}$$

defined as the work necessary to produce a strain ε_i per unit volume. For stability of the body, the quadratic form of (18) must be positive definite, i.e., greater than zero for all real values of ε_{ij} not equal to zero. This stipulation leads to restrictions on the c_{ij} which, for hexagonal symmetry (transverse isotropy) are:

$$c_{44} > 0$$

$$c_{11} > |c_{12}| \tag{19}$$

$$(c_{11} + c_{12})\, c_{13} > 2\, c_{13}^2$$

The s_{ij} are subject to the same restrictions.

STRESS-STRAIN RELATIONS FOR TRANSVERSELY ISOTROPIC MEDIA

Symmetry elements in the material further reduce the number of independent elastic coefficients. A transversely isotropic or hexagonally symmetric body contains one axis of rotational symmetry, z, oriented such that material properties are the same in all directions perpendicular to it, with the orthogonal plane of circular symmetry defined by the x- and y-axes. In this case the same system of equations must be obtained for reversal of direction of the z-axis and for rotations of the x- and y-axes through any angle about z (e.g., Jaeger; 1962). Expanding (7) and eliminating the algebra:

$$\begin{aligned}
\sigma_1 &= c_{11}\varepsilon_1 + c_{12}\varepsilon_2 + c_{13}\varepsilon_3 \\
\sigma_2 &= c_{12}\varepsilon_1 + c_{11}\varepsilon_2 + c_{13}\varepsilon_3 \\
\sigma_3 &= c_{13}\varepsilon_1 + c_{13}\varepsilon_2 + c_{33}\varepsilon_3 \\
\sigma_4 &= c_{44}\varepsilon_4 \\
\sigma_5 &= c_{44}\varepsilon_5 \\
\sigma_6 &= \tfrac{1}{2}(c_{11}-c_{12})\,\varepsilon_6 \quad .
\end{aligned} \tag{20}$$

Thus, there are five independent, nonzero coefficients, with $c_{66} = \frac{1}{2}(c_{11}-c_{12})$.

$$\begin{pmatrix}
c_{11} & c_{12} & c_{13} & & & \\
c_{12} & c_{11} & c_{13} & & & \\
c_{13} & c_{13} & c_{33} & & & \\
 & & & c_{44} & & \\
 & & & & c_{44} & \\
 & & & & & c_{66}
\end{pmatrix} \tag{21}$$

Hooke's law in the form of equations (8) is valid for boundary-value problems conforming to the generalized state of plane stress, as approximated by low-frequency, resonant-bar techniques for wave-propagation studies.

Hooke's law in the form of equations (7) is valid for the boundary-value problem of the generalized state of plane strain. As stipulated by Leipholz (1974), a body in plane strain is characterized by the assumption that displacement U_z is zero and that the nonzero displacements are functions of x and y only:

$$U_z = 0, \quad U_x = U_x(x,y), \quad U_y = U_y(x,y) \quad . \tag{22}$$

Plane-strain conditions are approximated by wave propagation by ultrasonic-frequency, pulse-transmission techniques. Velocities under these conditions are given by:

$$V_{PL} = V_{33} = \sqrt{\frac{C_{33}}{\rho}}$$

$$V_{P||} = V_{11} = V_{22} = \sqrt{\frac{C_{11}}{\rho}}$$

$$V_{SHL} = V_{31} = V_{32} = \sqrt{\frac{C_{44}}{\rho}} = V_{SV||} = V_{13}$$

$$V_{SH||} = V_{12} = \sqrt{\frac{C_{66}}{\rho}} \tag{23}$$

$$V_{p45^\circ} = \left[\frac{C_{11} + C_{33} + 2C_{44} + (C_{11} - C_{33})^2 + (C_{13} + C_{44})^2}{4\rho} \right]^{1/2}$$

Velocity notations are as labeled in Figure 1. The first numerical subscript refers to the direction of wave propagation; the second subscript denotes the direction of particle displacement.

EXPERIMENT DESCRIPTION

From equations (23) it is evident that determination of the five independent elastic stiffnesses for a hexagonally symmetrical medium by an ultrasonic, pulse-transmission technique requires velocity measurements in three directions. The directions of wave propagation must correspond to: (1) the normal to the plane of circular symmetry, (2) an axis in the plane of circular symmetry with shear-disturbance particle vibration normal to stratification and parallel to stratification, and (3) an axis at an angle to the plane stratification such that $0 < \theta < 90$. Algebraic computations are simplified for an axis oriented 45° to the plane of circular symmetry. Three cores of fissile, silty Cotton Valley shale were cut with the cylindrical axes corresponding to the required orientations. Each core measured 25.4 mm in diameter and 14.6 mm in length with ends flat and parallel to within .05 mm.

The cores were evacuated for two weeks at 40°C, 760 mm Hg vacuum. They were then transferred to a saturating vessel, re-evacuated at 20°C, 760 mm Hg vacuum, and then flooded with degassed, deionized water at a pressure of 250 bars for a period of several days to assure full saturation. After the sample was jacketed and assembled in the pressure vessel the pore-pressure lines were evacuated and then flooded with degassed, deionized water. It is well documented that acoustic measurements in rocks are sensitive to the presence of small volumes of free gas in the pore space (Domenico, 1976; Gregory, 1976).

Measurements were conducted at room temperature under conditions of separately applied and controlled pore pressure (P_p) and confining pressure (P_c). The confining medium was a dielectric silicone fluid of 200

centistokes viscosity. For each core, velocities were measured as functions of differential pressure, $\Delta P = P_c - P_p$, at a constant pore pressure of 50 bars. Fifty bars of pore pressure was sufficient to maintain full water saturation with the absence of a free gas phase in the pore fluid.

P-wave and S-wave velocities were calculated from measurements of first-arrival, transient-pulse, travel times through the cores. The driver and receiver piezoelectric transducer arrays were stacked composites consisting of a longitudinally polarized disc atop a shear-polarized plate. The material for all transducers was a lead-zirconium-titanate ceramic, PZT-5A. The transducer composites were epoxied to titanium endplug/buffer rods.

Frequency, amplitude, pulse width, and repetition rate of the input pulses were optimized to reduce scattering, diffraction, and reflection effects and to maximize definition of the first-arrival. Refer to Tosaya (1982) for a detailed review of optimal pulse parameters and sample dimensions. There are primarily three factors contributing to errors in the velocity calculations: (1) errors in determining sample length, (2) errors in time measurements of received pulses, and (3) imperfect coupling between the transducer holders and the sample. After all sources of error were considered, it was found that longitudinal- and shear-wave velocities could be determined to better than 2% and 3%, respectively.

RESULTS AND DISCUSSION

Figure 2 presents the verification of transverse isotropy for Cotton Valley shale. Measurements of compressional- and torsional-wave velocities made on a vacuum-dry core under small, constant uniaxial loading demonstrate that velocities do not vary with direction in the plane of circular symmetry. Compressional velocity is significantly higher in the plane of fissility than in the direction orthogonal to it which is consistent with the weakness of interlayer O-OH bonding in clay particles compared to intralayer O-O bonding. See Lambe and Whitman (1969), Mitchell (1976), and Van Olphen (1977) for discussions of interionic bonding in crystal structures of clays. Tosaya (1982) discusses the effects of interlayer bonding and pore-fluid/clay interactions on wave attenuation in shales. The measured P-wave velocity anisotropy is

$$\frac{V_{33}-V_{11}}{V_{33}} = 60\% \quad . \tag{24}$$

Simultaneous measurements of torsional velocity yield an anisotropy of

$$\frac{V_{t3}-V_{t1}}{V_{t3}} = 25\% \tag{25}$$

Because of symmetry constraints, the velocity of a torsional wave propagating in the X_3 direction is equivalent to the velocity of pure-shear waves travelling in the same direction:

$$V_{t3} = V_{31} = V_{32} \quad . \tag{26}$$

However, the velocity of a torsional wave propagating normal to the axis of circular symmetry has components of pure shear parallel and normal to the plane of fissility. From Hearman (1961) and Duvall (1965):

$$V_{t1} = V_{t2} = \sqrt{\frac{\overline{G}_1}{\rho}} \qquad (27)$$

where $\overline{G}_1$, the average modulus of rigidity, is

$$\overline{G}_1 = \frac{2G_{12}G_{13}}{G_{12}+G_{13}} \quad . \qquad (28)$$

The scanning-electron photomicrographs of Figure 3 permit direct inspection of the high degree of preferred orientation of clay platelets that is texturally characteristic of homogeneous, consolidated, fissile shales. Dominance of the platy clay morphologies in determining the texture of a shale is evidently valid over a large range of volumetric clay contents. The clays in all three shales of Figure 3 are primarily illitic in composition, but clay content by volume varies from 35% in the Cotton Valley sample (Figure 3A,B) to 72% in the Beth Elkhorn shale (Figure 3E,F). Pierre shale (Figure 3C,D) is intermediate with 57% clay. These photographs suggest that 35% clay is sufficient to encapsulate detrital minerals with more equant grain morphologies. Indeed, the thin-section photomicrographs of Cotton Valley silty shale (Figure 4) clearly indicate that the detrital quartz grains are suspended in a clay matrix.

The directional velocity data for fully water-saturated cores of Cotton Valley shale are presented in Figure 5. All velocities increase with

differential pressure with corresponding increases in Young's and shear moduli. Two important observations can be made from these data. The first is that velocity anisotropy, $\frac{V_{33}-V_{11}}{V_{33}}$ and $\frac{V_{12}-V_{31}}{V_{12}}$, increases with increasing stress level.

The second observation is that the slopes of the compressional-wave velocity curves do not level off at high differential pressures, an effect that is in marked contrast to P-wave velocity behavior in sandstones (Figure 6). Jones and Wang (1981) presented P-wave velocity data for undrained samples of Pierre shale that showed a high, positive, linear response to confining pressures up to 4 kilobars. The contrasting velocity responses of saturated sandstones and shales to increasing differential pressure, $\frac{\partial V_p}{\partial P_c}\Big|_{P_p}$, reflect continuous closure of pores and cracks with pressure in shales as well as increased alignment of clay grains in the plane of low shear resistance — the plane of fissility. Comprehensive discussion of these effects can be found in Tosaya (1982). The result of continuous pore closure and increased grain alignment is increased development of the degree of preferred orientation of clay grains with increasing differential pressure. If the individual clay platelets were isotropic rather than hexagonally anisotropic, then the effect of increasing differential pressure would be to increase physical and acoustical isotropy of the rock because continuous closure of pores would lead to homegenization of the medium. However, since the individual clay platelets are highly anisotropic, the physical and acoustical anisotropy of shales is expected to increase with depth or differential pressure until the intrinsic anisotropy of the zero-porosity, statistically weighted volume fraction of the dominant clay mineral is reached. Clays in the Cotton Valley samples are primarily illitic in structure. Data on the intrinsic elastic anisotropy of illite are not

available; however, the crystallographic structure of illite is similar to that of muscovite, for which the intrinsic velocity anisotropy, $\frac{V_{33}-V_{11}}{V_{33}}$, is 80% (Simmons and Wang, 1971). Jones and Wang (1981) found that the velocity anisotropy of Pierre shale recovered from a depth of 5000 feet was higher than the anisotropy of a sample recovered from a depth of 3000 feet. Kaarsberg (1959) found that anisotropy increased with compaction in natural and artificial argillaceous aggregates. The data of Figure 5 indicate that the maximum velocity anisotropies attained in saturated cores of Cotton Valley shale over the pressure range of this experiment were 13% and 19% for P and S, respectively.

Values of the five independent elastic stiffnesses ($C_{66} = \frac{1}{2}(C_{11}-C_{12})$) corresponding to the measured velocities are presented in Figure 7. Maximum anisotropy of the elastic stiffnesses in the pressure range of this experiment are 27% and 30% for $\frac{C_{11}-C_{33}}{C_{33}}$ and $\frac{C_{66}-C_{44}}{C_{44}}$, respectively.

CONCLUSIONS

The foregoing discussion indicates that:

(1) Acoustical and physical anisotropy in homogeneous, well consolidated Cotton Valley shale increases with stress level due to continuous closure of pores and cracks and to increased alignment of clay grains. This result is consistent with the observations of Jones and Wang (1981) for measurements in Pierre shale, but contrary to the findings of Podio, et al., (1968) for laminated, poorly consolidated Green River shale.

(2) Fissility may be well developed in shales with relatively low clay contents such as Cotton Valley silty shale.

(3) Once transverse isotropy has been established, the five independent elastic stiffnesses may be determined from ultrasonic-frequency velocity measurements in three oriented cylindrical cores.

(4) Boundary values consistent with the use of Hooke's law in the form $\varepsilon_{ij} = s_{ijkl}\sigma_{kl}$ correspond to generalized plane-stress conditions, approximated by resonant-frequency, long-bar acoustical measurements.

(5) Boundary values consistent with the use of Hooke's law in the form $\sigma_{ij} = c_{ijkl}\varepsilon_{kl}$ correspond to plane-strain restrictions, approximated ultrasonic-frequency, transient-pulse, short-core acoustical measurements.

REFERENCES

Anderson, D.L., 1961, Elastic wave propagation in layered anisotropic media: J. Geophys. Res., Vol. 66, p. 2953-2963.

Backus, G.E., 1962, Long-wave elastic anisotropy produced by horizontal layering: J. Geophys. Res., Vol. 67, p. 4427-4440.

Boas, W., and Mackenzie, J.K., 1950, Anisotropy in metals: in Chalmers, ed., Progress in Metals 2, Interscience Publishers, Inc., New York, p. 90-120.

Dieter, G.E., Jr., 1961, Mechanical Metallurgy, McGraw-Hill Book Co., New York, 615 pp.

Domenico, S.N., 1976, Effect of brine-gas mixture on velocity in an unconsolidated sand reservoir: Geophysics, Vol. 41, p. 882-894.

Duvall, W.I., 1965, The effect of anisotropy on the determination of dynamic argillaceous aggregates by sound-propagation and x-ray diffraction methods: J. Geol., Vol. 67, p. 447-472.

Gregory, A.R., 1976, Fluid saturation effects on dynamic elastic properties of sedimentary rocks: Geophysics, Vol. 41, p. 895-921.

Hearmon, R.F.S., 1961, An introduction to Applied Anisotropic Elasticity, Oxford University Press, 136 pp.

Helbig, K., 1981, Systematic classification of layer-induced transverse isotropy: Geophys. Prospecting, Vol. 29, p. 550-577.

Jaeger, J.C., 1962, Elasticity, Fracture, and Flow, Second Edition, Methuen and Co., Ltd., London, 208 pp.

Jones, L.E.A., and Wang, H.F., 1981, Ultrasonic velocities in Cretaceous shales from the Williston Basin: Geophysics, Vol. 46, p. 288-297.

Kaarsberg, E.A., 1959, Introductory studies of natural and artificial argillaceous aggregates by sound-propagation and x-ray diffraction methods: J. Geol., Vol. 67, p. 447-472.

Lambe, T.W., and Whitman, R.V., 1969, Soil Mechanics, John Wiley and Sons, New York, 553 pp.

Leipholz, H., 1974, Theory of Elasticity, Noordhoff International Publishing, the Netherlands, 400 pp.

Lekhnitskii, S.G., 1963, Theory of Elasticity of an Anisotropic Elastic Body, Holden-Day, Inc., San Francisco, 404 pp.

McDonal, F.J., Angona, F.A., Mills, R.L., Sengbush, R.L., Van Nostrand, R.G., and White, J.E., 1958, Attenuation of shear and compressional waves in Pierre shale: Geophysics, Vol. 23, p. 421-439.

Mitchell, J.K., 1976, Fundamentals of Soil Behavior, John Wiley and Sons, New York, 422 pp.

Nye, J.F., 1972, Physical Properties of Crystals, Oxford University Press, 322 pp.

Podio, A.L., Gregory, A.R., and Gray, K.E., 1968, Dynamic properties of dry and water-saturated Green River shale under stress: Soc. Petroleum Engr. Jour., Vol. 8, p. 389-404.

Postma, G.W., 1955, Wave propagation in a stratified medium: Geophysics, Vol. 20, p. 780-806.

Ricker, N., 1953, The form and laws of propagation of seismic wavelets: Geophysics, Vol. 18, p. 10-36.

Rytov, S.M., 1956, Acoustical properties of a thinly laminated medium: Soviet Physics — Acoustics, Vol. 2, p. 68-80.

Sokolnikoff, I.S., 1956, Mathematical Theory of Elasticity, Second Edition, McGraw-Hill Book Co., New York, 476 pp.

Tosaya, C.A., 1982, Acoustic identification and detection of abnormal pore pressures in shale lithologies: submitted to Geophysics.

Uhrig, L.F., and Van Melle, F.A., 1955, Velocity anisotropy in stratified media: Geophysics, Vol. 20, p. 774-779.

Van Olphen, H., 1977, An Introduction to Clay Colloid Chemistry, 2nd Edition, Wiley Interscience Publication, New York, 301 pp.

White, J.E., 1965, Seismic Waves: Radiation, Transmission, and Attenuation, McGraw-Hill Book Co., Inc., New York, 302 pp.

FIGURE CAPTIONS

FIGURE 1. Orientation of axes with respect to symmetry of solid. Velocity notation: first numerical subscript refers to direction of propagation, second subscript denotes direction of particle vibration.

FIGURE 2. Confirmation of transverse isotropy. P-wave and S-wave velocities measured circumferentially about a 2-in. diameter core of vacuum-dry Cotton Valley shale in the plane of circular symmetry show no variations larger than the measurement error. Velocities measured parallel to fissility are significantly higher than those measured perpendicular to plane of fissility.

FIGURE 3. Scanning-electron photomicrographs of 3 shales with different clay contents viewed parallel (A,C,E) and perpendicular to plane of fissility. Scales of photos vary. (A), (B) Cotton Valley shale, 35% clay. (C), (D) Pierre shale, 57% clay. (E), (F) Beth Elkhorn shale, 72% clay.

FIGURE 4. Thin section photomicrographs of Cotton Valley shale showing encapsulation of quartz grains by clay. White areas are mostly quartz; black areas are predominantly clay. (A) Magnification 40x, long dimension of photo is 2.2 mm. (B) Magnification 100x, long dimension of photo is .9 mm.

FIGURE 5. Directional velocity data for fully saturated Cotton Valley shale. Directions are as labeled in Figure 1. Note that anisotropy increases with increasing differential pressure.

FIGURE 6. Compressional-wave velocity plotted against confining pressure in fully water-saturated cores of sandstone and shale at low pore pressure. From Tosaya (1982).

FIGURE 7. Elastic stiffnesses plotted as functions of differential pressure, derived from measured velocities according to equations (23).

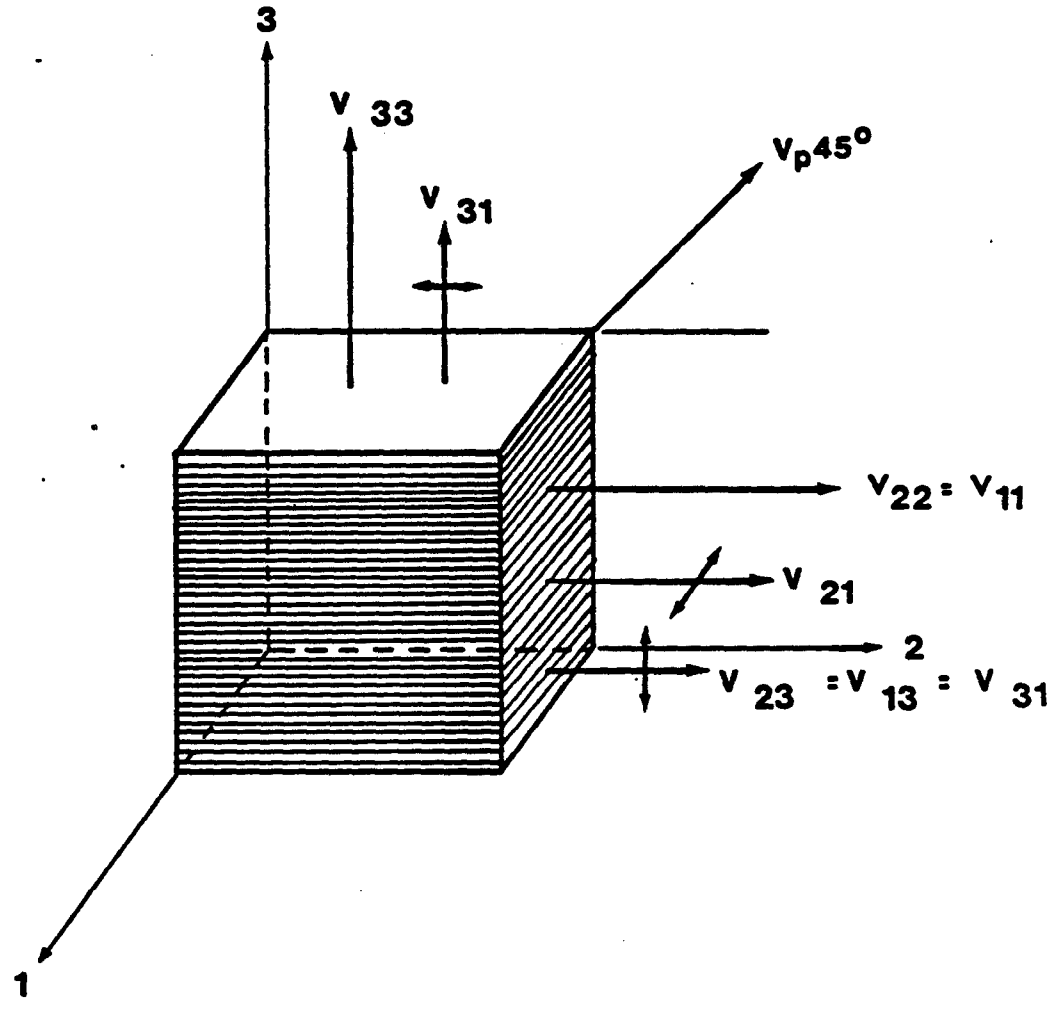

FIGURE 1

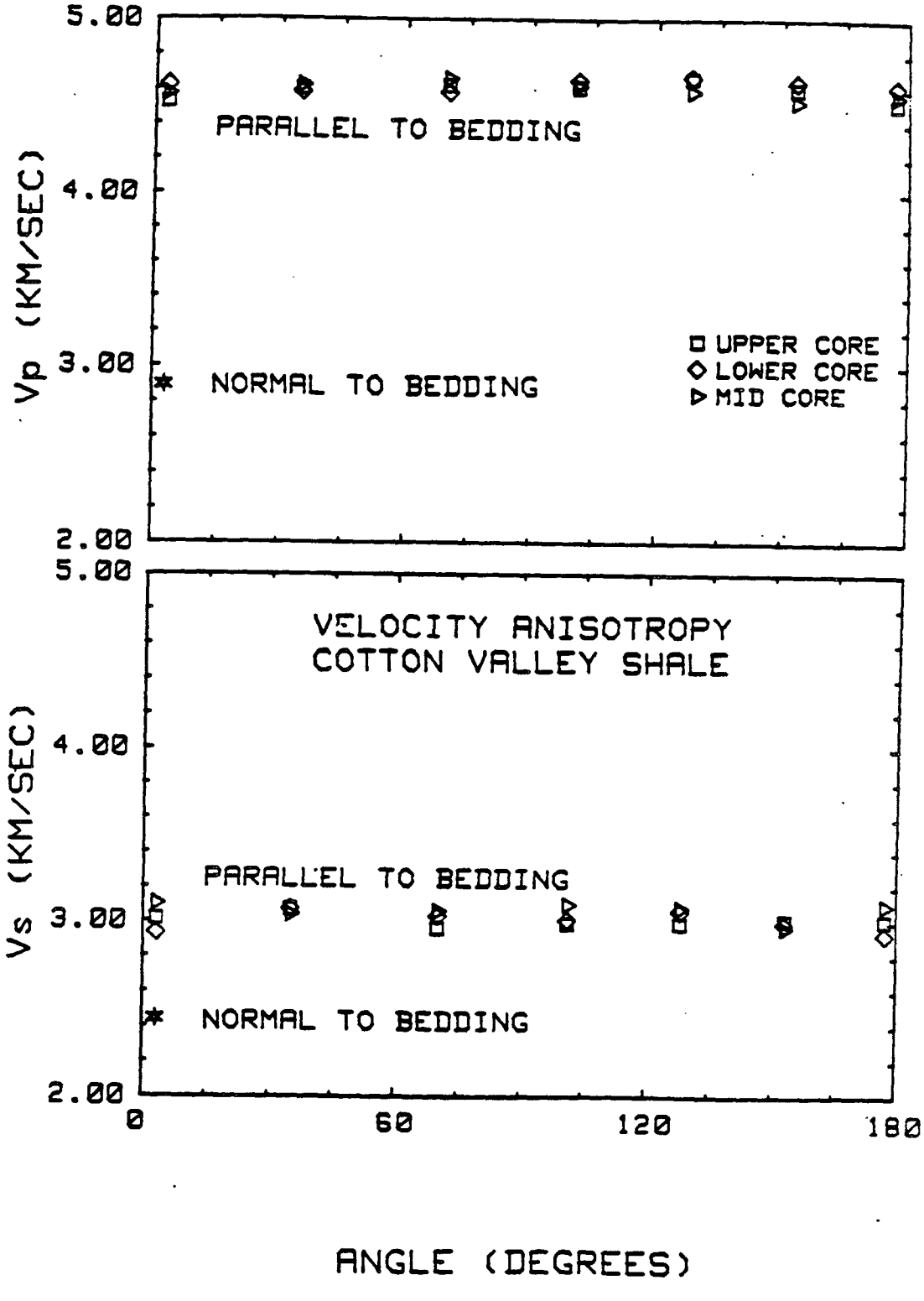
5.00
4.00
3.00
2.00
Vp (KM/SEC)
PARALLEL TO BEDDING
NORMAL TO BEDDING
UPPER CORE
LOWER CORE
MID CORE
VELOCITY ANISOTROPY
COTTON VALLEY SHALE
Vs (KM/SEC)
PARALLEL TO BEDDING
NORMAL TO BEDDING
0
60
120
180
ANGLE (DEGREES)

FIGURE 2

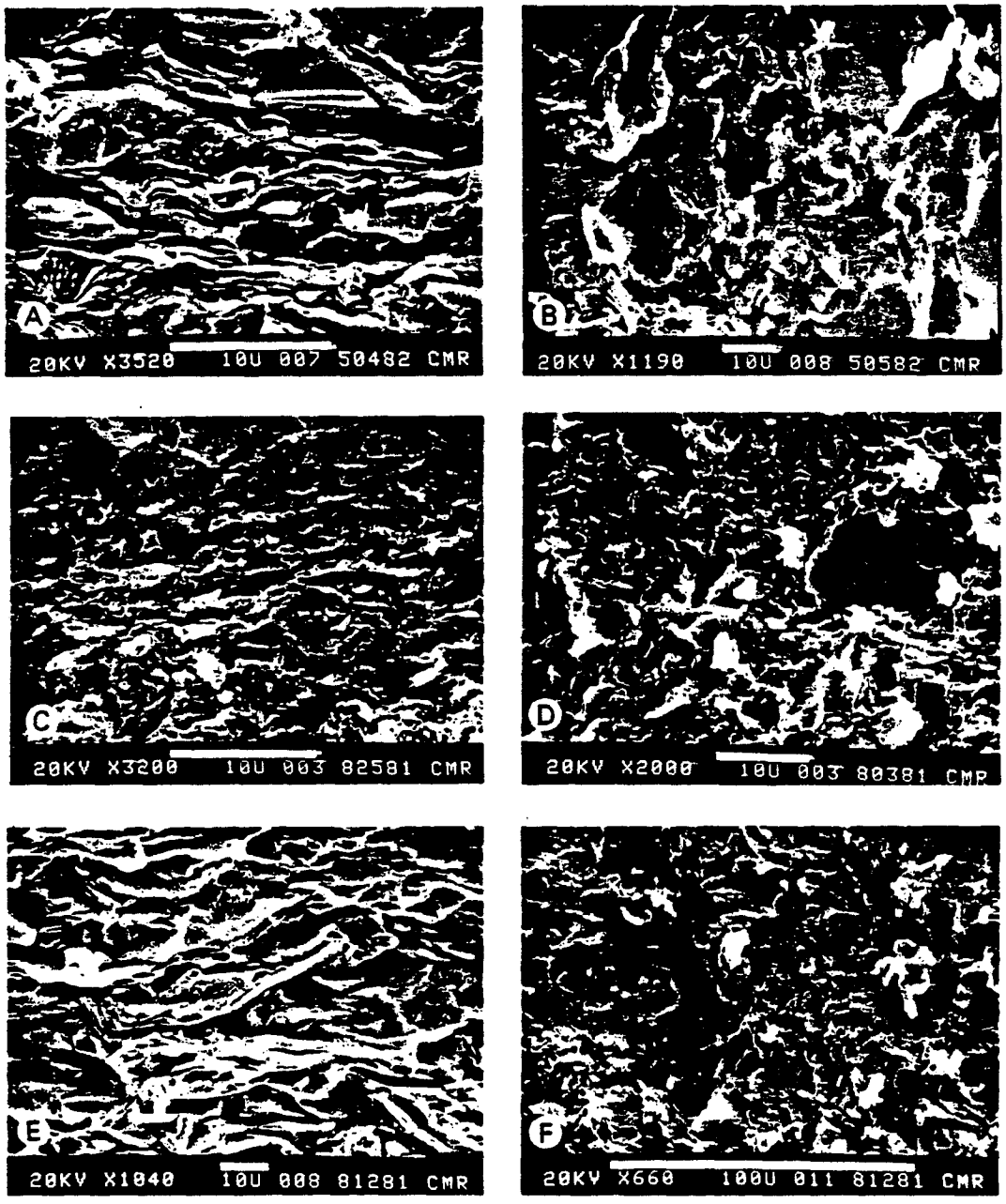
A
20KV X3520 10U 007 50482 CMR
B
20KV X1190 10U 008 50582 CMR
C
20KV X3200 10U 003 82581 CMR
D
20KV X2000 10U 003 80381 CMR
E
20KV X1040 10U 008 81281 CMR
F
20KV X660 100U 011 81281 CMR

Figure 3

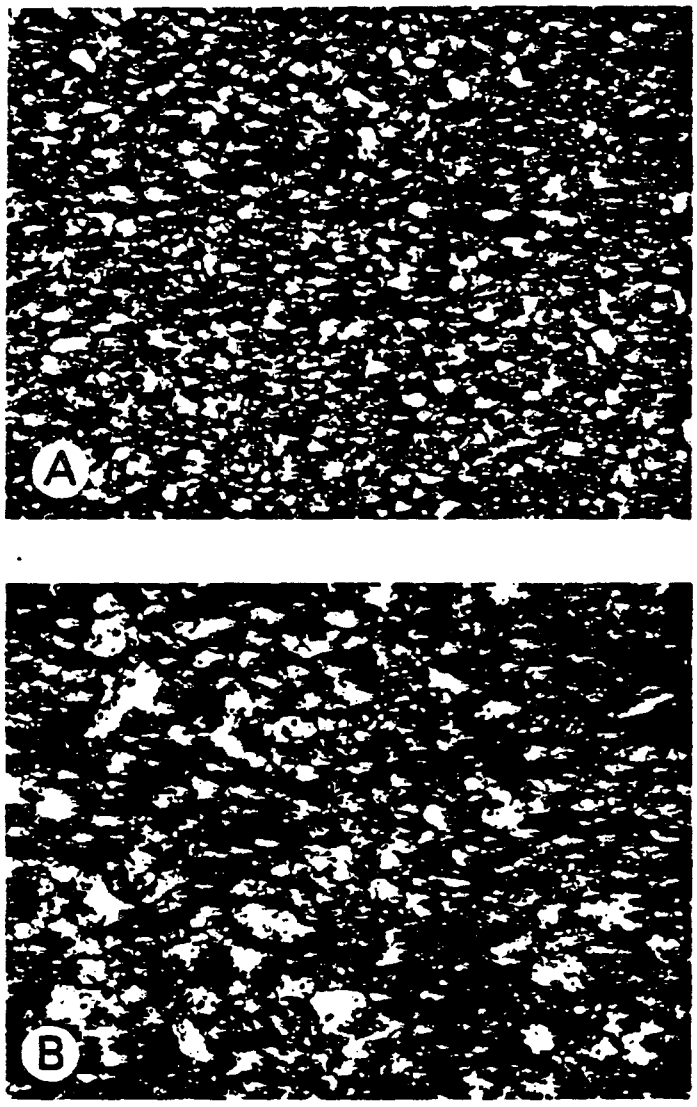

Figure 4

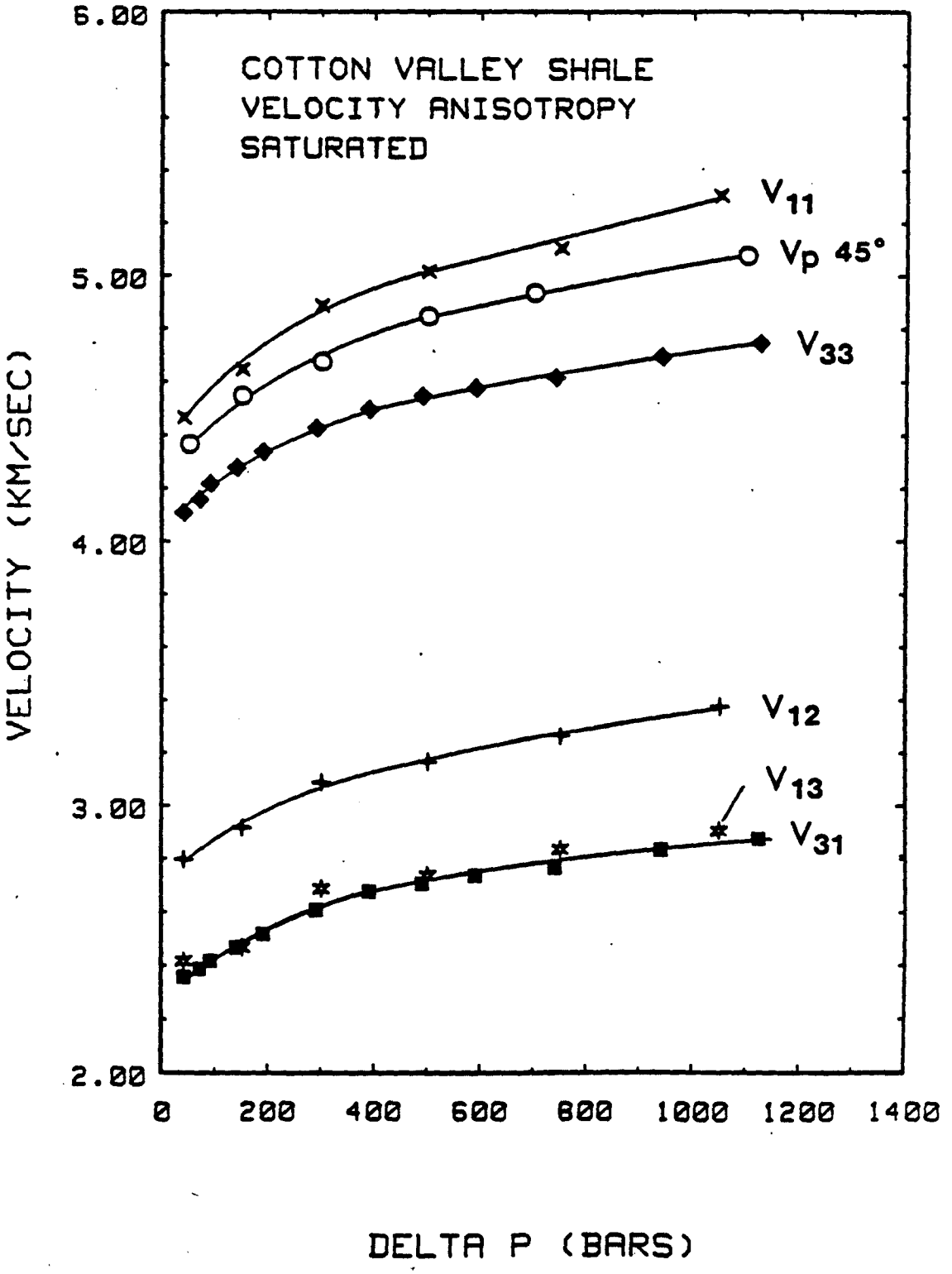
COTTON VALLEY SHALE
VELOCITY ANISOTROPY
SATURATED
V_{11}
V_p 45°
V_{33}
V_{12}
V_{13}
V_{31}
6.00
5.00
4.00
3.00
2.00
VELOCITY (KM/SEC)
0
200
400
600
800
1000
1200
1400
DELTA P (BARS)

FIGURE 5

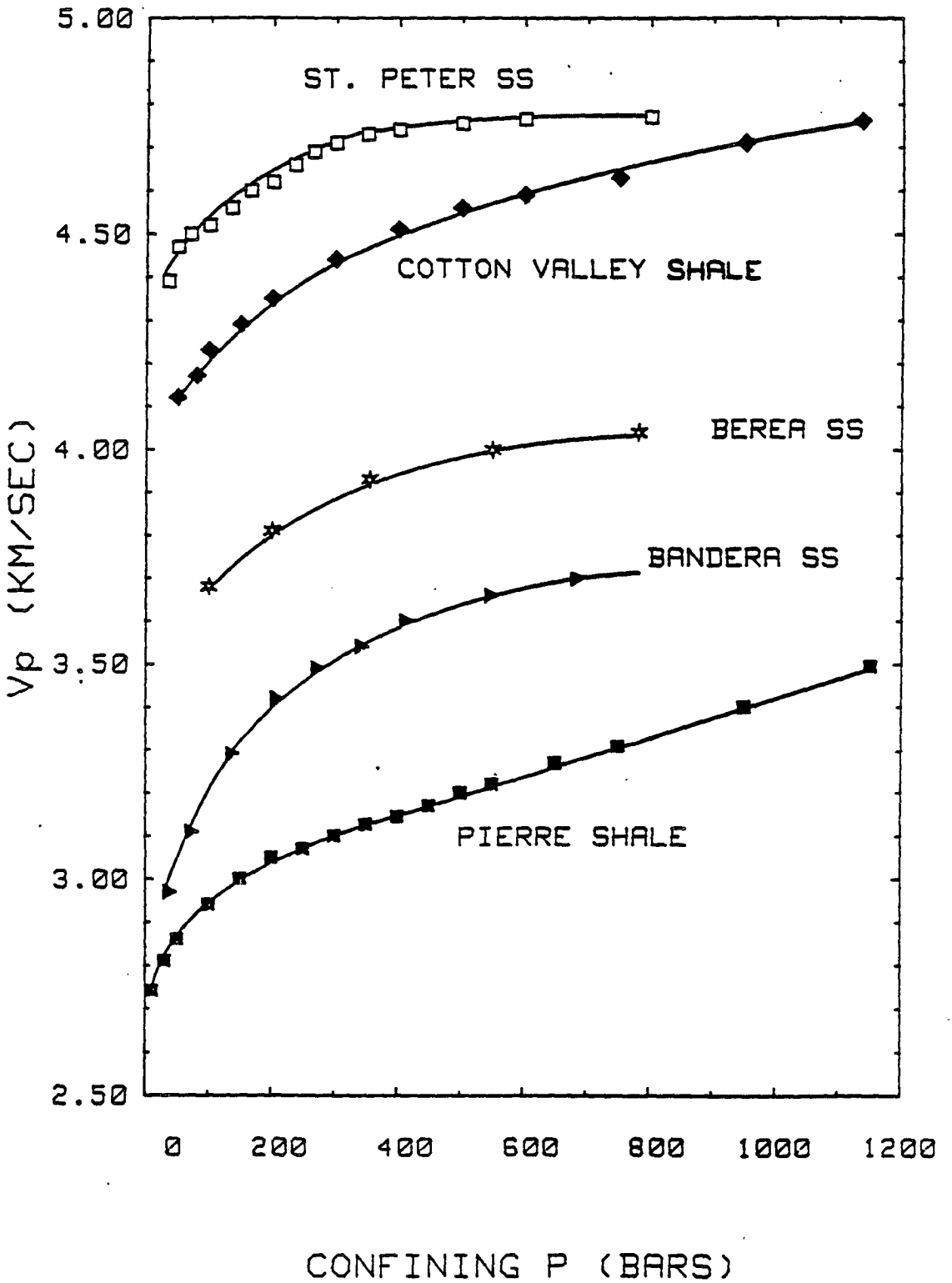
5.00
4.50
4.00
3.50
3.00
2.50
Vp (KM/SEC)
ST. PETER SS
COTTON VALLEY SHALE
BEREA SS
BANDERA SS
PIERRE SHALE
0
200
400
600
800
1000
1200
CONFINING P (BARS)

FIGURE 6

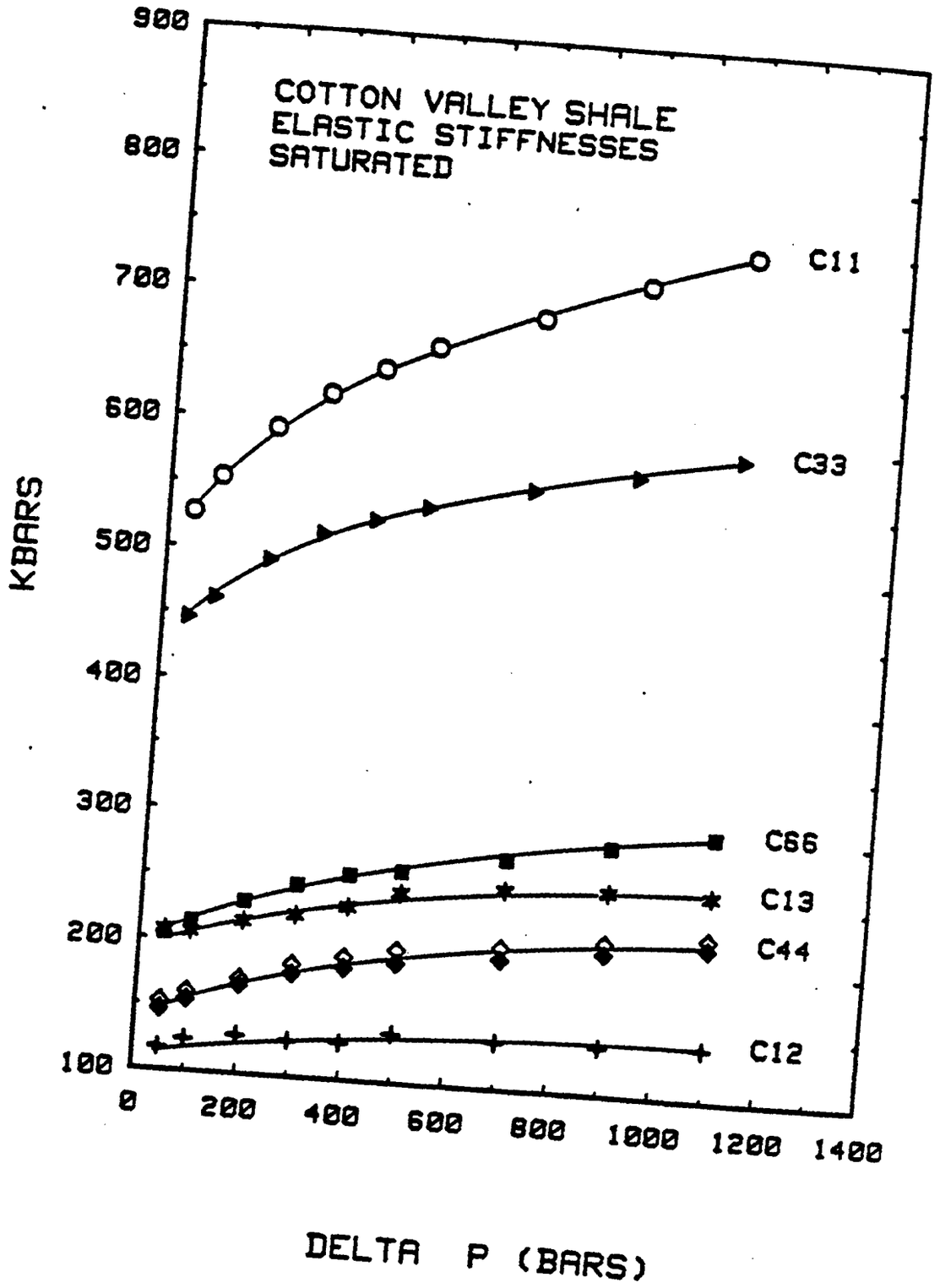
COTTON VALLEY SHALE
ELASTIC STIFFNESSES
SATURATED
C11
C33
C66
C13
C44
C12
KBARS
900
800
700
600
500
400
300
200
100
0
200
400
600
800
1000
1200
1400
DELTA P (BARS)

FIGURE 7